AN IRON SENSING E3 UBIQUITIN LIGASE REGULATES IRON HOMEOSTASIS

APPROVED BY SUPERVISORY COMMITTEE

Richard Bruick, Ph.D.

Wade Winkler, Ph.D.

Kevin Gardner, Ph.D.

Russell DeBose-Boyd, Ph.D.

DEDICATION

To my parents, Brent and Lissa Thompson, who always encouraged me to obtain the best education possible. Also to my wife Ale, my son Ezra, and my daughter Alice, for making everything worthwhile.

AN IRON SENSING E3 UBIQUITIN LIGASE REGULATES IRON HOMEOSTASIS

by

JOEL WILLIAM THOMPSON

DISSERTATION

Presented to the Faculty of the Graduate School of Biomedical Sciences

The University of Texas Southwestern Medical Center at Dallas

In Partial Fulfillment of the Requirements

For the Degree of

DOCTOR OF PHILOSOPHY

The University of Texas Southwestern Medical Center at Dallas

Dallas, Texas

June, 2011

ACKNOWLEDGEMENTS

First and foremost I would like to thank my mentor, Rick Bruick, who has been the mastermind behind this work. I am fortunate enough to have been given the opportunity to join the ideal lab with the ideal mentor for me to conduct my Ph.D. research. Rick has always gone out of his way to truly mentor me. He has taught me how to approach scientific questions and answer them in the most efficient and productive manner. Under Rick's guidance I have learned how to diligently design, conduct, and interpret experiments. Most importantly, Rick has instilled in me the desire to consistently perform high quality research, for which I will always be grateful.

I would also like to thank Ameen Salahudeen and Julio Ruiz. Under Rick's direction, the three of us worked as a team to identify and characterize FBXL5. Ameen and Julio are not only great colleagues but also great friends who have helped me tremendously. I am also deeply appreciative to the rest of the Bruick Lab including, Srinivas Chollangi, Hewen Ma, Yan Bai, and Cameron Shokri, for all of their assistance during my dissertation research. I would also like to thank Srinivas Chollangi, Ameen Salahudeen, and Sunil Laxman, for critical reading of this dissertation.

I have been privileged to collaborate with various people at UT Southwestern who without their assistance my research would not have been possible. I would especially like to thank Shugang Wei and the High Throughput Screening Facility, Lisa Kinch and the Grishin Lab, and Diana Tomchick and the Structural Biology Core.

Additionally, I would be remiss if I did not acknowledge the administrators of the UT Southwestern Graduate School of Biomedical Sciences. Specifically, I would like to express my appreciation to Stuart Ravnik and Nancy McKinney for all of their help and support.

Lastly, I would like to thank my dissertation committee, Wade Winkler, Kevin Gardner, and Russell DeBose-Boyd, for sacrificing their time to evaluate my progress, for all of their helpful suggestions during my committee meetings, and for their insightful comments on this dissertation.

AN IRON SENSING E3 UBIQUITIN LIGASE REGULATES IRON HOMEOSTASIS

JOEL WILLIAM THOMPSON

The University of Texas Southwestern Medical Center at Dallas, 2011

RICHARD KEITH BRUICK, Ph.D.

Human iron homeostasis must be tightly regulated to provide sufficient iron for vital cellular processes while preventing the toxic accumulation of free iron. IRP2 plays a critical role in cellular iron homeostasis by coordinating the posttranscriptional regulation of a variety of genes involved in iron metabolism. Posttranslational regulation of IRP2 is essential for its ability to maintain cellular iron homeostasis. The protein is stabilized under iron deficient conditions but polyubiquitinated and degraded by the proteasome when iron is plentiful. However, the E3 ubiquitin ligase that targets IRP2 for degradation is unknown. Moreover, the mechanisms cells use to sense iron levels and correlate changes of this metabolite to differences in IRP2 stability remain poorly understood. To

identify the E3 ubiquitin ligase responsible for IRP2 degradation, a high throughput RNAi screen was conducted. The top hit from the screen, FBXL5, interacts with and polyubiquitinates IRP2. Interestingly, FBXL5 is inversely regulated to IRP2. The protein is stabilized under conditions of excess iron and destabilized when iron is limiting. Deletion experiments identified the N terminus of FBXL5 as the region of the protein required for its iron dependent regulation. Bioinformatics predicted the N terminus encodes an iron binding hemerythrin domain. Consistent with this prediction X-ray crystallography demonstrated that the FBXL5 N-terminal domain adopts a hemerythrin fold with a diiron center. Mutation of iron ligating residues in the hemerythrin domain to abolish iron binding leads to constitutive destabilization of FBXL5. Collectively, these findings indicate that the hemerythrin domain acts as a ligand dependent regulatory switch controlling FBXL5's expression. Moreover, these data suggest that iron dependent regulation of FBXL5 exerts reciprocal effects on IRP2 stability. Thus, FBXL5 possesses an iron binding hemerythrin domain enabling cells to gauge bioavailable iron levels and control IRP2 expression accordingly, resulting in a tightly regulated circuit in the maintenance of iron homeostasis.

TABLE OF CONTENTS

PRIOR PUBLICATIONS

A.A. Salahudeen, J.W. Thompson, J.C. Ruiz, H. Ma, L.N. Kinch, Q. Li, N.V. Grishin, and R.K. Bruick. An E3 Ligase Possessing an Iron Responsive Hemerythrin Domain is a Regulator of Iron Homeostasis. (2009) *Science* 326, 722.

LIST OF FIGURES

LIST OF TABLES

LIST OF DEFINITIONS

ATP - adenosine triphosphate
DFO - deferoxamine mesylate
DNA - deoxyribonucleic acid
DTT - dithiothreitol
E1 - ubiquitin activating enzyme
E2 - ubiquitin conjugating enzyme
E3 - ubiquitin ligase
FAC - ferric ammonium citrate
HBEC - human bronchial epithelial cell line
HEK 293 - human embryonic kidney cell line
HEK 293T - human embryonic kidney cell line expressing large T antigen
HeLa - human cervical carcinoma cell line
HEPES - 4-(2-hydroxyethyl)-1-piperazineethanesulfonic acid
HOIL-1 - haem-oxidized IRP2 ubiquitin ligase-1
Hr - Hemerythrin
IPTG - isopropyl β-D-thiogalactopyranoside
IRE - Iron Responsive Element
IRP - Iron Regulatory Protein
MG132 - proteasome inhibitor Z-Leu-Leu-CHO
PAGE - polyacrylamide gel electrophoresis
PBS - Phosphate Buffered Saline
PCR - polymerase chain reaction
qRT-PCR - quantitative real time PCR
RNA - ribonucleic acid
RNAi - RNA interference
SDS - sodium dodecyl sulfate
SCF - Skp1, Cul1, F-box containing E3 ubiquitin ligase complex
Sf9 - Spodoptera frugiperda ovarian cell line
siRNA - small interfering RNA
shRNA - short hairpin RNA
Tris - tris(hydroxymethyl)methylglycine
UPS - ubiquitin-proteasome system
UTR - untranslated region

CHAPTER ONE

INTRODUCTION

IRON AND LIFE ON EARTH

Iron is one of the most abundant metals on Earth and the second most abundant element in the Earth's crust. It can function as an electron donor or acceptor interconverting between its ferrous (Fe^{+2}) and ferric (Fe^{+3}) oxidation states. Due to the abundance and chemical properties of iron, life on Earth evolved to depend on this transition metal (Crichton and Pierre, 2001).

Nearly every prokaryote and all eukaryotes require iron for life (Klausner et al., 1993). Iron functions as a cofactor in a variety of proteins including heme, iron-sulfur clusters, and oxygenases. On account of iron's ease in donating and accepting electrons, iron is employed by proteins to carry out oxidation-reduction reactions. Iron-utilizing proteins are necessary for critical biological processes such as transport and storage of oxygen, deoxyribonucleotide synthesis, chromatin regulation, and oxidative phosphorylation. However, while iron is generally required for sustaining life, when present in excess it can have deleterious consequences. Copious amounts of free iron generate radical species through Fenton chemistry that cause oxidative damage to proteins, nucleic acids, and lipids. Consequently, the acquisition, usage, and storage of iron are regulated in most organisms in order to maintain iron homeostasis (De Domenico et al., 2007).

HUMAN IRON HOMEOSTASIS

While humans require iron for diverse biological processes, the vast majority (~80%) of iron in the body is found in erythrocytes and their precursor cells where it is required for the synthesis and function of heme. Due to the high iron demand of red blood cells, iron deficiency causes anemia, a disease that affects more than a billion individuals worldwide. At the other end of the iron related disorders spectrum is hemochromatosis, a disease of iron overload, which can cause heart disease, diabetes, and cirrhosis of the liver. Thus, the challenge for humans is to maintain sufficient iron levels to sustain life while avoiding the potentially detrimental effects of excess iron (Hentze et al., 2004). In order to manage this dilemma humans regulate iron homeostasis at both the systemic and cellular levels.

Systemic Iron Homeostasis

Intestinal Iron Acquisition and Efflux to the Plasma

Regulation of iron homeostasis begins in the intestine, the absorption site of dietary iron. In order for iron to enter the bloodstream it must first traverse polarized intestinal epithelial cells called enterocytes. The apical side of enterocytes contains multiple finger-like appendages called villi to facilitate absorption of nutrients from the lumen. The basolateral side is adjacent to the circulation to enable secretion of absorbed nutrients into the blood. Dietary iron is largely in the insoluble ferric state and must be reduced to the soluble ferrous state before it can be absorbed. This reductive step is mediated by duodenal cytochrome b (DCYTB), a ferrireductase located on the apical side of enterocytes (McKie et al., 2001). This membrane bound protein shares significant homology to cytochrome b561 and based on this similarity is believed to be a heme

protein that uses ascorbate as an electron donor (Andrews and Schmidt, 2007). DCYTB is widely regarded as the primary ferrireductase responsible for reducing dietary iron. However, deletion of DCYTB in the mouse does not result in iron deficiency indicating that additional enzymes or pathways can compensate for its function (Gunshin et al., 2005b). Nevertheless, DCYTB is upregulated under iron deficient conditions and hypoxia suggesting this reductase plays an important role in intestinal iron absorption (McKie et al., 2001).

Once dietary iron has been reduced, Divalent Metal Transporter 1 (DMT1) transfers it across the apical membrane and into the enterocyte cytosol (Fig. 1-1). In addition to iron, DMT1 can transport other divalent metals such as manganese, cobalt, zinc, copper, lead, and cadmium, using a proton-coupled mechanism. In addition to enterocytes, DMT1 is expressed in the endosomes of virtually all cell types. Moreover, DMT1 is highly conserved from bacteria to man (De Domenico et al., 2007). Loss of DMT1 expression in mice inhibits intestinal iron uptake and causes anemia (Gunshin et al., 2005a). Human patients with loss of function mutations to DMT1 are not only anemic but also present with hepatic iron overload (Beaumont et al., 2006; Mims et al., 2005).

Following intestinal absorption iron can be stored in the cytosol bound to the storage protein ferritin or exported into the plasma via the actions of ferroportin (Fig. 1-1). Ferroportin is predicted to contain 12 transmembrane domains and is localized on the basolateral membrane of enterocytes. Ferroportin is also expressed on the cell surface of hepatocytes and macrophages where it plays a key role in releasing stored iron and iron recycled from effete erythrocytes, respectively (Andrews and Schmidt, 2007). Global ferroportin knockout causes embryonic lethality in mice and intestine specific knockout

results in severe anemia due to abrogated iron efflux from enterocytes (Donovan et al., 2005). In humans, ferroportin loss of function mutations lead to iron-limited erythropoiesis, and iron overload in machrophages and hepatocytes (Pietrangelo, 2004).

In 1956 it was discovered that copper-deficient pigs develop anemia suggesting an intimate relationship between iron and copper homeostasis (Bush et al., 1956). Two copper binding ferrioxidases, ceruloplasmin and hephaestin, are required for iron export from a variety of tissues including the intestines (Osaki and Johnson, 1969; Ragan et al., 1969; Vulpe et al., 1999). Similar to DMT1, ferroportin can only transport ferrous iron. Moreover, for reasons that remain poorly understood, ferroportin is unable to export iron in the absence of an ancillary enzyme providing extracellular ferrioxidase activity. Hephaestin provides the majority of this activity in the intestines whereas in hepatocytes and machrophages ceruloplasmin is probably used exclusively (Andrews and Schmidt, 2007). Due to iron overload in a variety of parenchymal tissues, humans with mutations to ceruloplasmin can develop anemia, neuropathies, retinopathies, and diabetes. Similar symptoms are also seen in Wilson's disease, a disease caused by defects in ceruloplasmin processing (Gouider-Khouja, 2009).

Delivery Of Iron To Tissues

Iron transported into the serum is bound by the glycoprotein transferrin (Fig. 1-1), which has an extremely high affinity ($K_D=10^{-23}$ M) for ferric iron. Transferrin serves two important roles in human physiology. First, by rapidly binding iron exported from enterocytes and other tissues, transferrin protects blood from the potentially harmful effects of free iron. Second, transferrin distributes iron throughout they body via the

circulation (De Domenico et al., 2007). Interestingly, humans with non-functioning transferrin develop iron overload in the liver and pancreas (Hamill et al., 1991).

In the majority of cells in the body the integral membrane protein, transferrin receptor 1 (TfR1), is responsible for iron uptake from the blood. To accomplish this, TfR1 binds circulating holo-transferrin. The resulting transferrin-TfR1 complex undergoes endocytosis and is delivered to the endosome (Fig. 1-1). In the acidic environment of the endosome ferric iron dissociates from transferrin and is subsequently converted to ferrous iron by the ferrireductase STEAP3. DMT1 transports ferrous iron from the endosome to the cytosol. TfR1, still bound to apo-transferrin, is recycled back to the cell membrane. At the more neutral pH of blood TfR1 releases apo-transferrin and the receptor can undergo additional cycles of holo-transferrin mediated endocytosis (Andrews, 2008; Hentze et al., 2004). Underscoring the importance of TfR1 is the embryonic lethal phenotype of TfR1 knockout mice (Levy et al., 1999).

Iron Storage and Recycling

Excess cellular iron is stored in the protein ferritin. There are two forms of ferritin, H (for heavy and heart) and L (for liver and light). The H form is predominantly expressed in the heart and has a molecular weight of 21 kDa, while the L form is predominantly expressed in the liver and spleen and has a molecular weight of 19 kDa. Ferritin exists as a multimer consisting of 24 subunits comprised of a mixture of the H and L forms (Theil, 2003). Interestingly, ferritin complexes adopt a sphere-like structure that allows for the storage of up to 4500 iron atoms in its hollow interior. Although the L form has no catalytic function, the ferritin H subunit displays ferrioxidase activity and converts ferrous iron to the less reactive ferric form for storage (De Domenico et al.,

2007; Hentze et al., 2004). Thus, ferritin not only sequesters excess iron for future use when demand may increase, but it also protects cells from the potentially toxic effects of free iron (Fig. 1-1).

The amount of dietary iron absorbed daily accounts for less than 0.1% of the total amount of iron in the body. Moreover, the body is constantly loosing iron through perspiration, bleeding, sloughing off of gut enterocytes, and exfoliation of skin and other cells. Therefore, in order to meet demand, there is an intrinsic need to recycle iron within the body. To this end, red blood cells, the greatest consumer of body iron, upon being damaged or dilapidated are phagocytosed by tissue macrophages localized in the spleen and liver. Engulfed erythrocytes are lysed and heme is catabolized by heme oxygenase, liberating iron from the porphyrin ring. Scavenged iron can then be stored in machrophages or in hepatocytes bound to ferritin. When demand for systemic iron increases, iron caches in macrophages and hepatocytes can be mobilized through the efflux of iron into the blood via ferroportin (Andrews and Schmidt, 2007; Hentze et al., 2010).

Regulation of Systemic Iron Homeostasis

The main regulator of systemic iron homeostasis is hepcidin, a circulating hormone peptide primarily excreted by the liver (Andrews, 2008). Hepcidin is a member of the defensin family of peptides characterized by their cysteine-rich sequences and antimicrobial properties. Hepcidin binds ferroportin and this interaction initiates the phosphorylation, internalization, and monoubiquitination of ferroportin. Ubiquitinated ferroportin is delivered to the lysosome where it is degraded. Internalization and degradation of ferroportin effectively reduces serum iron levels (Nemeth et al., 2004).

Hepcidin is regulated at the transcriptional level. When serum iron levels are sufficient to satisfy systemic demand, the gene encoding hepcidin, HAMP, is upregulated, and hepcidin expression increases resulting in decreased ferroportin levels with concomitant reduction of iron efflux into the blood from enterocytes, hepatocytes, and macrophages (Nicolas et al., 2002). Targeted deletion of HAMP in mice leads to severe iron overload (Nicolas et al., 2001). Moreover, humans with mutations in the HAMP gene develop juvenile hemochromatosis (Roetto et al., 2003). As part of the innate immune response, hepcidin expression increases under conditions of infection. Many pathogens require iron for viability and therefore, as an added protection against infection, HAMP expression is upregulated to reduce circulating iron levels and create a less inhabitable environment for microorganisms. However, individuals who suffer from chronic infections can develop anemia due to constitutive downregulation of ferroportin resulting in decreased iron uptake from the diet and retention of iron in the liver and macrophages (Schaible and Kaufmann, 2004).

Hepcidin expression can be repressed during various conditions including iron deprivation and hypoxia. When systemic iron demand exceeds iron availability HAMP transcription decreases. Reduced hepcidin expression stabilizes ferroportin and increases the amount of iron transported into the serum from enterocytes. Additionally under conditions of iron scarcity when hepcidin expression is attenuated, iron stores in hepatocytes and macrophages can be made available for systemic use. During conditions of low O_2 availability (hypoxia), in order to increase the O_2 supplying capacity of blood, erythropoiesis is stimulated. However, an upregulation of red blood cell production

requires iron and consequently under hypoxic conditions hepcidin expression is downregulated (Nicolas et al., 2002).

Cellular Iron Homeostasis

Iron Responsive Elements

During the decade spanning the mid 1970's to mid 1980's, a pair of critical observations were made that initiated the field of cellular iron homeostasis research. The first observation demonstrated that translation of ferritin increases when bioavailable iron levels are high and decreases when iron is scarce (Zahringer et al., 1976). The second observation revealed that the stability of TfR1 mRNA increases when iron availability is low and decrease when iron is plentiful (Rao et al., 1986). Together these data indicated that under conditions where cellular iron levels are in excess, TfR1 is downregulated to decrease iron acquisition and ferritin synthesis is upregulated to increase iron storage. Conversely, in iron deficient cells, TfR1 is upregulated and ferritin synthesis is inhibited resulting in increased iron uptake and availability. Thus, a new paradigm emerged suggesting mammalian cells coordinate the posttranscriptional regulation of genes involved in iron metabolism in order to maintain iron homeostasis (Klausner et al., 1993). However, the underlying mechanisms facilitating this coordinated regulation remained enigmatic.

In 1987 the laboratories of Munro and Klausner independently reported the same seminal discoveries. Iron responsive translational control of ferritin was dependent on its 5' untranslated region (UTR). Deletion of the ferritin 5' UTR abrogated posttranscriptional iron dependent regulation, and fusion of the 5'UTR to a heterologous mRNA was sufficient to confer iron dependent translational control. Further experiments

mapped a ~30 nucleotide RNA sequence in the 5' UTR that was both necessary and sufficient for iron dependent translational regulation (Aziz and Munro, 1987; Hentze et al., 1987). This highly conserved sequence was termed an iron responsive element (IRE). Both the H and L ferritin subunits contain a single IRE in their 5' UTRs and these IREs were predicted to adopt stem-loop structures. Subsequent experiments using NMR spectroscopy and x-ray crystallography (Addess et al., 1997; Walden et al., 2006) confirmed that the ferritin IREs contain a six-nucleotide loop followed by a 5 base-pair stem, an unpaired cytosine, and a lower stem (Fig. 1-2).

In 1987 it was also discovered that iron responsive regulation of TfR1 mRNA stability was dependent on the TfR1 3' UTR (Owen and Kuhn, 1987). Ensuing investigations identified five putative RNA stem-loop motifs in the 3' UTR with predicted structures remarkably similar to the IREs in ferritin (Casey et al., 1988a). Structural and mutational experiments confirmed the presence of these IREs and demonstrated that three of the five were required for iron dependent control of TfR1 stability (Casey et al., 1988b; Casey et al., 1989). Thus, both ferritin and TfR1 contain cis-acting IREs. However, the location of the IRE within the UTR has opposite affects on the iron dependent regulation of the gene. Since the discovery of IREs in TfR1 and ferritin, there has been other IRE containing genes identified such as DMT1, ferroportin, HIF-2α, mAconitase, eALAS, APP, CDC14A, and alpha-synuclein. While the physiological significance of many of these more recently discovered IREs requires further analysis, it is becoming clearer that disparate cell types employ these cis-acting regulatory elements to maintain iron homeostasis under a variety of tissue dependent contexts (Hentze et al., 2004; Hentze et al., 2010).

Iron Regulatory Protein 1

After the initial finding that iron dependent regulation of ferritin and TfR1 was mediated by cis-acting IREs, it was discovered that a cytosolic protein could bind these highly conserved RNA elements. This IRE interacting protein displayed increased binding activity under iron deficient conditions and decreased activity under iron replete conditions. Furthermore, the decrease in IRE binding activity under high iron conditions could be reversed by addition of a reducing agent to cell extracts (Leibold and Munro, 1988; Rouault et al., 1988; Yu et al., 1992). In 1990 the Klausner group was able to purify the protein responsible for the IRE binding activity from human liver extracts using IRE-affinity chromatography and two-dimensional gel electrophoresis (Rouault et al., 1990). Following sequencing of the purified protein, the cDNA encoding the IRE binding protein was cloned, and the protein was later referred to as Iron Regulatory Protein 1 (IRP1).

Elucidation of IRP1's preferential IRE binding activity led to a mechanistic understanding of iron dependent regulation of IRE containing genes. Under iron deficient conditions IRP1 binding to the IRE on the 5'UTR of ferritin sterically hinders the ribosome from binding to the mRNA and initiating translation. However, under iron replete conditions IRP1 fails to interact with IREs allowing binding of the ribosome to the ferritin mRNA with concomitant upregulation of the protein. In the case of TfR1, IRP1 binding to multiple IREs in the 3'UTR prevents endonucleolytic degradation of the transcript and increases stability of the mRNA. When iron is abundant in the cell, IRP1 looses its IRE binding ability leaving the TfR1 transcript susceptible to degradation thereby decreasing its translation (Klausner et al., 1993).

In addition to its IRE binding activity, IRP1 can also functions as a cytosolic aconitase enzyme, interconverting two intermediates of the TCA cycle, citrate and isocitrate. Similar to mitochondrial aconitase, IRP1 binds a cubane iron-sulfur (Fe-S) cluster (Kaptain et al., 1991; Philpott et al., 1994). However, IRP1 can only assemble a Fe-S cluster under iron replete conditions. This finding also explained why IRP1's IRE binding activity correlates with bioavailable iron levels. Under conditions where iron is plentiful IRP1 binds a Fe-S cluster (holo-IRP1) and looses affinity for IREs. In contrast, when cellular iron levels are low IRP1 no longer binds a Fe-S cluster (apo-IRP1) and undergoes a conformational change exposing an IRE binding pocket. Under these conditions IRP1 interacts with IREs in the UTRs of genes such as ferritin and TfR1. Thus, IRP1's two functions are mutually exclusive. Moreover, the previous observation that adding a reducing agent to iron rich cell lysates reverses IRP1's inability to bind IREs, could now be explained mechanistically. IRP1 employs three critical cysteine residues to bind three iron atoms of a Fe-S cluster. Addition of a reducing agent reduces these active site cysteines precluding IRP1 from binding a Fe-S cluster, thus converting it into an IRE binding protein (Hentze et al., 2004; Rouault, 2006; Wallander et al., 2006).

Iron Regulatory Protein 2

Gel shift assays using rodent lysates for IRE binding activity demonstrated two distinct complexes interacting with radiolabeled IRE probes. While the slower migrating IRE protein complex contained IRP1, the identity of the protein in the faster migrating IRE complex remained unknown. The Klausner lab cloned the second protein the same year as IRP1 (Rouault et al., 1990) but characterization of this protein occurred later than IRP1. The second IRE binding protein was naturally named Iron Regulatory Protein 2

(IRP2), and possessed 57% identity and 75% homology to IRP1 at the amino acid level. IRP2 demonstrated preferential IRE binding under iron deficient conditions and was able to posttranscriptionally regulate IRE containing genes via the same mechanism as IRP1. However, in contrast to IRP1, IRP2 had no detectable aconitase activity. This is presumably due to the fact that IRP2 is missing two of the conserved aconitase active site cysteine residues and contains a unique 73 amino acid insert (Rouault et al., 1992; Samaniego et al., 1994). Various experiments conducted by the Leibold and Klausner labs indicated that IRP2 was regulated at the posttranslational level. IRP2 levels decrease substantially in cells treated with iron due to a decrease in protein stability, while mRNA levels remain unchanged as a function of iron bioavailability. Furthermore, treatment of cells with proteasome inhibitors stabilizes IRP2 suggesting that under conditions where iron is plentiful IRP2 is polyubiquitinated and tagged for degradation in the proteasome (Guo et al., 1995; Guo et al., 1994; Samaniego et al., 1994).

The ubiquitin-proteasome system (UPS) is an important regulator of many cellular processes including the cell cycle, protein quality control, apoptosis, immune responses, and differentiation. The proteasome is a large macromolecular complex that degrades proteins that have been posttranslationally modified with a polyubiquitin tag. Ubiquitin is a 76 amino acid containing protein with a molecular weight of around 8 kDa. Cells utilize a trio of enzymes to carry out polyubiquitination of proteins (Fig. 1-4). The first enzyme, termed an E1 activating enzyme, catalyzes adenylation of the C-terminal carboxylate moiety of ubiquitin. Following activation of ubiquitin, the E1 enzyme facilitates attachment of the ubiquitin C-terminal carboxylate to its active site cysteine residue creating a high-energy thioester bond. The second enzyme in the process, an E2

conjugating enzyme, facilitates the transfer of ubiquitin from the E1 enzyme to itself, once again via attachment of the C-terminal ubiquitin carboxylate to its active site cysteine residue. The last enzyme in the cascade is called an E3 ubiquitin ligase. In many cases the E3's function is to catalyze the transfer of ubiquitin directly from the E2 enzyme to the substrate protein. In this final step, the ubiquitin C-terminal carboxylate is covalently attached to the ε-amino group of a lysine residue on the substrate forming an isopeptide bond. After the initial monoubiquitination event occurs, polyubiquitin chains can then be formed via isopeptide bond formation between newly added ubiquitins and ubiquitins previously attached to the target protein. To date only two E1 enzymes have been identified. There are ~40 E2s and ~600 predicted E3 ligases in the human genome. Out of the three enzymes in the UPS cascade, E3s are often considered the most important because of their role in regulating substrate specificity as they bind the target protein directly (Nalepa et al., 2006; Ravid and Hochstrasser, 2008; Yamanaka et al., 2003). The regulatory elements that E3 ligases recognize and bind to on their substrates are referred to as degrons (Varshavsky, 1991).

Thus, while both IRP1 and IRP2 act as trans-acting elements to control the translation or mRNA stability of IRE containing genes, they are regulated by distinct iron dependent mechanisms. IRP1 binds a Fe-S cluster under iron replete conditions precluding its IRE binding activity, whereas under iron deficient conditions it assumes its apo form and functions as an IRE binding protein (Fig. 1-5). IRP2 is degraded in the proteasome when iron is plentiful, while the protein is stabilized under iron limiting conditions allowing it to accumulate and bind IREs (Fig. 1-6).

Physiological Roles of IRP1 and IRP2

The functions of IRP1 and IRP2 to regulate cellular iron homeostasis by coordinating the posttranscriptional regulation of IRE containing genes was well studied during the 1990's in a variety of in vitro and cell culture models. However, it wasn't until the 2000's that the physiological roles of these IRE binding proteins was characterized. Underscoring the physiological importance of both IRPs is the lethal phenotype of global $IRP1^{-/-}$ $IRP2^{-/-}$ mice observed during the blastocyst stage of embryonic development (Smith et al., 2006). While demonstrating the necessity of IRPs for viability, these double knockout mice do not address IRPs relevance for maintaining physiological iron homeostasis. This fundamental question has been answered through the generation of single IRP knockout mice and tissue specific $IRP1^{-/-}$ $IRP2^{-/-}$ mice.

IRP2 null mice display inappropriate accumulation of ferritin, DMT1, and ferroportin in a variety of tissues. They also developed excessive iron accumulation in the brain and mild neurodegenerative phenotypes including ataxia, bradykinesia, and loss of neuronal axons. Moreover, due to the loss of IRP2 expression, eALAS, an IRE containing gene encoding the rate-limiting enzyme in the heme biosynthetic pathway, is inappropriately upregulated causing erythropoietic protoporphyria. One of the more striking examples of aberrant iron homeostasis in the $IRP2^{-/-}$ mice is the development of microcytic anemia. This phenotype is ostensibly due to constitutive downregulation of TfR1 leading to iron deficiency in erythrocytes and their precursor cells (Galy et al., 2005; LaVaute et al., 2001; Meyron-Holtz et al., 2004a).

In contrast to IRP2 knockout mice, misregulation of iron metabolism is only observed in brown fat and kidneys in $IRP1^{-/-}$ mice. Moreover, IRP1 null mice do not

exhibit any other overt phenotypes (Meyron-Holtz et al., 2004a). These data suggest that IRP2 plays a more dominant role in regulating iron homeostasis in vivo. Consistent with this paradigm are cell culture studies comparing the IRE binding activities of IRP1 and IRP2 as a function of O_2 availability. Under typical cell culture conditions where O_2 is present at 21%, both IRP1 and IRP2 demonstrate increased IRE binding activity under iron deficient conditions. However, at the more physiologically relevant level of 3% O_2, IRP1, loses much of its ability to preferentially bind IREs under iron deficient conditions whereas IRP2 retains its IRE binding activity. Furthermore, at 3% O_2 levels IRE containing genes are regulated normally in IRP1 null cells, while IRP2 null cells misregulate the same genes (Meyron-Holtz et al., 2004b). One possible explanation for lack of IRP1 IRE binding activity under low O_2 conditions is an increase in the protein's aconitase activity, as the two functions are mutually exclusive. When exposed to supra physiological O_2 levels the Fe-S cluster may become more labile and render IRP1 more sensitive to changes in iron availability. In contrast, under physiological O_2 conditions, Fe-S clusters are more stable promoting IRP1 aconitase activity and inhibiting its IRE binding activity. Taken together, IRP1 and IRP2 have some overlapping functions, but IRP2 appears to play a more crucial role in the posttranscriptional regulation of IRE containing genes in vivo. This may be due to the distinct manner in which IRP2 is regulated as a function of iron availability.

Crosstalk Between Systemic and Cellular Iron Homeostasis

As previously described, systemic iron homeostasis is mainly regulated by the liver hormone hepcidin. Cellular iron homeostasis is primarily controlled through the IRE/IRP regulatory system. Recently, it has become increasingly evident that these two

systems are interconnected. One example of this crosstalk is the regulation of ferroportin. Hepcidin posttranslationally regulates ferroportin in order to prevent systemic iron overload. Ferroportin expression is also regulated posttranscriptionally by IRPs via an IRE its 5' UTR. In mice with intestine specific knockout of both IRPs, despite increased hepcidin expression, ferroportin is grossly overexpressed causing enterocyte iron deficiency (Galy et al., 2008). Thus, both systemic and cellular iron regulatory systems are required for proper iron export from the intestine. Moreover, these data suggest that ferroportin expressing cells such as enterocytes, which function to maintain systemic iron homeostasis, are intrinsically programmed to protect themselves against excessive iron efflux that could lead to iron deficiency (Hentze et al., 2010).

Initial Studies of the Mechanisms Governing Iron Dependent Regulation of IRP2

While the mechanism regulating IRP1's IRE binding activity was determined relatively quickly to involve an iron dependent "switch" controlled by assembly of an Fe-S cluster, the mechanisms controlling IRP2's iron dependent regulation has proven much more difficult to delineate. However, it is widely accepted that IRP2 is polyubiquitinated and degraded in the proteasome under iron replete conditions and stabilized when iron is limiting.

Initial efforts to understand the iron dependent regulation of IRP2 stability focused on identifying the mechanisms cells use to sense iron levels through IRP2, as IRP2 was thought to be a direct iron sensor. IRP1 and IRP2 share extensive amino acid sequence homology throughout the proteins, except for a unique 73 amino acid insert in IRP2. With this in mind, the Rouault lab focused investigations on the unique region of IRP2 with the rationale that it may be important for mediating iron dependent regulation

of IRP2. To test this hypothesis, a stable cell line expressing a truncated IRP2 constructs lacking the unique 73 amino acid insert (IRP2 Δ73) was generated. This IRP2 Δ73 construct failed to respond to changes in cellular iron levels and remained stable under iron replete conditions. Furthermore, insertion of the unique IRP2 region to the homologous position within IRP1 was sufficient to confer iron dependent regulation on the resulting chimera protein. Taken together, these data suggested that the unique 73 amino acid region of IRP2, termed the iron-dependent degradation domain (IDD), was both necessary and sufficient to confer iron dependent regulation on the IRPs (Iwai et al., 1995).

With the IDD identified as a possible region within IRP2 required for its iron dependent regulation, further work focused on identifying posttranslational modifications within the IDD. The IDD contains five conserved cysteine residues, which were predicted by the Rouault lab to bind iron. Iron binding by the IDD was postulated to catalyze oxidation of nearby amino acids through an oxygen radical species dependent mechanism. To test this hypothesis recombinant IRP1 and IRP2 were expressed and purified from insect cells and subjected to in vitro oxidation assays. When incubated in the presences of DTT, O_2, and iron, recombinant IRP2, but not IRP1, displayed oxidation of amino acid side chains as measured by the generation of carbonyl groups. IRP2 immunoprecipitated from mammalian cells also displayed increased oxidation that was dependent on conserved cysteine residues in the IDD. In vitro ubiquitination assays using mammalian cell lysates for activity and recombinant IRP2 as the substrate were also carried out. These results indicated that iron oxidized IRP2 was a much better substrate for in vitro polyubiquitination than native IRP2. In all, these data suggested a mechanism

for iron dependent regulation of IRP2 in which oxidation of the protein signals for its ubiquitination and degradation in the proteasome (Iwai et al., 1998).

While previous work provided evidence that IRP2 was oxidized, the specific amino acids oxidized on the protein had not been determined. It was assumed that oxidation occurred in or near the IDD domain as it contained a putative iron binding motif, but no experimental evidence to substantiate this idea had been published. To this end, work led by the Levine lab in collaboration with the Rouault lab focused on delineating specific amino acids within IRP2 that were oxidized. Using recombinant IRP2 protein from yeast, a series of in vitro oxidation reactions were carried out. Using the same protocol as previous reports, recombinant protein was either left untreated or incubated with iron and DTT. Differentially treated recombinant IRP2 was subjected to proteolysis and analyzed by HPLC-MS. These data demonstrated that oxidized IRP2 contained one peptide with 2 less mass units then the corresponding peptide from the native protein. This peptide was sequenced and found to encode a region overlapping with part of the IDD. Moreover, this region contained three cysteine residues from the IDD, cysteines 168, 174, and 178. Subsequently it was determined that the loss of 2 mass units in the peptide corresponded to cysteine 178 being oxidized to dehydrocysteine. As a result the Levine group proposed that oxidized cysteine 178 might be recognized by components of the UPS and target IRP2 for proteasomal degradation (Kang et al., 2003). This model however, varied from those previously published suggesting iron binding by cysteine residues in the IDD would promote oxidation of neighboring side chains and not the cysteine residues themselves.

With multiple reports suggesting that IRP2 becomes oxidized on its IDD domain and that this oxidation event stimulates degradation of IRP2, one important question remained—what was the E3 ubiquitin ligase that polyubiquitinates IRP2? To address this question the Iwai group undertook a yeast two-hybrid screen. In this screen the IRP2 IDD domain was used as bait and yeast were cultured under either anaerobic or aerobic conditions. Using this approach haem-oxidized IRP2 ubiquitin ligase-1 (HOIL-1) was identified as a yeast clone that interacted with the IDD domain under aerobic conditions while the interaction was blocked under anaerobic conditions. Co-transfection of IRP2 and HOIL-1 in mammalian cell demonstrated an interaction by co-immunoprecipitation assays. Furthermore, ubiquitination assays using recombinant IRP2 as substrate suggested that HOIL-1 enhanced IRP2 polyubiquitination in vitro. Owing to previous reports that IRP2 degradation is enhanced by treatment with heme and that IRP2 may bind heme, the Iwai lab tested whether heme treatment also stimulated IRP2 polyubiquitination by HOIL-1 in vitro. Heme loaded IRP2 was a better substrate for HOIL-1 than oxidized IRP2 in vitro. Moreover, recombinant IRP2 treated with heme in vitro displayed an absorbance peak at around 420 nm similar to known heme binding proteins suggesting that IRP2 binds heme (Yamanaka et al., 2003). Lastly, the Iwai group demonstrated that recombinant IDD binds heme in vitro (Ishikawa et al., 2005). Taken these data together, a model was proposed in which the IDD binds heme to promote oxidation and subsequent ubiquitination of IRP2 by HOIL-1. This model diverged from previous models that postulated IRP2 bound iron, and that iron binding induced oxidation of IRP2 causing the protein to be degraded.

Returning to Square One—Iron Dependent Regulation of IRP2

Beginning with reports that IRP2 was regulated through an oxidation dependent phenomenon to the studies that HOIL-1 controlled IRP2 stability, investigations into the mechanisms regulating IRP2 have been controversial. Shortly after the initial studies proposing the iron dependent oxidation model of the IDD, multiple groups published results questioning this paradigm of IRP2 regulation. One of the first reports to challenge this model demonstrated that deletion of the IDD domain did not abolish iron dependent regulation of IRP2 as the protein still showed preferential accumulation under iron replete conditions (Wang et al., 2004). Thus, it appeared that the IDD domain was not necessary for iron dependent regulation of IRP2. One possible explanation for the discrepancy among reported data is that IRP2 regulation can be saturated. Using mammalian cell culture systems overexpressing IRP2 Δ73 could overwhelm the endogenous IRP2 E3 ligase and lead to constitutive stabilization of the exogenous protein lacking the IDD.

As further evidence that the IDD domain did not play a role in regulating IRP2 stability in cell culture, the Rouault lab expressed IRP2 mutants where the putative iron binding cysteine residues had been changed to alanine or serine. Similar to WT IRP2, IRP2 constructs containing mutations to the putative iron binding cysteines of the IDD domain preferentially accumulated under iron deficient conditions (Bourdon et al., 2003). Thus, iron binding by the IDD cysteines to promote oxidation of cysteine 178 was not required for IRP2 regulation. Instead it appeared that previously generated data suggesting the requirement of IRP2 oxidation for proper regulation could be attributed to an in vitro artifact.

Taking into account reports that the IDD domain is not required for IRP2 regulation, data demonstrating the IDD is sufficient to confer iron dependent regulation on IRP1 becomes particularly perplexing. However, two groups have shown that when IRP1's ability to bind Fe-S clusters is compromised, the protein is regulated in an analogous manner to IRP2—i.e. the protein accumulates under iron deficient conditions and is degraded when iron is plentiful (Clarke et al., 2006; Wang et al., 2007). One of the ways in which this phenotype has been observed is by mutating the cysteine residues required for IRP1 Fe-S cluster binding. These data suggest that apo-IRP1 and IRP2 may be regulated through a common mechanism involving a degron found within both proteins. Moreover, reexamining the data with the IDD-IRP1 chimera protein it is reasonable to speculate that insertion of the IDD domain in IRP1, although not predicted to inhibit Fe-S cluster binding may do so by structurally altering the protein fold. This could cause the chimera protein to adopt a constitutive apo form and confer iron dependent regulation similar to mutating critical cysteine residues for Fe-S cluster assembly. Consistent with this explanation, no data has been published demonstrating that the IDD-IRP1 chimera retains aconitase activity.

After several lines of evidence were published that the IDD domain was not required for proper IRP2 regulation in cell culture, the Leibold lab also published a report questioning the validity of HOIL-1 being the E3 ligase for IRP2. For example, overexpression of HOIL-1 did not alter IRP2 half-life. Additionally, abrogation of HOIL-1 via RNAi had no affect on iron dependent regulation of endogenous IRP2. The Leibold lab did report an interaction between IRP2 and HOIL-1, although it did not occur in an iron dependent fashion (Zumbrennen et al., 2008). These data raised the question of how

HOIL-1 could ubiquitinate IRP2 in vitro. One well-known caveat of in vitro ubiquitination assays is that excessive concentrations of E2s or E3s can cause stochastic substrate polyubiquitination. When the in vitro ubiquitination assays performed by the Iwai lab are reviewed it becomes apparent that the reactions were conducted with very high concentrations of E2 and HOIL-1. Furthermore, the background ubiquitination of IRP2 in the absence of E2 or HOIL-1 is very strong suggesting that inclusion of E2 or HOIL-1 leads to non-specific ubiquitination of IRP2. Lastly, a role for HOIL-1 in regulating IRP2 stability in vivo has never been demonstrated. A HOIL-1 knockout mouse has been characterized without mention of misregulation of IRP2 or iron homeostasis. Instead, the report focused on aberrant NF-κB signaling in HOIL-$1^{-/-}$ mice (Tokunaga et al., 2009).

With respect to heme regulating IRP2 levels, the purported heme binding region of IRP2 is contained within the IDD domain. As previously mentioned, the IDD is dispensable for proper regulation of IRP2. This data alone suggests that heme binding does not regulate IRP2. Rather, the heme binding reported is ostensibly due to an in vitro artifact as heme notoriously binds to proteins non-specifically (Dycke et al., 2007). It has also been reported that adding exogenous heme to mammalian cells promotes IRP2 degradation similar to iron (Wang et al., 2004). These data can easily be reconciled as heme can function as an iron donor. Cells uptake heme and catabolize the cofactor releasing iron from the porphyrin ring. Thus, addition of exogenous heme or iron to mammalian cells may regulate IRP2 through a common mechanism.

SPECIFIC AIMS OF DISSERTATION RESEARCH

With published reports discrediting the prevailing model of IRP2 regulation, it seemed that the cellular iron homeostasis field needed to return to square one. Taking this into consideration I began my dissertation research with two fundamental questions:

1. What is the E3 ubiquitin ligase that targets IRP2 for proteasomal degradation?

2. What are the molecular mechanisms cell utilize to sense bioavailable iron levels with concomitant regulation of IRP2 stability?

Understanding the molecular mechanisms cells use to sense bioavailable iron levels and regulate IRP2 expression accordingly will lead to a better understanding of how cellular iron homeostasis is maintained. Due to crosstalk between cellular and systemic iron homeostasis systems, delineation of IRP2 regulatory pathway may also result in an increased understanding of how systemic iron homeostasis is maintained. Lastly, further insights into the underlying mechanisms controlling human iron homeostasis has the potential to impact human health through the development of novel therapies for the treatment of iron related pathologies including anemia and hemochromatosis.

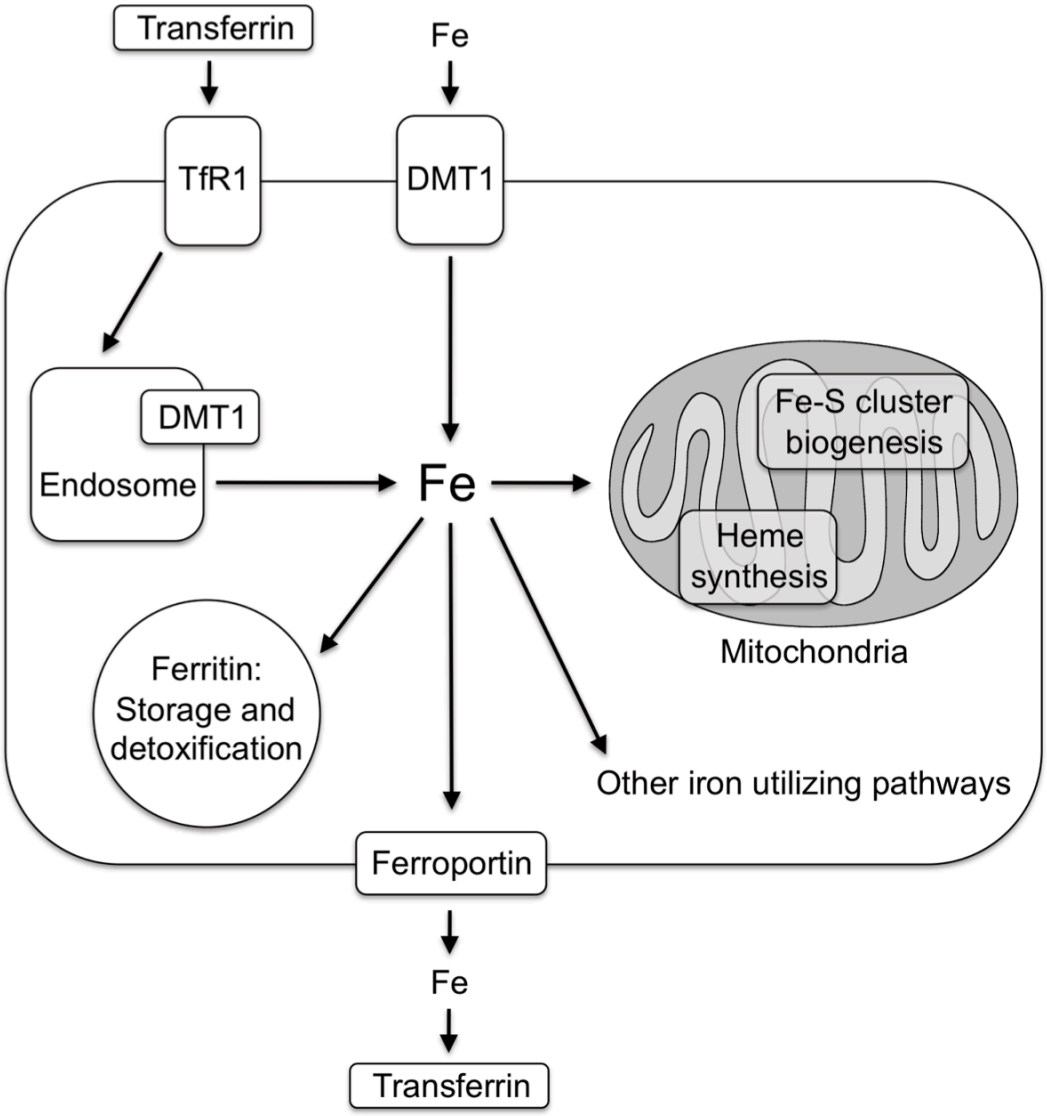

Figure 1-1. Human Iron Metabolism
A generic cell is depicted with the salient features of iron usage, import, storage, and export. Dietary iron is transported into the enterocyte cytosol via DMT1 and exported into the plasma by ferroportin. In the blood iron is bound by the transport protein transferrin. TfR1 binds holo-transferrin and the complex undergoes endocytosis. Following endocytosis and delivery to the endosome, iron is released from the complex and pumped into the cytosol by DMT1. Intracellular iron is utilized for a variety of purposes including iron-sulfur cluster and heme synthesis in the mitochondria. Excess cellular iron is stored in its inert form bound to ferritin. Macrophages and hepatocytes function as iron depots and efflux iron into the blood via ferroportin when systemic demand increases. (Figure adapted from Hentze et al., 2004)

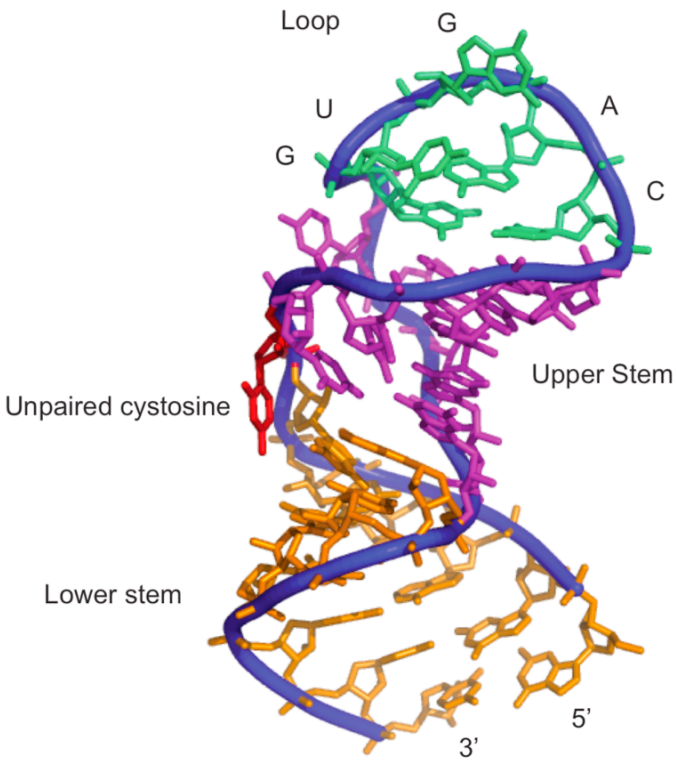

Figure 1-2. Iron Responsive Element
NMR structure of the H ferritin IRE (pdb code 1AQO). (Figure adapted from Rouault, 2006)

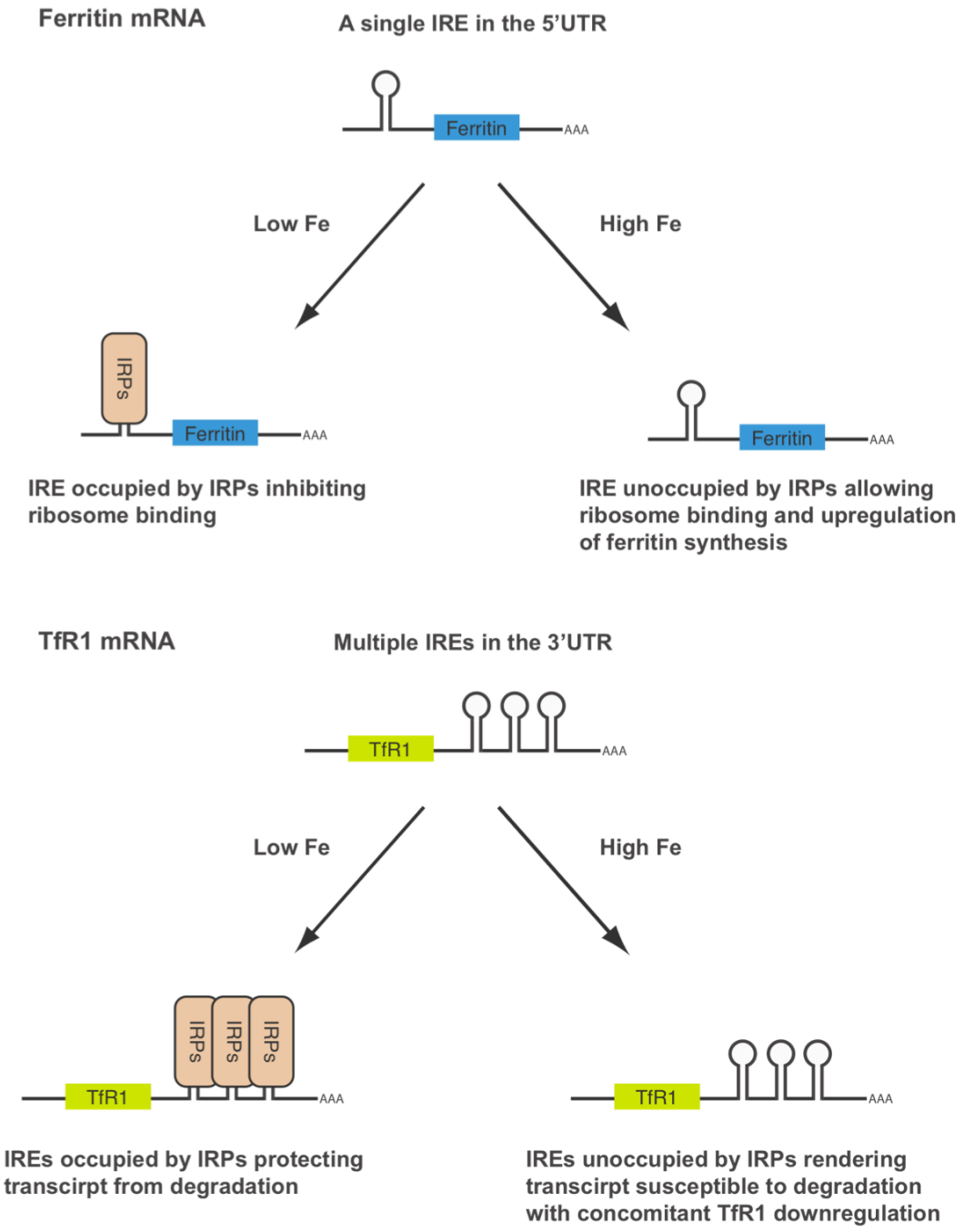

Figure 1-3. IRE Containing Genes Are Regulated By IRPs
Under iron replete conditions, IRPs binding to the ferritin IRE inhibits translation (top). IRPs binding to multiple IREs in the 3'UTR of TfR1 protects the mRNA from degradation (bottom). (Figure adapted from Rouault, 2006)

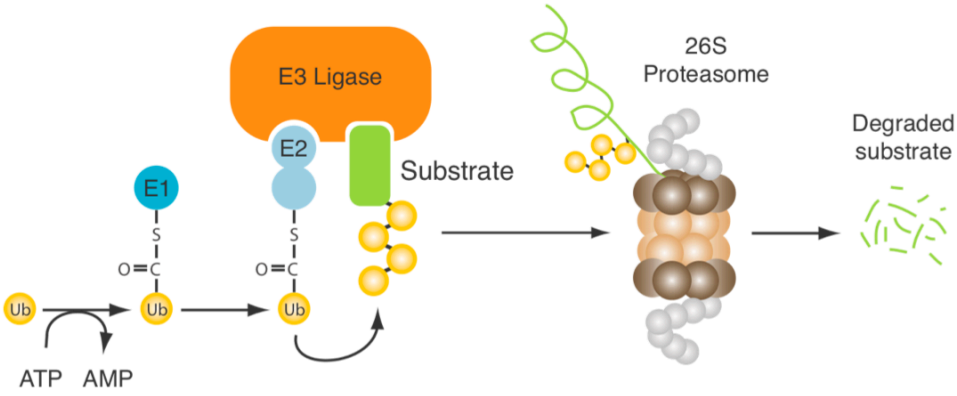

Figure 1-4. The Ubiquitin Proteasome System
Protein ubiquitination is dependent on a series of enzymes termed E1, E2, and E3. The E1 enzyme catalyzes the activation of ubiquitin in an ATP dependent fashion. Activated ubiquitin is transferred to an active site cysteine on the E1 enzyme. The E2 enzyme catalyzes the transfer of ubiquitin from the E1 enzyme to its own catalytic cysteine residue. In last step of the cascade, the E3 facilitates transfer of ubiquitin to lysines on its target protein, tagging it for degradation in the proteasome. (Figure adapted from Nakayama and Nakayama, 2006)

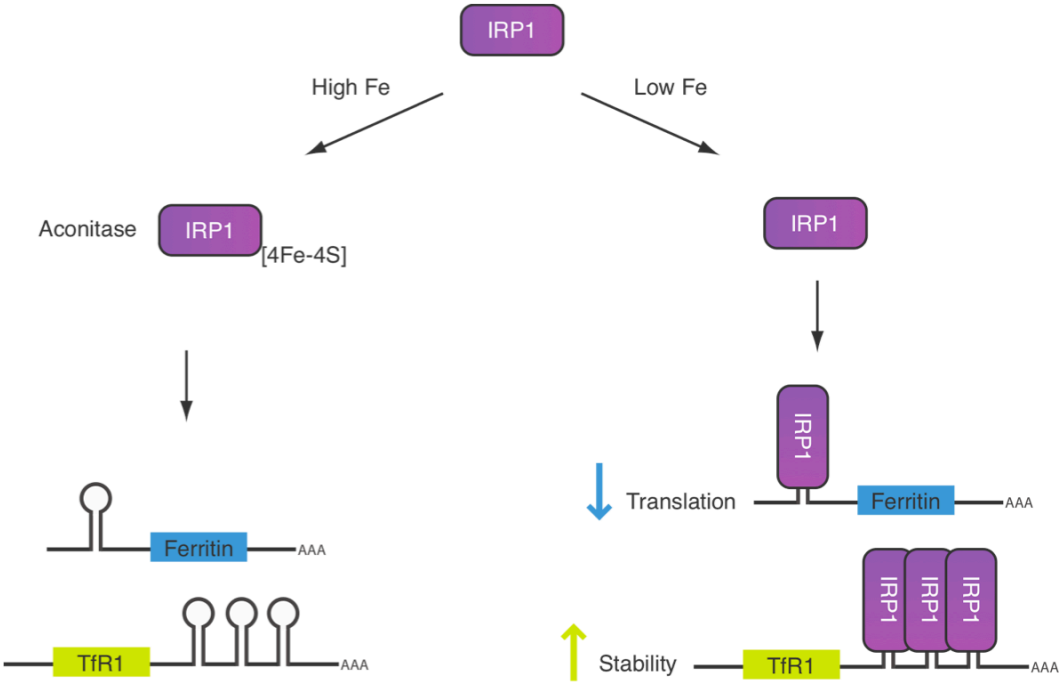

Figure 1-5. Iron Dependent Regulation of IRP1
Under iron replete conditions IRP1 ligates an iron-sulfur cluster and functions as a cytosolic aconitase. In contrast, under iron deficient conditions, the protein binds to IREs found in the UTRs of genes such as ferritin and TfR1, regulating their translation and mRNA stability, respectively.

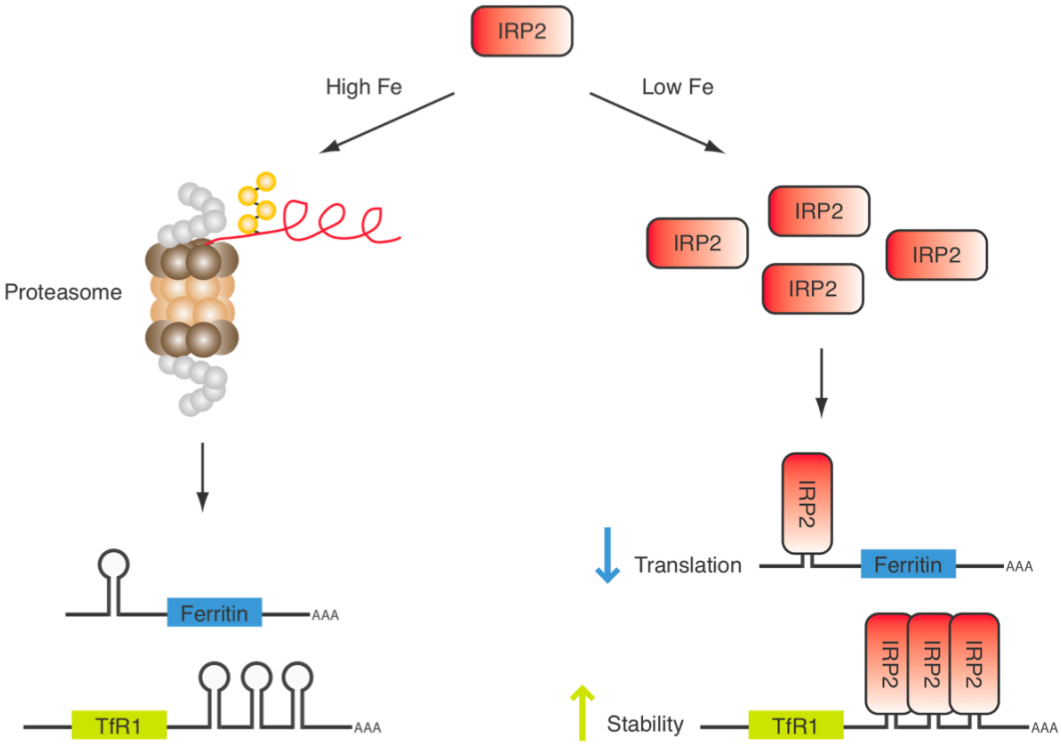

Figure 1-6. Iron Dependent Regulation of IRP2
Under conditions where iron is plentiful, IRP2 is polyubiquitinated and degraded by the proteasome. However, when iron is scarce, IRP2 becomes stabilized and regulates IRE containing genes in an analogous manner to IRP1.

CHAPTER TWO

FBXL5 IS AN IRON RESPONSIVE E3 LIGASE TARGETING IRP2 FOR PROTEOLYTIC DEGRADATION

Introduction

Humans require adequate amounts of iron to carry out an assortment of biological processes. However, high concentrations of free iron can lead to cellular damage due to the generation of toxic radical species. For this reason it is crucial that iron homeostasis be properly maintained. Mammals have evolved to use the IRP/IRE regulatory systems to control iron homeostasis. Many genes important for cellular iron homeostasis, like TfR1 and ferritin, contain cis-acting regulatory elements in their 5' or 3' UTRs. These IRE containing genes are regulated in a coordinated fashion via the actions of IRPs. IRP2 is regulated as a function of iron availability and preferentially binds IREs under iron deficient conditions. This is due to its selective degradation by the proteasome under iron replete conditions (Andrews and Schmidt, 2007; Hentze et al., 2010; Muckenthaler et al., 2008; Rouault, 2006). Several different groups in the mid 1990's to mid 2000's attempted to delineate the mechanisms controlling iron dependent degradation of IRP2 in the proteasome. Much of this work focused on identifying modifications and interacting partners of the IRP2 IDD (Ishikawa et al., 2005; Iwai et al., 1998; Iwai et al., 1995; Kang et al., 2003; Yamanaka et al., 2003). However, despite reports describing potential mechanisms of IDD oxidation and the identification of a putative IRP2 E3 ligase, these data were met with skepticism and controversy (Hentze et al., 2004; Wang et al., 2004; Zumbrennen et al., 2008). Thus, it appeared that the E3

ligase regulating IRP2 stability awaited identification. Moreover, the mechanisms by which cell sense iron levels and correlate changes of this metabolite to differences in IRP2 stability also remained enigmatic. To address these outstanding questions in the cellular iron homeostasis field, a high throughput siRNA screen to identify candidate IRP2 E3 ligases was performed.

IRP2 AlphaScreen

First, to identify the E3 ubiquitin ligase regulating IRP2 stability, a clonal HEK 293 cell line stably expressing an IRP2 construct containing HA and 3X FLAG epitopes at its N and C-termini, respectively, was generated. Using an amplified luminescent proximity homogenous assay (AlphaScreen), relative levels of the IRP2 reporter can be determined. This assay is carried out in a 96-well format making it amenable to high throughput screening. In AlphaScreen, cells are first plated and allowed to incubate for the necessary time. Following incubation and cell lysis, donor and acceptor beads conjugated to α-FLAG and α-HA antibodies, respectively, are added to the lysates. Lastly, a plate reader measures relative IRP2 levels.

AlphaScreen works due to the different chemistries preformed by the donor and acceptor beads. The plate reader emits light with a wavelength of 680 nm. The acceptor bead contains phthalocyanine that uses energy from the excitation light to convert ambient oxygen into a singlet excited oxygen species. This singlet oxygen has a short half-life (~4 μsec) and can only diffuse ~200 nm in solution before it decays back to its ground state. If the acceptor bead is within proximity, energy is transferred from the singlet oxygen species to a thioxene derivate within the bead, which produces light with a wavelength of ~520-620 nm. Thus, the plate reader emits light at one wavelength and

simultaneously measures the generation of light at a lower wavelength to give a relative signal (Ullman et al., 1994).

In the IRP2 AlphaScreen presented here, when HEK 293 reporter cells are incubated with the highly selective iron chelator deferoxamine mesylate (DFO), conditions of low iron availability are induced leading to high levels of IRP2 accumulation. Consequently, the donor and acceptor beads are brought within close proximity by interacting with the epitope tags on IRP2. This results in a high signal by AlphaScreen (Fig. 2-1). However, when reporter cells are treated with excess iron in the form of ferric ammonium citrate (FAC), IRP2 is degraded and accumulates at very low levels. Under these conditions the donor and acceptor beads are rarely adjacent to each other, resulting in a lower signal by AlphaScreen (Fig. 2-1).

A sample of the IRP2 AlphaScreen data is shown in Figure 2-2. Similar to endogenous IRP2 in the parental HEK 293 cell line, the HA-IRP2-FLAG reporter accumulates when cells are treated with DFO and is degraded following FAC treatment. Untreated cells display intermediate accumulation levels. Most importantly, relative IRP2 levels as measured by AlphaScreen strongly correlate with data from immunoblot analyses (Fig. 2-2). Thus, the IRP2 AlphaScreen provides a simple, high throughput assay to measure relative IRP2 levels as an alternative to immunoblotting.

siRNA Screen

With the development of the IRP2 AlphaScreen, this assay could now be used in combination with RNA interference (RNAi) to screen to for candidate E3 ubiquitin ligase regulating IRP2 stability. Knowing beforehand the enzymatic activity of the protein we wanted to identify, a specific short interfering RNA (siRNA) library was generated. This

library contained 800 genes that were either known or predicted to encode proteins involved in the ubiquitin-proteasome system (UPS), such as E3 ligases. Specifically, Qiagen siRNAs were employed under a format where four siRNAs targeting a single gene were arrayed in a one-gene one-well format. HEK 293 cells expressing the HA-IRP2-FLAG reporter were plated on 96-well plates, reverse transfected with siRNAs in triplicate, and incubated for 48 hours. Prior to lysis, cells were treated with FAC overnight to induce low expression levels of IRP2. Lastly, the AlphaScreen assay was implemented to measure relative IRP2 levels (Fig. 2-3). Inappropriate accumulation of IRP2 following knockdown of a particular gene, may suggest the gene is involved in regulating IRP2 stability. Among the 800 different genes assayed, 71 had the ability to induce the IRP2 reporter ~7.5 fold over background (Chapter 5 and Table 1, Appendix).

To confirm the results from the primary screen, a secondary screen was carried out with Dharmacon siRNAs. The secondary screen format varied slightly from the primary screen in order to minimize potential artifacts. One of the most common artifacts in using RNAi is the introduction of off-target effects (Jackson and Linsley, 2004). Another artifact that was inherent to the IRP2 screen was the possibility of finding genes whose expression regulates iron uptake and/or availability. Inhibiting cellular iron uptake and reducing bioavailable iron levels could stabilize IRP2 in a similar fashion to knocking down the IRP2 E3 ligase. In order to address the first caveat and minimize the introduction of off target effects, the secondary screen was carried out using four siRNAs targeting a single gene with each siRNA plated in a single well. Using this approach if a gene has multiple siRNAs that induce IRP2 accumulation under iron replete conditions, then this would suggest the phenotype is unlikely to be caused by an off-target effect. To

address the second potential artifact, the secondary screen was carried out in sextuplicate with three plates being treated with 1 μM FAC and three with 25 μM FAC. Treating cells with high concentrations of exogenous iron can lead to iron entering the cell via non-TfR1 dependent pathways such as sodium channels (de Silva et al., 1996; Tsushima et al., 1999). Thus, by treating cells with 25 μM FAC, iron should enter cells regardless of whether the TfR1-endosomal iron uptake pathway is compromised. Accordingly, if knockdown of a particular genes gives a high AlphaScreen signal in cells treated with 1 μM FAC but the signal is reduced in cells treated with 25 μM FAC, this may suggest the gene does not affect polyubiquitination of IRP2. Alternatively, knockdown of the gene may inhibit iron uptake or availability. Using this approach for the secondary screen, 292 siRNAs corresponding to 73 genes were screened. In addition to the ~71 top hits from the primary screen, RBX1 and SKP1 were also screened (see below). Among the 73 genes screened, F-box and leucine-rich repeat protein 5 (FBXL5) knockdown led to the greatest induction of the IRP2 reporter. Among the top five hits in cells treated with 25 μM FAC, FBXL5 had three siRNAs including the top hit (Table 2, Appendix). Moreover, stabilization of the IRP2 reporter following FBXL5 knockdown did not change with 1 μM or 25 μM FAC treatment (data not shown).

RNAi Mediated Suppression of SCF^{FBXL5} Stabilizes IRP2

FBXL5 is a member of the F-box protein family defined by their conserved ~40-50 amino acid F-box domain (Jin et al., 2004). F-box proteins associate with E3 ubiquitin ligases termed SCF complexes. SCF E3 ligases are composed of a scaffolding protein CUL1 that interacts with RBX1 on its C terminus and SKP1 on its N terminus. RBX1 is a ring-box protein that binds to an activated E2 conjugating enzyme. SKP1 is an adaptor

protein that links a F-box protein to the SCF complex by interacting with its F-box domain. Typically the F-box domain is on the N-terminal half of F-box proteins while other protein domains are found on the C terminus. F-box proteins contain domains that mediate protein-protein interactions such as WD40, armadillo repeats, kelch repeats, and leucine-rich repeats (Cardozo and Pagano, 2004; Ho et al., 2008; Jin et al., 2004; Nakayama and Nakayama, 2006). The function of the F-box protein is critical as it binds target proteins bringing them into the optimal conformation to be polyubiquitinated by the multimeric SCF complex (Fig. 2-5).

Since abrogation of FBXL5 expression with multiple siRNAs stabilized the IRP2 reporter under high iron conditions, this data suggested that an SCF complex containing FBXL5 (SCF^{FBXL5}) may regulate IRP2 ubiquitination. Previous work done in the lab by Julio Ruiz also indicated an SCF complex might play a role in IRP2 regulation. Using a proteomics approach, CUL1 was identified as a possible interacting partner of IRP2 (Julio Ruiz, unpublished data). Moreover, knockdown of CUL1 led to stabilization of the IRP2 reporter as measured by AlphaScreen (Julio Ruiz, unpublished data). Consistent with these data, CUL1 was the 15^{th} best hit in the primary screen and stabilized the IRP2 reporter ~11 fold over background (Table 1, Appendix). Taking these data into consideration, RBX1 and SKP1 siRNAs were added to the secondary screen. In the secondary screen SKP1 had three siRNAs in the top 15 hits, CUL1 had two siRNAs in the top 15, and RBX1 had one siRNA in the top 20 hits (Table 2, Appendix).

As previously mentioned, knockdown of FBXL5 expression led to the greatest stabilization of the IRP2 reporter. Compared to a non-targeting (NT) control siRNA, reduction of FBXL5 expression by two different siRNAs led to complete stabilization of

HA-IRP2-FLAG as measured by AlphaScreen under iron replete conditions. Knockdown of the core subunits of the SCF complex led to intermediate stabilization of the IRP2 reporter. Similar results were observed for endogenous IRP2 in HEK 293 cells, following knockdown of each member of the SCF^{FBXL5} complex with two unique siRNAs (Fig. 2-5). Taken together these data suggest that SCF^{FBXL5} may regulate IRP2 stability.

While FBXL5 was the top hit from the RNAi screen and appeared to be the most promising IRP2 E3 ligase candidate, we did not want to overlook any additional genes controlling IRP2 protein accumulation. To this end, the top 30 hits from the secondary siRNA screen (excluding the SCF^{FBXL5} complex subunits) were assayed to determine whether their knockdown caused inappropriate accumulation of endogenous IRP2 under high iron conditions. In these assays FBXL5 was used as a positive control. A subunit of the endosomal ATPase, D1, was used as a negative control. Abrogation of D1 expression via RNAi is predicted to diminish acidification of the endosome and as a result inhibits TfR1 mediated iron uptake (data not shown). However, when cells are treated with high amounts of exogenous iron, iron can enter the cell via endosome independent pathways as previously described. Therefore, knockdown of D1 does not cause accumulation of IRP2 if cells are treated with high concentrations of iron. As shown in Figure 2-6, none of the top 30 hits when depleted by RNAi, showed an effect equal to or greater than knockdown of FBXL5. Thus, following two rounds of RNAi screening, and assaying for genes whose knockdown stabilize endogenous IRP2, the SCF^{FBXL5} complex emerged as the leading IRP2 E3 ligase candidate.

FBXL5 is Required for Proper Regulation of IRP2 and IRE Containing Genes

Previous work demonstrated that knockdown of FBXL5 stabilized a reporter IRP2 construct and endogenous IRP2 (Fig. 2-5). However, both of these experiments were carried out in HEK 293 cells. Therefore the question remained whether abrogation of FBXL5 expression leading to inappropriate accumulation of IRP2 was unique to HEK cells or if this was a widespread phenotype. To this end, HeLa cells were transfected with two different FBXL5 siRNAs. Similar to HEK cells, RNAi mediated suppression of FBXL5 stabilized IRP2 in HeLa cells incubated with exogenous iron (Fig. 2-7A). Moreover, knockdown of FBXL5 by three different siRNAs in non-tumorigenic human bronchial epithelial cells (HBEC) also results in stabilization of IRP2 (Fig. 2-7B). Thus, FBXL5 regulates IRP2 stability in a variety of human cell types including non-transformed cells.

As discussed in Chapter One, oxidation of the IDD domain was proposed to signal for IRP2 ubiquitination by the E3 ligase HOIL-1 (Yamanaka et al., 2003). However, IRP2 truncation constructs lacking the IDD are still regulated in an iron dependent manner (Hanson et al., 2003; Wang et al., 2004). Furthermore, knockdown of HOIL-1 expression does not stabilize IRP2 in the presence of excess iron (Zumbrennen et al., 2008). Consistent with these results, our lab independently demonstrated that a HEK 293 cell line stably expressing FLAG-tagged IRP2 Δ73 preferentially accumulated in cells treated with iron but displayed lower accumulation levels under iron limiting conditions. Moreover, knockdown of FBXL5 led to inappropriate accumulation of FLAG-IRP2 Δ73 under iron replete conditions (Fig. 2-8).

Although IRP1's IRE binding activity is regulated via its ability to assemble a Fe-S cluster, it has been shown that apo-IRP1 can be targeted for proteasomal degradation under iron deficient conditions similar to IRP2. One of the ways in which this phenotype has been observed is by mutating three cysteine residues required for IRP1's Fe-S cluster binding (Clarke et al., 2006). Using HEK 293 stable cell lines expressing either myc-tagged wild-type (WT) IRP1 or a variant unable to bind Fe-S clusters ($IRP1^{3C<3S}$), we tested whether knockdown of FBXL5 had any affect on IRP1. Although no change was seen in WT IRP1, knockdown of FBXL5 by three unique siRNAs led to stabilization of $IRP1^{3C<3S}$ in a similar fashion to endogenous IRP2 (Fig. 2-9). Together these data indicate that FBXL5 regulates both IRP2 and apo-IRP1. Moreover, these data suggest that FBXL5 may interact with IRP2 and IRP1 via a common degron.

Normally under iron rich conditions IRP2's IRE binding activity is downregulated due to decreased protein levels. However, loss of FBXL5 expression leads to inappropriate accumulation of IRP2. To determine whether following FBXL5 knockdown inappropriately stabilized IRP2 is functional, an electrophoretic mobility shift assay (EMSA) was performed. Using the HEK 293 IRP2 reporter cell line, cells were transfected with either a NT or FBXL5 siRNA, treated with DFO or FAC, and lysed. Lysates were then incubated with a ^{32}P-labeled ferritin IRE and resolved on a non-denaturing gel. As expected, cells transfected with a NT siRNA and treated with DFO showed greater IRP/IRE binding activity than cells treated with FAC. However, under iron replete conditions, cells transfected with a FBXL5 siRNA showed increased IRP/IRE binding compared to cells transfected with a NT siRNA. In order to separate

IRP1/IRE and IRP2/IRE complexes, antibodies were added to supershift the respective complexes. Addition of an α-IRP1 antibody demonstrated that IRP1's IRE binding activity was not affected substantially by FBXL5 knockdown under iron replete conditions. Consistent with previous results, this data suggests that diminishing FBXL5 expression via RNAi does not simply inhibit iron uptake or availability. However, addition of an α-FLAG antibody to cell lysates depleted of FBXL5 expression under high iron treatment demonstrated that IRP2's IRE binding activity increases to levels similar to low iron treatment (Fig. 2-10).

Next, we wanted to determine whether increased IRP2 IRE binding activity in FBXL5 depleted cells also causes misregulation of IRE containing genes. To this end, a tetracycline-inducible FBXL5 short hairpin RNA (shRNA) cell line was employed. Following incubation of cells with DFO or FAC and in the absence or presence of tetracycline, relative levels of TfR1 mRNA were measured by qRT-PCR. Under iron deficient conditions TfR1 expression increases in part due to the protective effect of IRPs binding to multiple IREs in the transcript's 3' UTR. Under iron replete conditions however, IRP binding is reduced and the transcript becomes more readily degraded causing a decrease in TfR1 expression. In tetracycline inducible FBXL5 shRNA cells, TfR1 mRNA levels increase by ~2.5 fold following inhibition of FBXL5 expression under iron rich conditions (Fig. 2-11). Thus, loss of FBXL5 expression under iron replete conditions results in inappropriate IRP2 accumulation and increased IRE binding activity with concomitant misregulation of IRE containing genes.

FBXL5 Interacts with and Ubiquitinates IRP2

While RNAi is a powerful tool and provided compelling evidence that FBXL5 regulates IRP2, it is unable to answer whether or not this regulation is direct. To address this question co-immunoprecipitation experiments were performed. V5-tagged FBXL5 or vector were transiently transfected into HEK 293 cells stably expressing FLAG-tagged IRP2. Following immunoprecipitation with FLAG resin, the precipitates were resolved by SDS-PAGE and blotted with α-FLAG and α-V5 antibodies. These data demonstrate that FBXL5-V5 interacts with IRP2-FLAG. As a negative control, FBXL5-V5 was transiently transfected into HEK 293 cells and immunoprecipitations were carried out using FLAG resin. However, no FBXL5-V5 was observed in the immunoprecipitates suggesting that FBXL5-V5 does not interact non-specifically with FLAG beads (Fig. 2-12A). In a reciprocal experiment, HEK 293 cells stably expressing FBXL5-FLAG were used. Immuoprecipitation of FBXL5-FLAG resulted in co-immunoprecipitation of endogenous IRP2. In contrast, IRP2 failed to co-immunoprecipitate from HEK 293 cell lysate incubated with FLAG resin (Fig. 2-12B).

Next we wanted to investigate whether FBXL5 could polyubiquitinate IRP2 in vitro. Ameen Salahudeen expressed SCF^{FBXL5} recombinantly in insect cells and purified the complex by multiple chromatographic steps. Then using the purified complex as a source of E3 ligase activity he performed a series of in vitro ubiquitination assays. Recombinant SCF^{FBXL5} can only polyubiquitinate IRP2 in the presence of ATP, ubiquitin, and recombinant E1/E2. Furthermore, addition of exogenous iron to the reactions did not enhance ubiquitination of IRP2 (Fig. 2-13A). To confirm that the laddering pattern of IRP2 observed in the in vitro assay was due to specific polyubiquitination of IRP2, a

parallel assay was carried out using GST-tagged ubiquitin lacking lysine residues (K_0-GST-Ub) in place of wild-type ubiquitin. This assay resulted in discrete higher molecular weight bands of IRP2 consistent with multiple monoubiquitination events on IRP2 (Fig. 2-13B). Moreover, the two aforementioned assays were performed with tubulin as the substrate instead of IRP2. In these assays SCF^{FBXL5} failed to ubiquitinate tubulin indicating the complex does not display non-specific activity in vitro (Fig. 2-13C and 2-13D). Collectively, the above results indicate that IRP2 is a direct substrate of SCF^{FBXL5}.

FBXL5 Accumulation is Regulated as a Function of Iron and Oxygen Availability

With the identification of the E3 ligase, SCF^{FBXL5}, that could regulate IRP2 protein accumulation, the first experimental aim of my dissertation research was completed. Moving on to my second aim, there was still no clear understanding of how cells gauge bioavailable iron levels in order to regulate IRP2 stability. With the discovery of the SCF^{FBXL5} complex however, there was now an upstream regulator of IRP2 that could be studied. Because there are many predicted SCF complexes with a plethora of cellular targets, we focused our work on the characterization of the substrate recognition subunit, FBXL5, instead of the core SCF components.

First, we wanted to determine whether FBXL5 is regulated by iron availability. To this end, HEK 293 cells were transiently transfected with an FBXL5-V5 expressing plasmid or empty vector and incubated with DFO or FAC to induce conditions of low or high iron, respectively. Intriguingly, FBXL5-V5 was poorly expressed under iron deplete conditions but showed a dramatic increase in accumulation under conditions of excess iron (Fig. 2-14). Moreover, Ameen Salahudeen demonstrated that endogenous FBXL5 substantially accumulates under iron replete conditions but displays very low expression

levels when iron is limiting (Fig. 2-15). Thus, FBXL5 is regulated in an iron dependent manner reciprocal to IRP2.

We next examined whether FBXL5's responsiveness to iron availability occurred on a time scale that was consistent with regulation of IRP2 stability. HEK 293 cells were treated with FAC overnight, switched to DFO treated media, and then harvested 0, 1, 2, 4, or 6 hours later. In agreement with previously published data (Guo et al., 1995), IRP2 was fully stabilized within six hours following DFO treatment. Conversely, in HEK 293 cells incubated with DFO overnight and switched to FAC treated media, IRP2 was degraded and reached basal levels of expression within six hours. Performing parallel experiments using a HEK 293 cell line stably expressing FBXL5-FLAG revealed that FBXL5 is fully degraded within six hours after iron depletion but fully stabilized in six hours post addition of excess iron (Fig. 2-16). Thus, not only is FBXL5 regulated in an inverse fashion to IRP2, this regulation occurs in a temporal manner consistent with FBXL5 regulating IRP2 stability.

In addition to being regulated by bioavailable iron levels, IRP2 is regulated in an O_2 dependent manner. Under normoxic conditions (21% O_2) IRP2 has a half-life of ~6 hours which increases to greater than 12 hours in hypoxic (1% O_2) treated cells (Hanson et al., 2003). We wanted to test whether O_2 plays a role in mediating FBXL5 protein accumulation. HEK 293 cells stably expressing FBXL-FLAG were treated with high or low iron concentrations under normoxic or hypoxic conditions. While FBXL5-FLAG accumulated in cells treated with iron under normoxic conditions, protein accumulation was greatly diminished with hypoxic treatment (Fig. 2-17). Thus, FBXL5 is regulated by O_2 in a reciprocal manner to IRP2.

Conclusion

While it has been known for over a decade that IRP2 is posttranslationally regulated via proteasomal degradation, the E3 ligase controlling this process has remained controversial. To identify the E3 ligase tagging FBXL5 for degradation, a high throughput siRNA screen was performed. In contrast to previous work that was based on the IDD dependent model of IRP2 regulation, we undertook an unbiased approached to identify an IRP2 E3 ligase. Our approach centered on assaying protein accumulation of an IRP2 reporter following knockdown of an E3 ligase RNAi library. Using this approached we screened for genes whose knockdown resulted in inappropriate IRP2 accumulation in iron replete cells. The results of this screen suggested that the E3 ligase complex SCF^{FBXL5} might be regulating IRP2 protein stability.

Further experiments demonstrated that knockdown of FBXL5 stabilized IRP2 in various human cell lines. Moreover, abrogation of FBXL5 via RNAi led to increased IRP2 IRE binding activity and aberrant IRE gene regulation. Consistent with direct regulation of IRP2 by FBXL5, endogenous IRP2 co-immunoprecipitated with FBXL5-FLAG. Furthermore, using in vitro reconstitution assays, SCF^{FBXL5} was able to catalyze the polyubiquitination of IRP2. Taken together, these data indicate that IRP2 is a direct proteolytic target of the E3 ligase complex SCF^{FBXL5}.

Remarkably, FBXL5 is regulated in an inverse manner to IRP2. While IRP2 is stabilized under iron deficient conditions and destabilized under iron replete conditions, FBXL5 is expressed at very low levels under low iron treatment and expressed at much higher levels with excess iron treatment. Moreover, while hypoxia increases IRP2 half-life, FBXL5-FLAG expression is greatly reduced in cells cultured at 1% O_2. In all, these

data suggest that changes in IRP2 protein stability as a function of iron and O_2 availability may be mediated through the regulation of FBXL5 (Fig. 2-18).

The mechanisms by which cells sense intracellular iron levels in order to regulate IRP2 stability are poorly understood. However, identification of the iron regulated IRP2 E3 ligase, FBXL5, provides a starting point to begin to delineate these mechanisms. Therefore, we hypothesized that elucidation of FBXL5's iron dependent regulation had the potential to provide a mechanistic understanding of how cells gauge bioavailable iron concentrations in order to control IRP2 stability.

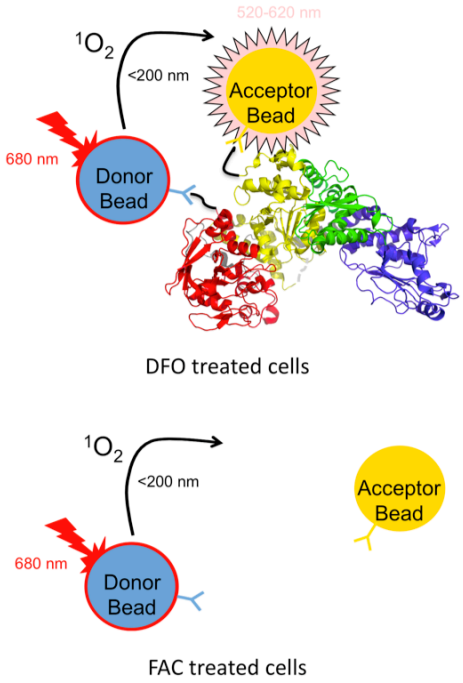

Figure 2-1. Cartoon of IRP2 AlphaScreen
In HA-IRP2-FLAG expressing HEK cells treated with DFO, IRP2 is stabilized resulting in the donor and acceptor beads being brought within close proximity. Thus, the relative signal is high by AlphaScreen (top). In contrast, cells treated with FAC have low levels of HA-IRP2-FLAG expression. As a result, the donor and acceptor beads are not within close proximity and the AlphaScreen signal is low (bottom).

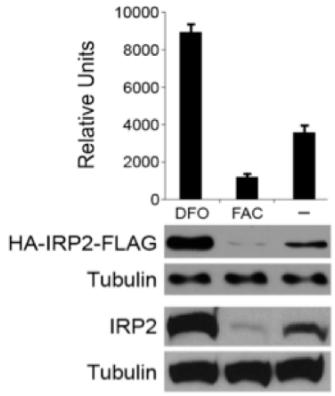

Figure 2-2. AlphaScreen and Immunoblot Data of IRP2 Accumulation
Relative levels of HA-IRP2-FLAG as measured by AlphaScreen (top), or by immunoblot analysis (middle). Assessment of endogenous IRP2 levels by immunoblot analysis in parental HEK 293 cells. AlphaScreen assays were performed in triplicate with mean data reported +/- SE. (Salahudeen et al., 2009)

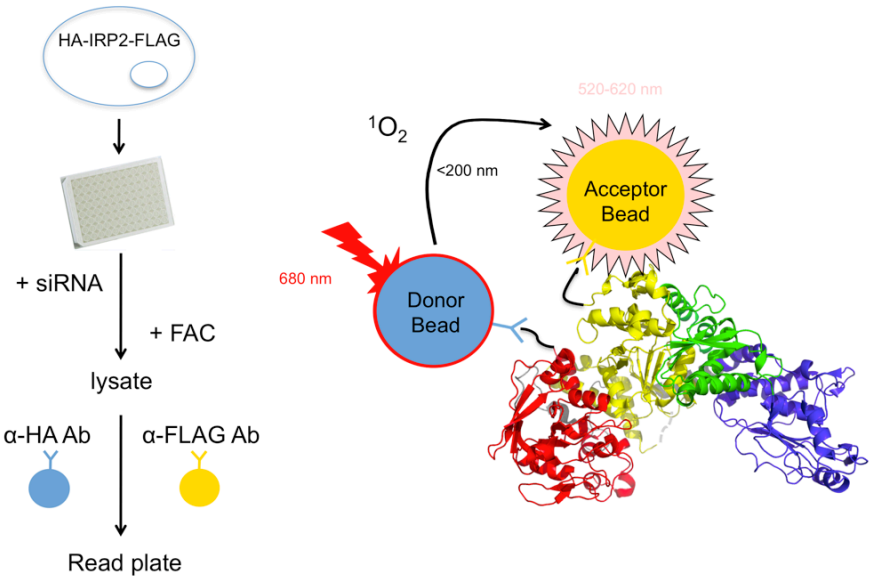

Figure 2-3. Schematic of RNAi Screen to Identify Candidate IRP2 E3 Ligases
HA-IRP2-FLAG expressing cells were reverse transfected with siRNAs. Cells were treated with FAC to induce low levels of IRP2 expression. Using the AlphaScreen readout, siRNAs that had the ability to induce inappropriate accumulation of IRP2 under iron replete conditions were considered hits.

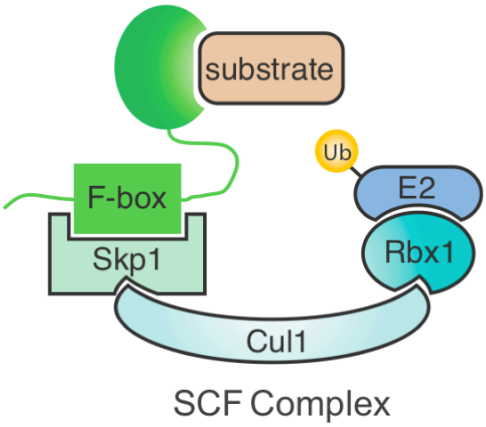

Figure 2-4. Cartoon of SCF Complex
SCF complexes are composed of Cul1, a scaffolding protein that interacts with Rbx1 on its C terminus and Skp1 on its N terminus. Rbx1 interacts with an E2 enzyme and Skp1 binds to the F-box domain of a F-box protein. The F-box protein functions to link the substrate to the complex and facilitate polyubiquitination. Together these proteins form a multimeric E3 ligase.

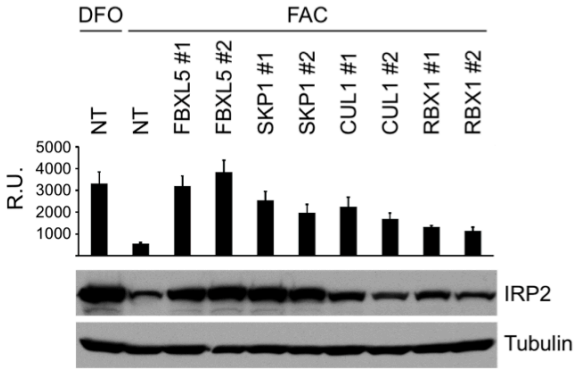

Figure 2-5. Knockdown of SCF^{FBXL5} Stabilizes IRP2

RNAi mediated suppression of SCF^{FBXL5} induces the IRP2 reporter as measured by AlphaScreen (top) and causes inappropriate accumulation of endogenous IRP2 as measured by immunoblot analysis (bottom). (Salahudeen et al., 2009)

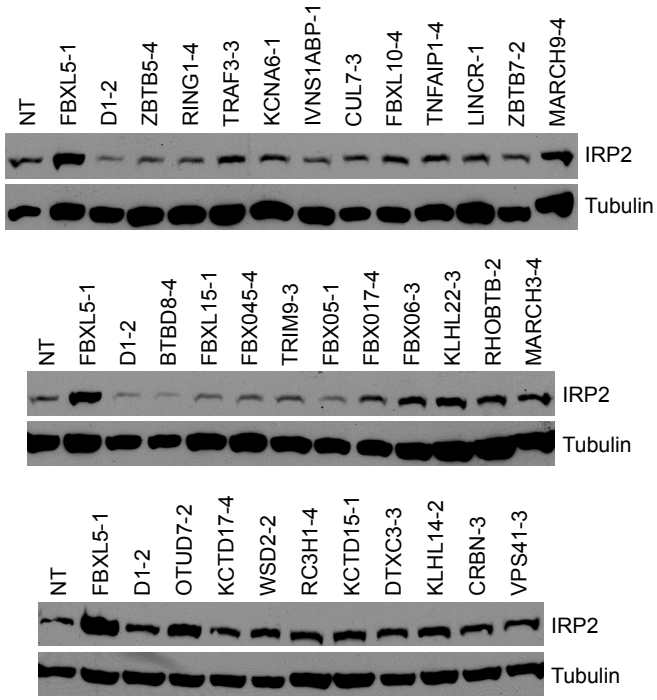

Figure 2-6. FBXL5 Knockdown Results in the Greatest Accumulation of Endogenous IRP2 Among the Top Hits from the Secondary RNAi Screen.
HEK 293 cells were transfected with the top 30 hits from the IRP2 siRNA screen (excluding the putative SCF^{FBXL5} components) to determine their efficacy in stabilizing endogenous IRP2 under iron replete conditions.

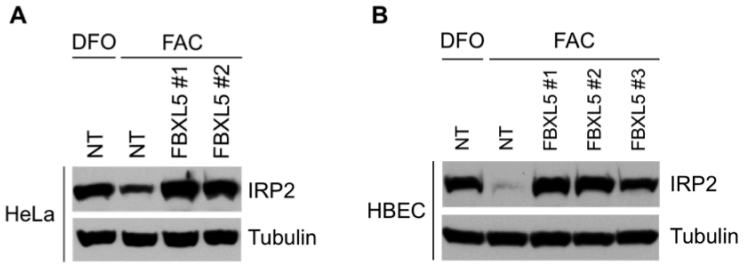

Figure 2-7. FBXL5 Knockdown in Additional Human Cell Lines
Immunoblot analysis of IRP2 accumulation in HeLa cells (**A**) and non-tumorigenic HBEC cells (**B**) following knockdown of FBXL5. (Salahudeen et al., 2009)

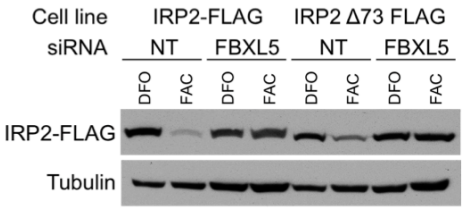

Figure 2-8. RNAi Mediated Suppression of FBXL5 Stabilizes IRP2 Δ73
Immunoblot analysis demonstrates that FBXL5 knockdown stabilizes wild-type IRP2 and an IRP2 truncation construct lacking the IDD. (Salahudeen et al., 2009)

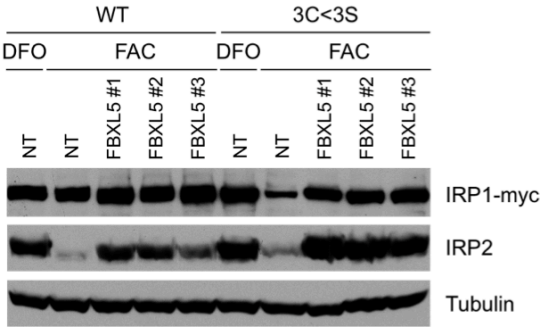

Figure 2-9. Knockdown of FBXL5 Stabilizes IRP1$^{3C<3S}$

An IRP1 mutant construct lacking the ability to bind a Fe-S cluster (3C<3S) displays aberrant accumulation under iron replete conditions following FBXL5 knockdown as measured by immunoblot analysis. (Salahudeen et al., 2009)

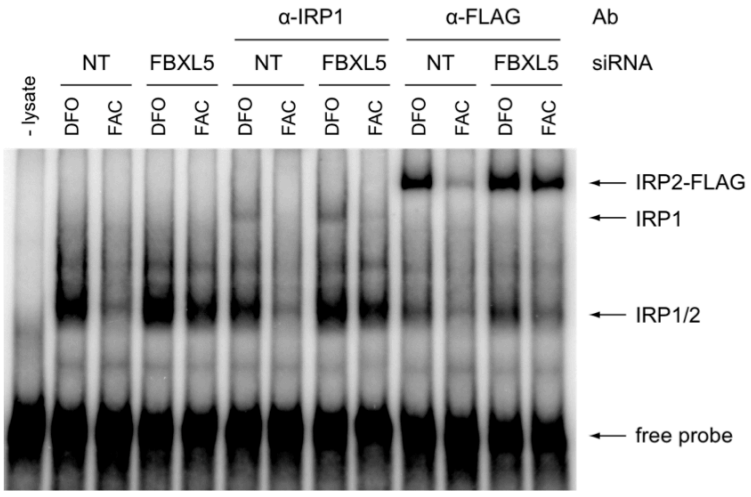

Figure 2-10. Knockdown of FBXL5 Causes Increased IRP2 IRE Binding Activity

IRE binding activity of IRPs was measured by EMSA. HA-IRP2-FLAG expressing HEK cells were transfected with either a NT or FBXL5 siRNA. Due to the co-migration of IRP-IRE complexes, antibodies were added to lysates to supershift individual complexes. (Salahudeen et al., 2009)

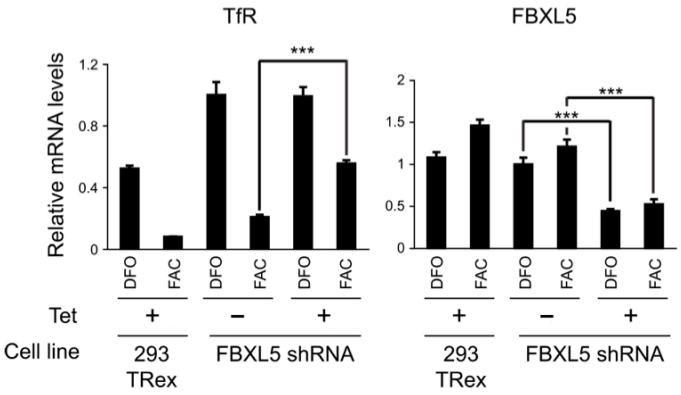

Figure 2-11. Abrogation of FBXL5 Expression Results in Misregulation of TfR1

Relative TfR1 and FBXL5 mRNA accumulation levels as measured by qRT-PCR. Values are expressed as the mean +/- SE. *** = p<.001 by Student's T-test. (Figure courtesy of Ameen Salahudeen and Hewen Ma; Salahudeen et al., 2009)

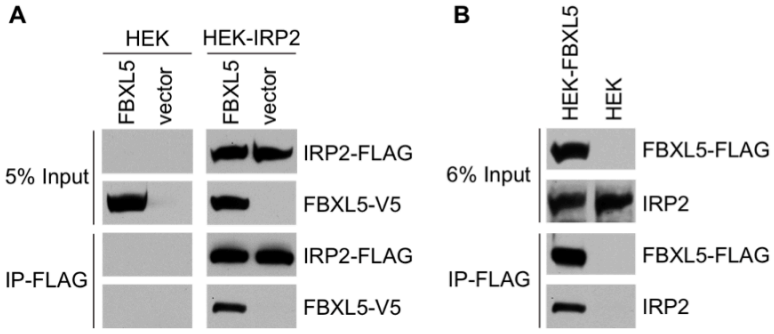

Figure 2-12. FBXL5 Interacts with IRP2
(**A**) FBXL5-V5 co-immunoprecipitates with IRP2-FLAG in HEK 293 cells. (**B**) Endogenous IRP2 co-immunoprecipitates with FBXL5-FLAG. (Salahudeen et al., 2009)

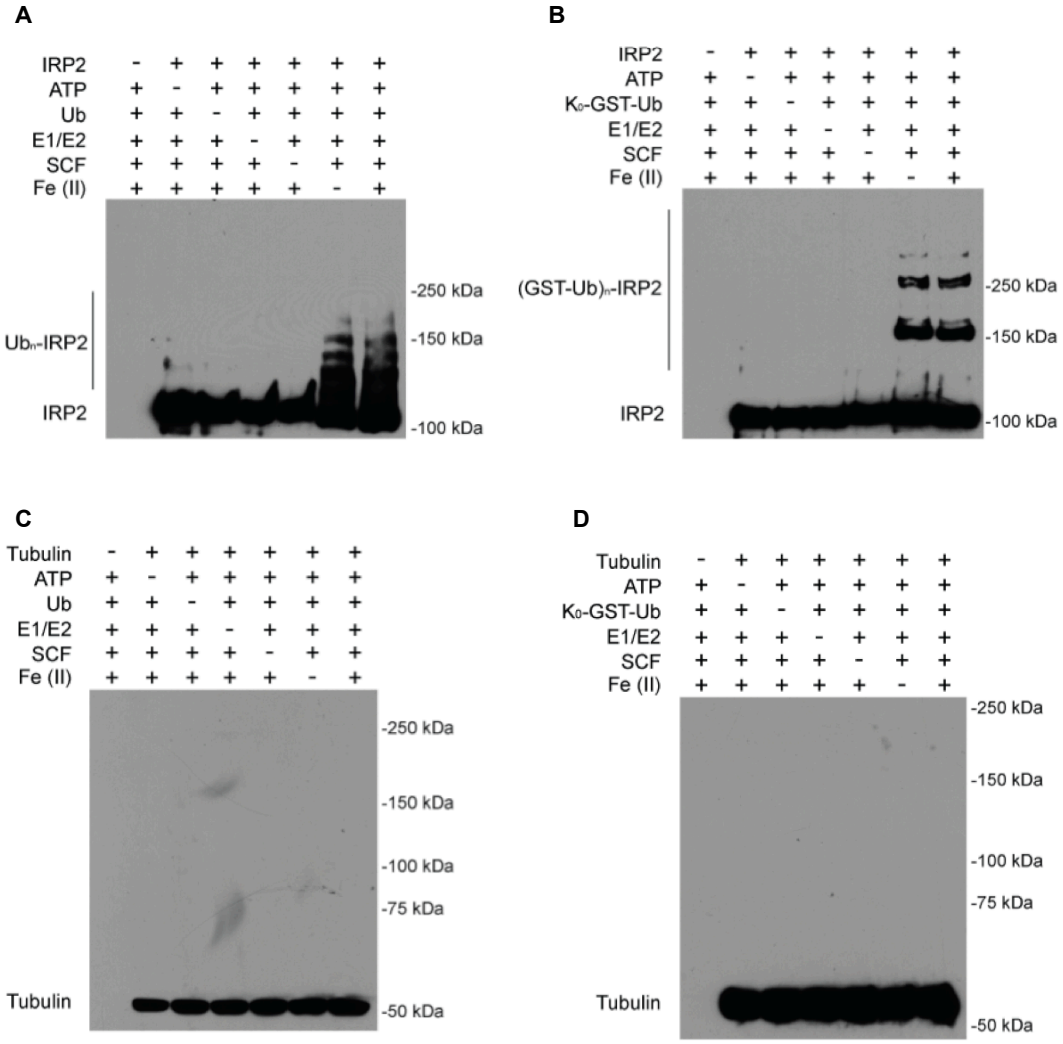

Figure 2-13. SCF^{FBXL5} Polyubiquitinates IRP2 In Vitro
Recombinant SCF^{FBXL5} ubiquitinates IRP2 in *in vitro* assays using wild-type ubiquitin (**A**) or ubiquitin fused to GST lacking lysine residues (K_0-GST-Ub; **B**). Equivalent assays using Tubulin as the substrate in place of IRP2 demonstrated that SCF^{FBXL5} does not display promiscuous activity in vitro (**C** and **D**). (Figure courtesy of Ameen Salahudeen; Salahudeen et al., 2009)

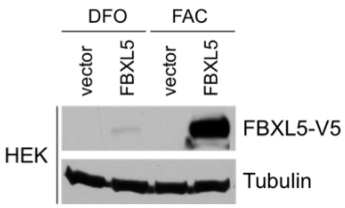

Figure 2-14. FBXL5 Preferentially Accumulates Under Iron Replete Conditions
HEK 293 cells were transfected with empty vector or a plasmid encoding FBXL5-V5 and treated with DFO or FAC. Immunoblot analysis with an α-V5 antibody was used to asses protein accumulation.

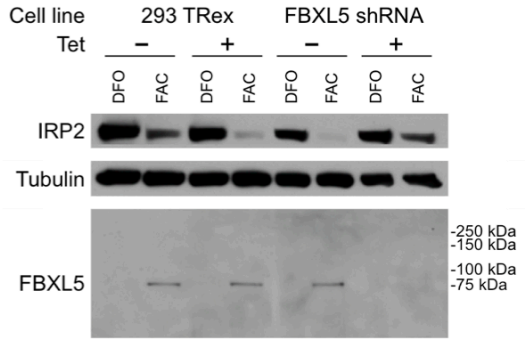

Figure 2-15. Endogenous FBXL5 is Regulated as a Function of Iron Availability
Tetracycline inducible FBXL5 shRNA 293 TRex cells were treated in the absence or presence of tetracycline, and with DFO or FAC. Endogenous FBXL5 and IRP2 accumulation was measured by immunoblot anlaysis. (Figure courtesy of Ameen Salahudeen; Salahudeen et al., 2009)

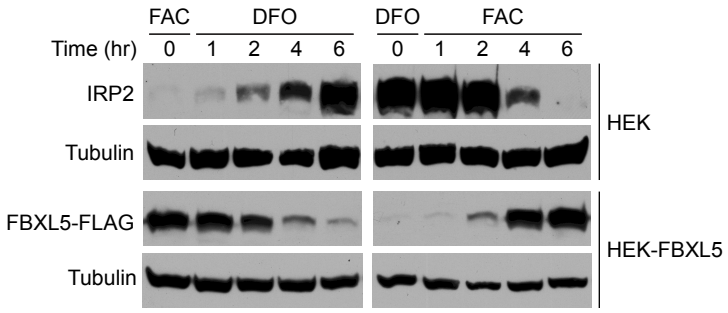

Figure 2-16. FBXL5 is Inversely Regulated in a Temporal Manner to IRP2

HEK 293 cells were incubated overnight with either high (FAC) or low (DFO) iron conditions and switched to low or high iron conditions, respectively. IRP2 protein levels were analyzed by immunoblotting at various time points as indicated (top). Parallel assays were performed measuring FBXL5-FLAG accumulation in a HEK 293 stable cell line (bottom). (Salahudeen et al., 2009)

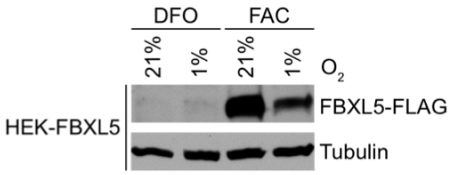

Figure 2-17. O_2 Availability Regulates FBXL5 Protein Accumulation
Immunoblot analysis of stably transfected FBXL5-FLAG under high or low O_2 and iron treatment. (Salahudeen et al., 2009)

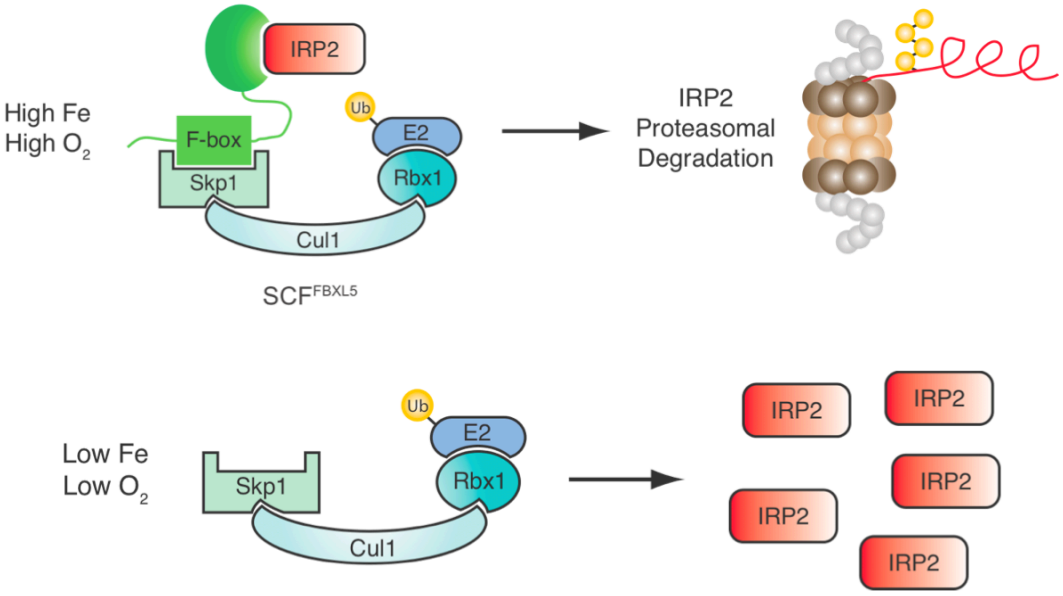

Figure 2-18. Model of Regulated IRP2 Stability Mediated by FBXL5 Accumulation
Under conditions where iron or O_2 are plentiful, FBXL5 accumulates and the SCF^{FBXL5} complex assembles resulting in IRP2 proteasomal degradation. However, if iron or O_2 are limiting, FBXL5 fails to accumulate precluding formation of SCF^{FBXL5} and stabilizing IRP2.

CHAPTER THREE

AN IRON BINDING HEMERYTHRIN DOMAIN REGULATES FBXL5 STABILITY

Introduction

In mammals, IRP2 helps maintain iron homeostasis by coordinating the posttranscriptional regulation of a variety of genes responsible for iron acquisition, utilization, and sequestration. When iron is limiting, IRP2 binds to RNA hairpin structures found in the UTRs of its target genes such as ferritin and TfR1. Mechanistically, IRP2 is posttranslationally regulated in an iron and oxygen dependent manner. The protein is stabilized under iron or oxygen deficient conditions but polyubiquitinated and degraded by the proteasome when iron is plentiful (Hentze et al., 2004; Muckenthaler et al., 2008; Rouault, 2006; Wallander et al., 2006). However, the mechanisms cells use to sense iron and oxygen levels with concomitant regulation of IRP2 stability are poorly understood.

Using a high throughput RNAi screen, we identified an E3 ubiquitin ligase complex containing FBXL5 that regulates IRP2 stability (Chapter 2). FBXL5 interacts with and polyubiquitinates IRP2 (Figs. 2-12 and 2-13). Loss of FBXL5 function leads to inappropriate accumulation of IRP2 and results in misregulation of the IRP target gene TfR1 (Figs. 2-5, 2-7, and 2-11). Interestingly, FBXL5 is regulated in a fashion reciprocal to IRP2 (Fig. 2-16). FBXL5 is stabilized under iron replete conditions and destabilized when iron or oxygen is limiting (Fig. 2-17). Therefore, we hypothesize that IRP2 is directly regulated as a function of FBXL5 expression (Fig. 2-18). However, the

mechanisms controlling FBXL5's iron dependent regulation remain unknown. In order to begin to understand how cells sense intracellular iron levels to regulate IRP2 expression, we sough to delineate the mechanisms controlling FBXL5 protein accumulation.

Iron Dependent Regulation of FBXL5 Requires the Proteasome

FBXL5 mRNA levels do not change substantially in response to iron availability (Fig. 2-11). Moreover, ectopically expressed FBXL5 lacks the FBXL5 promoter and UTRs, yet fully recapitulates iron dependent regulation (Figs. 2-14 and 2-16) of endogenous FBXL5 (Fig. 2-15). Together these data indicate that FBXL5 is regulated posttranslationally. Several F-box proteins are regulated through the UPS (Cardozo and Pagano, 2004). To determine whether FBXL5 is regulated by the proteasome, two clonal HEK 293 FBXL5-FLAG stable cell lines were treated with the proteasome inhibitor MG132 or vehicle (DMSO) and incubated with FAC or DFO for six hours to induce high or low iron bioavailability, respectively. Immunoblot analysis demonstrated that destabilization of FBXL5-FLAG is reversed with proteasomal inhibition, suggesting that FBXL5 is preferentially polyubiquitinated and degraded via the proteasome under iron deficient conditions (Fig. 3-1).

The N Terminus of FBXL5 is Necessary and Sufficient to Confer Iron Dependent Regulation

Human FBXL5 is 691 amino acids in length with a molecular weight of 75 kDa. FBXL5 contains a canonical F-box domain near its N terminus and a pair of three leucine rich repeat regions. The first region is in the middle of the protein and the second is located on the C terminus. Additionally, FBXL5 contains a region between the two leucine rich repeats that we termed the Cys-rich region due its high number of conserved

cysteine residues (Fig. 3-2). After analyzing the proposed domain structure of FBXL5, we wanted to delineate the region of FBXL5 required for its iron dependent regulation. To this end, a series of seven V5-tagged FBXL5 truncation constructs were generated that lacked different regions of FBXL5 (Fig 3-2). These constructs were transiently transfected into HEK 293T cells and treated with either DFO or FAC. Six of the seven truncation constructs phenocopied full-length (FL) FBXL5 and preferentially accumulated under iron replete conditions. In contrast, an FBXL5 construct lacking the first 197 amino acids (ΔN-term) constitutively accumulated irrespective of cellular iron status (Fig. 3-2). Thus, the N terminus of FBXL5 is required for its iron dependent regulation.

To determine whether the N terminus of FBXL5 was sufficient to confer iron dependent regulation, HEK 293T cells were transiently transfected with full-length FBXL5 and the N terminus of FBXL5 alone (amino acids 1-161). Interestingly, the N terminus of FBXL5 was regulated in an analogous manner to the full-length protein—i.e. the protein accumulates under iron replete conditions but displays a considerable reduction in accumulation under iron limiting conditions (Fig. 3-3).

In order to determine whether the N terminus of FBXL5 was sufficient to confer iron dependent regulation to a heterologous protein, chimera constructs containing amino acids 1-161 of FBXL5 fused to the N or C termini of firefly Luciferase were generated. HEK 293T cells were transiently transfected with the chimera constructs and wild-type Luciferase, followed by treatment with DFO or FAC. Wild-type Luciferase activity and protein accumulation levels did not change as a function of iron availability. However, the chimera proteins activities increased ~2-2.5 fold in lysates from FAC treated cells

compared to DFO treated cells. Moreover, increased Luciferase activity correlated with protein accumulation levels as measured by immunoblot analysis (Fig. 3-4). Taken together, the N terminus of FBXL5 is both necessary and sufficient to confer iron dependent regulation.

The N Terminus of FBXL5 is Predicted to Encode a Hemerythrin Domain

To ascertain potential mechanisms by which the N terminus confers iron dependent stability to FBXL5, we turned to bioinformatics. In collaboration with the Grishin lab at UT Southwestern we were able to predict that the N terminus of FBXL5 encodes a hemerythrin domain. Hemerythrin (Hr) domains from marine invertebrates have been well characterized and homologous domains from bacteria are beginning to be investigated (Holmes et al., 1991; Holmes and Stenkamp, 1991; Isaza et al., 2006; Kao et al., 2008; Sheriff et al., 1987; Stenkamp et al., 1985). In marine invertebrates, Hr domain containing proteins are believed to function as O_2 transport and storage proteins similar to the mammalian proteins hemoglobin and myoglobin, respectively. In addition to these roles, it has also been postulated that Hr proteins functions as iron sensors, iron depots, and O_2 sensors. Structurally, Hr domains are characterized by a helical bundle fold containing four α helices and an O_2 binding diiron center. The binuclear iron center is typically ligated by seven amino acids comprised of five histidines, one aspartic acid, and one glutamic acid. The first iron atom (Fe1) of the diiron center is coordinated by three histidines and the second iron (Fe2) is coordinated by two histidines. The glutamic and aspartic acid residues bridge both Fe1 and Fe2 using each oxygen from their carboxylate group. Moreover, the diiron center is bridged by an ostensibly solvent derived μ-hydroxyl group in the deoxy (when O_2 is not bound) state. In the oxy state, O_2 binds the μ-

hydroxyl using one oxygen atom and interacts with Fe2 using its other oxygen (Fig. 3-5). Upon O_2 binding, the μ-hydroxyl becomes a μ-oxo group and O_2 is reduced forming a peroxide species that is stabilized by hydrophobic residues lining the binding pocket. In the deoxy state the iron atoms of the active site are in the ferrous (+2) state while in the oxy state they adopt the ferric (+3) state (French et al., 2008; Nordlund and Eklund, 1995; Stenkamp, 1994).

Structural Characterization of the FBXL5 Hemerythrin Domain

To complement our other approaches, we employed X-ray crystallography to confirm that the N terminus of FBXL5 contains a Hr domain. Ameen Salahudeen, and Diana Tomchick of the UT Southwestern Structural Biology Core, largely carried out this work. The FBXL5 N terminus (residues 1-161) was recombinantly expressed, purified, and crystals were generated. The structure was determined to 1.9 Å (Native form 1, Table 3, Appendix). Analogous to bacterial and invertebrate Hrs, the FBXL5 N terminus contains an up-down alpha-helical bundle with a diiron center (Fig. 3-6). Compared to solved Hr domain structures, the FBXL5 Hr is most structurally homologous to the Hr domain from the bacterial protein DcrH (Fig. 3-7).

While the FBXL5 Hr has the same general tertiary structure as other Hrs, there are several features that are unique to this vertebrate Hr. In contrast to previously characterized Hrs, the FBXL5 Hr contains a fifth helix (Fig. 3-6) packed against the apex of the canonical four-alpha-helical bundle (α helices: α1, 12-31; α2, 37-45 and 47-73; α3, 84-98; α4, 102-141; α5, 144-158; Fig. 3-8). Helix α5 forms an interhelical salt bridge with helix α2 (E146-R72) and is required for iron dependent regulation of FBXL5 (see below). Overall, the FBXL5 Hr has an elongated length (58 Å versus ~40-50 Å), but

similar diameter and height (~20 Å) compared to other Hrs (Isaza et al., 2006; Stenkamp, 1994; Figs. 3-6 and 3-7). This increased length is due to helices α2 and α4, spanning 37 and 40 amino acids, respectively. In contrast, in the DcrH Hr, which has longer helices than the invertebrate Hrs, helices α2 and α4 have 29 and 33 residues, respectively (Fig. 3-8). In the FBXL5 Hr, helices α2 and α4 extend well beyond the diiron center. These helices, together with helix α5 and an unstructured region at the beginning of the domain, form a predominantly alpha helical rich bundle on the opposite side of the diiron center to the canonical O_2 binding pocket. Similar to the canonical four-alpha helical bundle, this smaller bundle contains a hydrophobic core composed of invariant amino acids that may stabilize the domain. Another distinct feature of the FBXL5 Hr structure is its unassignable residues (81-83) between a loop and the start of helix α3 (Fig. 3-6).

Examination of the amino acid side chains responsible for coordinating iron demonstrates that FBXL5's diiron center deviates from the scheme previously observed in Hrs (Fig. 3-9). All Hr domains structure solved to date employ 5 coordinating histidines, while the FBXL5 Hr has four (H80 and H126 coordinate Fe1, while H57 and H80 coordinate Fe2, using their ε nitrogens). In place of an aspartic acid and glutamic acid to bridge the diiron center, the FBXL5 Hr employs two glutamic acids (E61 and E130). As with other Hrs, the diiron center is bridged by a μ-hydroxyl. In this structure however, no O_2 was bound to the diiron center. However, the most significant variation in the FBXL5 diiron center may be the presence of a glutamic acid (E58) in lieu of a histidine binding Fe1. Unexpectedly, E58 interacts with both Fe1 and the μ-hydroxyl.

In addition to the primary shell of amino acids that coordinate iron, the FBXL5 Hr contains a secondary shell of amino acids that form a hydrogen bond network to three

of the iron-ligating residues (Figs. 3-8 and 3-9). The carbonyl of N62 is hydrogen-bonded to Nδ of H80, the carboxylate of E131 is hydrogen bonded to Nδ of H15, and the Nε of H158 is hydrogen bonded to Nδ of H57.

The coordination geometry of the diiron site is also unique to the vertebrate FBXL5 Hr (Table 4, Appendix). Notably, the Fe-O_{μ}-Fe angle in the FBXL5 Hr is more acute (98.1°) than those previously observed in invertebrate (116.7°) and bacterial (132.4°) Hrs (Isaza et al., 2006; Stenkamp, 1994). The Fe-Fe distance is also smaller (3.12 Å versus ~3.41-3.28 Å) than other Hrs (Isaza et al., 2006; Stenkamp, 1994). Despite these differences, the spatial conservation of the iron-ligating residues with respect to the diiron center is remarkably similar to the DcrH Hr (Fig. 3-10).

Next we wanted to determine whether we could obtain an X-ray crystal structure of the FBXL5 Hr domain in a different form from our first structure. We hypothesized that in the protein used to generate the Native form 1 crystals, the reducing agent in the buffer could have reduced the core iron atoms and prevented O_2 binding. We therefore generated the second crystal structure of the Hr domain in the absence of reducing agent (Native form 2, Table 3, Appendix). However, while adding reducing agent to the purified domain was sufficient to elicit a mild change in the UV-Visible spectrum of the protein (data not shown), the crystal structure of the FBXL5 Hr did not differ appreciably in the absence or presence of reducing agent. In the absence of reducing agent no ordered electron density corresponding to O_2 was observed in the diiron site. This occurred despite crystallization conditions under ambient O_2 concentrations sufficient to obtain crystals of oxy-Hr in previous reports (Holmes and Stenkamp, 1991; Stenkamp, 1994). Moreover, generation of crystals under anoxic conditions yielded an essentially identical

Hr structure (Srinivas Chollangi, unpublished data). Thus, despite trying different crystallization conditions, the FBXL5 Hr was found to adopt a single structure in our samples.

We subsequently began to investigate possible reasons for the lack of O_2 binding to the diiron center in the Hr domains crystallized. Although the iron-binding residues of the FBXL5 Hr domain are generally spatially conserved with the DcrH Hr, there are significant spatial variations in the hydrophobic amino acids lining the O_2 binding pocket. In the FBXL5 Hr, the canonical O_2 binding pocket adjacent to Fe2 and the μ-hydroxyl is obstructed by F123 and M127 (Fig. 3-10). F123 is located in the center of the helical bundle and in close proximity (~4 Å) to the μ-hydroxyl. M127 also protrudes into the binding pocket and is in close proximity (~4 Å) to both the μ-hydroxyl and Fe2. In the DcrH Hr, W114, the homologous hydrophobic residue to F123, is positioned closer to the periphery of the hydrophobic core and adjacent to Fe1. The analogous residue to M127 in the DcrH Hr, L115, is more distal (~6 Å) to both Fe2 and the μ-hydroxyl, and consequently the binding pocket in the DcrH Hr has much larger dimensions than the FBXL5 Hr. Moreover, although Fe1 is solvent accessible due to its proximity to a putative substrate channel, Fe2 appears to be obstructed from the same channel by F123 (data not shown). Thus, in addition to sterically blocking O_2 binding to Fe2 and the μ-hydroxyl, F123 may also occlude Fe2's accessibility to O_2. Lastly, another potential hindrance to O_2 binding the diiron center is residue E58, which interacts with the μ-hydroxyl and would preclude O_2 from binding the Fe2 and forming a hydrogen bond with the μ-oxo species.

Iron Binding via its Hemerythrin Domain Regulates FBXL5 Stability

The confirmation that the N terminus of FBXL5 contained an iron binding Hr domain suggested an intriguing mechanism by which FBXL5 could serve as a direct iron sensor. We postulated that iron binding via the Hr domain was crucial for regulating FBXL5 protein stability. To test this hypothesis, the ability of the Hr domain to bind iron was perturbed. First, a series of FBXL5 constructs were generated containing individual mutations to all seven of the iron ligating residues in which the amino acids were changed to alanine (H15, H57A, E58A, E61A, H80A, H126A, E130A). These constructs and wild-type (WT) FBXL5 were transiently transfected into HEK 293T cells and treated with FAC or DFO. As expected, WT FBXL5 showed preferential accumulation under iron replete conditions. Contrastingly, all seven mutant FBXL5 constructs displayed constitutively low expression levels irrespective of bioavailable iron levels (Fig. 3-11A). These results demonstrate the importance of the primary iron binding residues in mediating iron dependent regulation of FBXL5.

In the crystal structure of FBXL5's Hr domain it was revealed that residues N62, E131, and H158, form hydrogen bonds with the primary iron binding residues H80, H15, and H57, respectively. We postulated that these secondary shell interactions may be crucial for the formation of the diiron center by bringing the imidazole moieties of residues H80, H15, and H57 into their optimal conformations to coordinate iron. Furthermore, we postulated that mutating any one of residues N62, E131, and H158 to alanine would preclude formation of the diiron center and render FBXL5 constitutively unstable. With this idea in mind, site directed mutagenesis was carried out to individually change the aforementioned amino acids to alanine (N62A, E131A, and H158A). These

mutant constructs and WT FBXL5 were transfected into HEK 293T cells and treated with DFO or FAC. In contrast to WT FBXL5, which showed increased accumulation under iron replete conditions, all three mutant FBXL5 constructs displayed low expression levels under both iron replete and deficient conditions (Fig. 3-11B). Thus, although residues N62, E131, and H158 do not directly bind iron, this data is consistent with these residues being important for mediating iron coordination.

In a typical Hr domain, in addition to the two bridging carboxylates, Fe1 is ligated by three histidines. However, in the FBXL5 Hr domain, Fe1 is ligated by two histidines (H126 and H80) and 1 glutamic acid (E58). Therefore, we wanted to determine whether a histidine residue could replace a glutamic acid at residue 58. Thus, a FBXL5 mutant construct where E58 had been changed to histidine (E58H), and WT FBXL5 were transiently transfected into HEK 293T cells. We observed that while WT FBXL5 responded normally to FAC and DFO treatment, E58H FBXL5 was constitutively unstable under both conditions (Fig. 3-13). Furthermore, when residue E58 was changed to the shorter side chain containing aspartic acid (E58D), or the amide containing glutamine (E58Q), both FBXL5 mutant proteins were unstable under high and low iron treatment (Fig. 3-11C). Thus, it appears for iron dependent regulation of FBXL5 a glutamic acid is critical at residue 58. This may be due to the length, flexibility, and chemical properties of glutamic acid that allows it to interact with both Fe1 and the μ-hydroxyl.

Next we wanted to determine whether the fifth helix of the Hr domain is required for proper regulation of FBXL5, as no other Hr-like domain structure has been reported that contains a five alpha-helical bundle. To this end, WT FBXL5 and a construct lacking

helix α5 (Δ143-161) were transiently transfected into HEK 293T cells and subjected to low or high iron treatment. Similar to mutation of the primary or secondary iron coordination shell ligands, removal of helix α5 led to constitutive destabilization of FBXL5 (Fig. 3-11D). This is not surprising due to the fact that helix α5 contains the secondary coordination shell residue (H158) and ostensibly functions to stabilize the canonical four helical bundle. Thus, precluding FBXL5's ability to bind iron through mutagenesis or deletion of iron binding residues in the Hr domain, destabilizes FBXL5 in a similar fashion to depleting cells of iron. Taken together, the above data suggests that the FBXL5 Hr domain may functions as a sensory module to gauge bioavailable iron levels and regulate FBXL5 stability.

The FBXL5 Hemerythrin Domain Preferentially Responds to Iron Treatment Compared to Other Metals

If the Hr domain functions in an iron sensory capacity it should preferentially respond to iron treatment. HEK 293 cells stably expressing a N-terminal FLAG and C-terminal HA tagged Hr construct (HEK-Hr) were incubated with DFO to induce basal expression levels of the domain. Following incubation with DFO, cells were treated with increasing amounts of iron, nickel, cobalt, zinc, copper, magnesium, or manganese. In contrast to iron, which promoted Hr accumulation under the lowest concentration, cobalt and zinc treatment only induced Hr domain accumulation at the highest concentration. Manganese treatment also appeared to induce intermediate accumulation of the Hr domain. Nickel, copper, and magnesium treatment had no effect (Fig. 3-12A). Thus, for the seven metals tested, Hr accumulation is most sensitive to iron treatment. Moreover, titration of HEK-Hr cells with lower concentrations of FAC demonstrated that the Hr

protein responds in a dynamic fashion to iron treatment (Fig. 3-12B), consistent with its function as an iron binding and sensing domain.

Analysis of a Regulatory Sequence in the FBXL5 Hemerythrin Domain

The FBXL5 N terminus accumulates under iron replete conditions in an analogous manner to full-length FBXL5 (Fig. 3-3). Moreover, fusion of the N terminus of FBXL5 to a heterologous protein is sufficient to confer iron dependent regulation (Fig. 3-4). Taken together, these data suggest that the N-terminal Hr domain may contain a degron that targets FBXL5 for polyubiquitination by an E3 ubiquitin ligase. To identify the region within the FBXL5 Hr domain that is responsible for targeting the protein for degradation we generated a series of progressively longer FBXL5 N-terminal truncation constructs. While Δ1-33, Δ1-59, and Δ1-76 proteins were constitutively unstable, the Δ1-81 and Δ1-100 proteins were stabilized under both FAC and DFO treatment suggesting the regulatory sequence targeting FBXL5 for degradation may be located following amino acid 76 (Fig. 3-13A). To follow up this observation a series FBXL5 constructs containing 5 amino acid deletions in the region spanning residues 67 to 91 were generated. Interestingly, deletion of residues 77-81 led to a substantial constitutive increase in FBXL5 accumulation (Fig. 3-13B) indicating these residues may be part of a degron that controls FBXL5 stability.

FBXL5 is Preferentially Polyubiquitinated Under Iron Limiting Conditions

Proteasome inhibition leads to increased FBXL5 accumulation consistent with the protein being regulated via polyubiquitination and proteasomal degradation (Fig. 3-1). To determine if FBXL5 is posttranslationally regulated via polyubiquitination, immunoprecipitation experiments were performed using HEK 293T cells stably

expressing FBXL5-FLAG. Cells were treated with either FAC or DFO, and in the absence or presence of the proteasome inhibitor MG132. FBXL5 was subsequently immunoprecipitated using FLAG resin. Immunoblot analysis of the immunoprecipitated FBXL5 demonstrated the protein displays enhanced polyubiquitination under iron deficient conditions (Fig. 3-14). However, FBXL5 is spared from high levels of ubiquitination when iron is plentiful, ostensibly stabilizing the protein.

The FBXL5 Hemerythrin Domain Undergoes a Conformation Change in its Apo State

Our data demonstrates that FBXL5's differential stability is regulated via the UPS. However, it remained unclear mechanistically how FBXL5's polyubiquitination status was increasing under iron deplete conditions. One possible hypothesis to explain these data is that under iron replete conditions the N terminus of FBXL5 adopts a hemerythrin fold, masking its degron. Conversely, under iron deficient conditions, when the Hr is no longer able to form a diiron center, the domain undergoes a conformation change causing a degron to be exposed. To test this hypothesis, a limited proteolysis experiment was carried out. HEK-Hr cells were treated with FAC or DFO, in addition to MG132 to block Hr degradation. Cell lysates were then generated and incubated with increasing amounts of trypsin. Hr domain from FAC treated cells was refractory to trypsinolysis while the Hr protein from the DFO treated cells was degraded following the same treatment (Fig. 3-15). Thus, this cell-based assay indicates the FBXL5 Hr domain in its unmettalated state undergoes a conformational change. Moreover, this data is consistent with a model in which under iron limiting conditions the Hr domain adopts a

conformation with its degron exposed, resulting in increased polyubiquitination and degradation of FBXL5.

Further Insights into the O_2 Dependent Regulation of FBXL5

Although a crystal structure of the FBXL5 Hr domain containing an O_2 bound diiron center was not obtained, our data demonstrates that O_2 plays a role in regulating the Hr domain's expression. Fusion of the Hr domain to a heterologous protein is sufficient to reduce fusion protein accumulation under low O_2 treatment (data not shown). In order to assess whether oxygen dependent regulation of the FBXL5 Hr was mediated through polyubiquitination and proteasomal degradation, we incubated HEK-Hr cells with either FAC or DFO, in the absence or presence of MG132, and under high (21%) or low (1%) O_2 conditions. As observed with FBXL5, treatment of the HEK-Hr cells with MG132 led to enhanced expression of the Hr protein, which was preferentially polyubiquitinated under iron deficient conditions. However, in FAC treated cells incubated under low O_2 conditions there was a moderate increase in polyubiquitination and a slight decrease in accumulation of the Hr domain versus cells incubated under high O_2 conditions (Fig. 3-16). Thus, O_2 may play a partial role in controlling the stability of the Hr domain via polyubiquitination and proteasomal degradation. However, this data varies from experiments using full-length FBXL5. FBXL5 shows a more dramatic decrease in expression under high iron treatment and low O_2 conditions (Fig. 2-18). Therefore, there may additional mechanisms independent of the Hr domain, which contribute to FBXL5's O_2 dependent regulation. To address this idea, full-length FBXL5 and a construct lacking the Hr domain (Δ1-161) were transiently transfected into HEK 293T cells. Cells were treated with DFO or FAC and incubated under high or low O_2 conditions. Similar to

previous results, full-length FBXL5 displayed reduced expression levels under low O_2 treatment and the Δ1-161 construct accumulated under both high and low iron conditions. Interestingly, in an analogous manner to full-length FBXL5, Δ1-161 FBXL5 levels were substantially lower in cells grown at 1% O_2 (Fig. 3-17). Thus, while the Hr domain is both necessary and sufficient to confer iron dependent regulation, it is not solely required for O_2 dependent regulation of FBXL5.

Iron Dependent Regulation of the FBXL5-IRP2 Interaction

Our studies demonstrate that an iron responsive N-terminal Hr domain controls FBXL5 stability. We also wanted to determine whether iron availability affects the activity of FBXL5. To this end, co-immunoprecipitation experiments were carried out using HEK 293T cells stably expressing FBXL5-FLAG. Cells were incubated with FAC or DFO and MG132 prior to lysis. While endogenous IRP2 co-immunoprecipitated with FBXL5-FLAG in lysates from FAC treated cells, this interaction was abolished in lysates from DFO treated cells (Fig. 3-18A). Moreover, HEK 293T cells were transiently co-transfected with IRP2-FLAG and several FBXL5-V5 constructs (WT, ΔN-term, and ΔF-box). Prior to lysis cells were treated with DFO or FAC. Ectopic expression of the ΔF-box protein had no affect on IRP2-FLAG. In contrast, cells transfected with WT FBXL5 displayed a slight reduction in IRP2-FLAG accumulation under iron deplete conditions. Although the FBXL5 ΔN-term protein expresses at high levels irrespective of iron availability, under iron deficient conditions it also failed to degrade IRP2-FLAG to levels observed with excess iron treatment. However, under iron deficient conditions, cells transfected with the ΔN-term construct did display decreased IRP2-FLAG expression compared to cells transfected with WT FBXL5 (Fig 3-18B). Together these data indicate

that in addition to FBXL5 stability, iron may regulate the physical interaction between IRP2 and FBXL5. Additionally, this data suggests that the Hr domain is not required for FBXL5's association with IRP2.

Conclusion

Previously using a functional genomics approach we identified the SCF^{FBXL5} complex as an E3 ligase regulating IRP2 stability. The substrate recognition subunit of the SCF complex, FBXL5, was regulated in an inverse fashion to IRP2. FBXL5 accumulates under iron replete conditions and is degraded under iron or O_2 depletion. We hypothesized that iron dependent regulation of FBXL5 may mediate proteolytic degradation of IRP2. However, the cellular mechanisms controlling the iron responsiveness of FBXL5 were unknown.

Treatment of cells with the proteasome inhibitor MG132 led to a substantial increase in FBXL5 expression, particularly under low iron conditions. Furthermore, immunoprecipitation experiments demonstrated that FBXL5 undergoes enhanced polyubiquitination under iron deficient conditions. Thus, it appears that degradation of FBXL5 is mediated via the UPS.

Using a series of FBXL5 truncation constructs it was determined that the N terminus of FBXL5 is required for its iron dependent degradation. Bioinformatics predicted that the N-terminal region of FBXL5 encodes a hemerythrin domain. X-ray crystallography confirmed the N terminus of FBXL5 adopts an Hr fold with a diiron center. Identification of the N-terminal Hr domain was paramount as it provided a basis to begin to dissect the mechanisms controlling iron dependent degradation of FBXL5.

The crystal structure of the FBXL5 Hr demonstrated that seven conserved amino acids bound a diiron center. Inhibiting the Hr domain's ability to bind iron by mutagenesis of its iron ligating residues rendered FBXL5 constitutively unstable similar to chelating iron from cell culture media. Moreover, the Hr domain showed preferential sensitivity to iron treatment compared to six other metals, as the protein fully accumulated with lower concentration of iron treatment than other metals. Taken these data together, we propose that the FBXL5 Hr domain functions as a direct iron sensor.

We next asked how the Hr domain was regulating FBXL5 stability. Because the Hr domain expressed alone is regulated in an analogous manner to FL FBXL5 and the domain is also sufficient to confer iron dependent regulation to a heterologous protein, it was reasonable to predict that a degron was encoded within the Hr domain. Deletion experiments in the N terminus of FBXL5 suggested that residues 77-81 may be part of this degron. Many characterized degrons are posttranslationally modified with a phosphate or hydroxyl group in order to promote an interaction with their cognate E3s (Schrader et al., 2009). However, we postulated that FBXL5 was regulated by an alternative mechanism. Instead of the degron being chemically modified, we proposed that the accessibility of the degron would be controlled in an iron dependent manner in order to regulate FBXL5's interaction with an E3 ligase. Consistent with this hypothesis, Hr domain protein expressed in cells treated with iron prior to lysis was insensitive to limited trypsinolyis. Conversely, Hr protein from DFO treated cells was efficiently degraded following trypsinolysis, indicative of a structural change in the domain.

On the basis of the above findings, we propose the following model for iron dependent regulation of FBXL5 stability. When cellular iron levels are high, the N

terminus of FBXL5 folds into a Hr domain with a diiron center. Under these conditions, a degron is masked and FBXL5 is stabilized. As a result the SCF^{FBXL5} complex forms, promoting polyubiquitination of its target substrates such as IRP2. However, under conditions where bioavailable iron is scarce, the FBXL5 Hr domain is unable to bind iron triggering a conformation change and exposing a degron. The degron is then recognized by an unknown E3 ligase and FBXL5 is tagged for proteasomal degradation (Fig. 3-19).

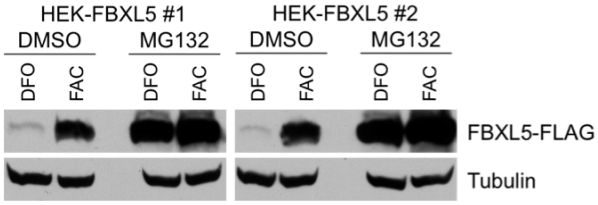

Figure 3-1. FBXL5 is Regulated Via the Ubiquitin Proteasome System
FBXL5-FLAG accumulation was measured by immunoblot analysis following treatment with MG132 or DMSO and FAC or DFO. (Salahudeen et al., 2009)

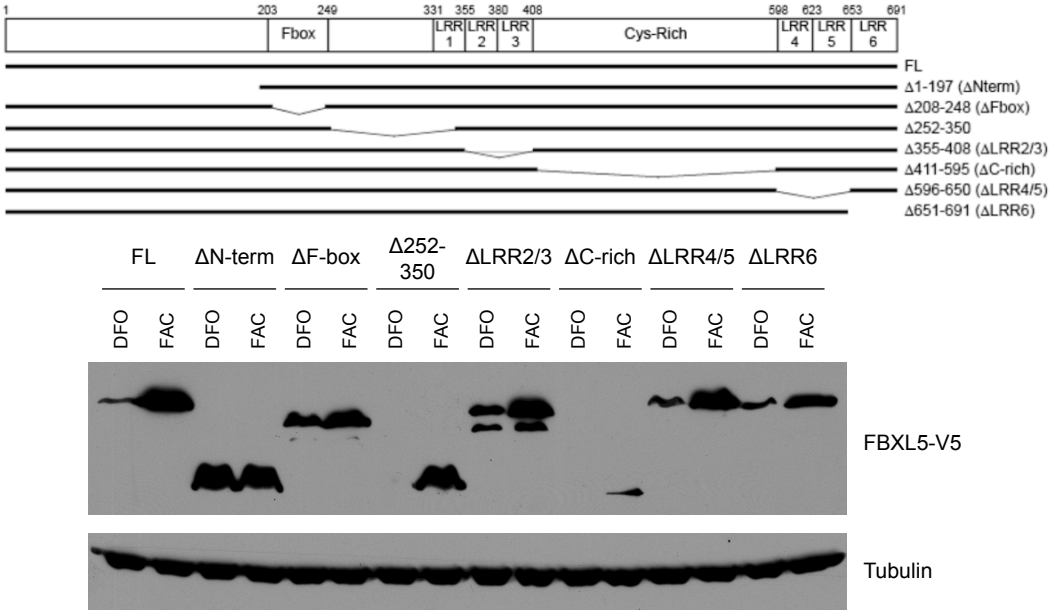

Figure 3-2. The N terminus of FBXL5 is Required for its Iron Dependent Regulation

Topology map of FBXL5 showing its predicted domain architecture and schematic of FBXL5 truncation constructs (top). HEK 293T cells were transfected with various FBXL5 deletion constructs as indicated and incubated with DFO or FAC. Protein accumulation was measured by immunoblot analysis (bottom). (Salahudeen et al., 2009)

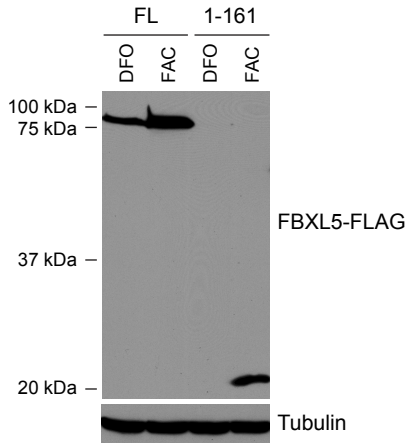

Figure 3-3. The FBXL5 N Terminus is Regulated in an Iron Dependent Manner
Assessment of FBXL5 full-length and N terminus protein accumulation under iron replete and iron deficient conditions by immunoblot analysis. (Salahudeen et al., 2009)

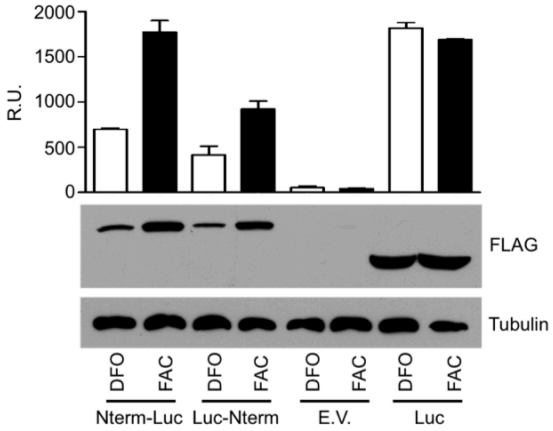

Figure 3-4. The N terminus of FBXL5 is Sufficient to Confer Iron Dependent Regulation to a Heterologous Protein

Expression constructs containing residues 1-161 of FBXL5 fused to the N or C terminus of Lucifersase were transiently transfected into HEK 293T cells. Luciferase activity (top) and fusion protein accumulation (bottom) were assayed under iron replete and iron deficient conditions. (Figure courtesy of Julio Ruiz)

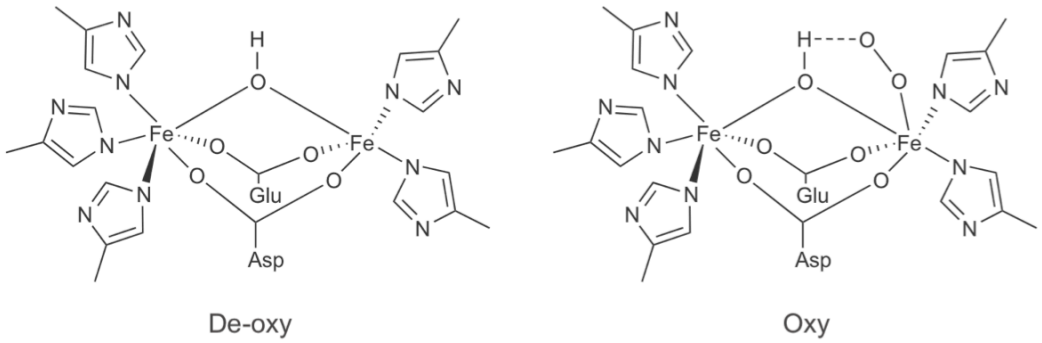

Figure 3-5. Schematics of Canonical Hemerythrin Domain Diiron Centers
Typically, five histidine residues ligate the Hr domain diiron center. Two residues, an aspartic acid and glutamic acid, interact with both iron atoms. Additionally, the diiron center is bridged by a μ-hydroxyl species. In the oxy state (right) the second iron atom and the μ-hydroxyl bind O_2, while this binding is absent in the de-oxy state (left).

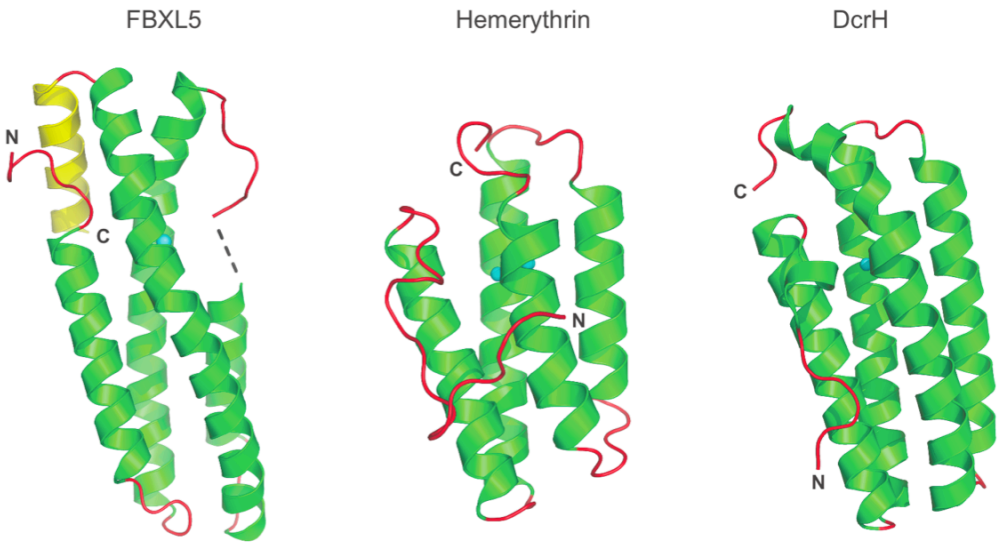

Figure 3-6. The N-terminal Domain of FBXL5 is a Helical Bundle, a Hemerythrin-like Fold
From left, ribbon representations of the N-terminal domain of *Homo sapien* FBXL5, *Thermiste dyscritum* hemerythrin (PDB code 2HMQ), and *Desulfovibrio vulgaris* DcrH (PDB code 2AWY). Helices are shown in green and loops in red. The additional fifth C-terminal helix found in FBXL5 is shown in yellow. The dotted black line in FBXL5 represents the disordered residues (81-83) in helix 3. (Figure courtesy of Ameen Salahudeen and Diana Tomchick)

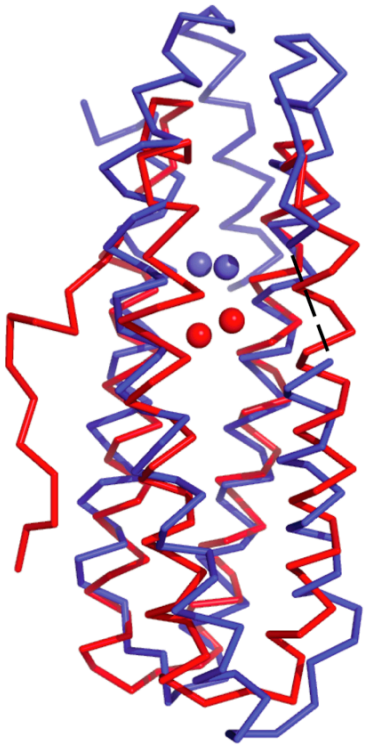

Figure 3-7. The N-terminal Domain of FBXL5 is Structurally Homologous to the DcrH Hr Domain
Shown in ribbon representation is a DaliLite superposition of chain A of Native 2 FBXL5 Hr (blue) and chain B of D. vulgaris met-DcrH Hr (red, PDB code 2AWY). One hundred and thirteen common residues align with a r.m.s.d. of 3.0 Å and a Z-score of 9.0.

Figure 3-8. Secondary Structure Alignment of the N Terminus of FBXL5 and the DcrH Hr Domain

A DaliLite superposition was used to generate a structural alignment of chain A of Native 2 FBXL5 Hr and chain B of D. vulgaris met-DcrH Hr (PDB code 2AWY). Secondary structure is shown on top with helices numbered in order from the N to C termini. Below is the amino acid sequence alignment based on the secondary structure alignment. Amino acids forming the primary iron coordination shell are highlighted in green, while the residues comprising the second iron coordination shell are highlighted in pink. The missing residues in the FBXL5 Hr structure are highlighted in gray. The sequence identity between the FBXL5 Hr and the DcrH Hr is 11%.

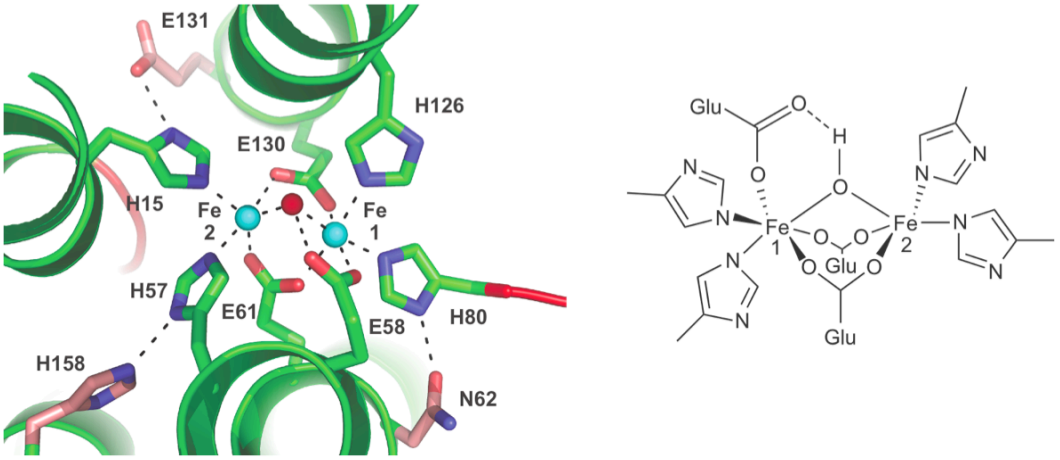

Figure 3-9. The FBXL5 Hemerythrin Diiron Center
On the left is a pymol representation of the diiron center. First coordination sphere iron ligands are shown as green sticks, and conserved second coordination sphere iron ligands are shown as pink sticks. Metal-ligand and hydrogen bonds are shown as dotted black lines. On the right is a schematic of the FBXL5 Hr diiron center. (Pymol representation courtesy of Diana Tomchick)

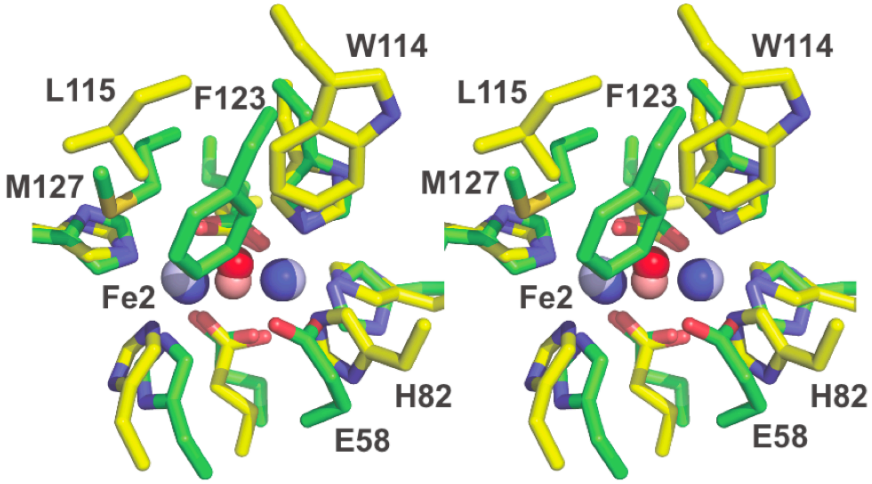

Figure 3-10. The Diiron Center of FBXL5 Resembles Deoxy-DcrH, but F123 Occludes the Hydrophobic O_2 Binding Pocket
Shown in stereo is a superposition of the diiron sites (dark blue and dark red) and first coordination sphere iron ligands (green) of chain A of Native 2 FBXL5 to the metal site (pale blue and pale red) and ligands (yellow) of chain A of deoxy-DcrH (PDB code 2AWC). The twelve common atoms align with an r.m.s.d. of 0.95 Å. Labeled are the Fe2 site and residues that differ between the two proteins. (Figure courtesy of Diana Tomchick)

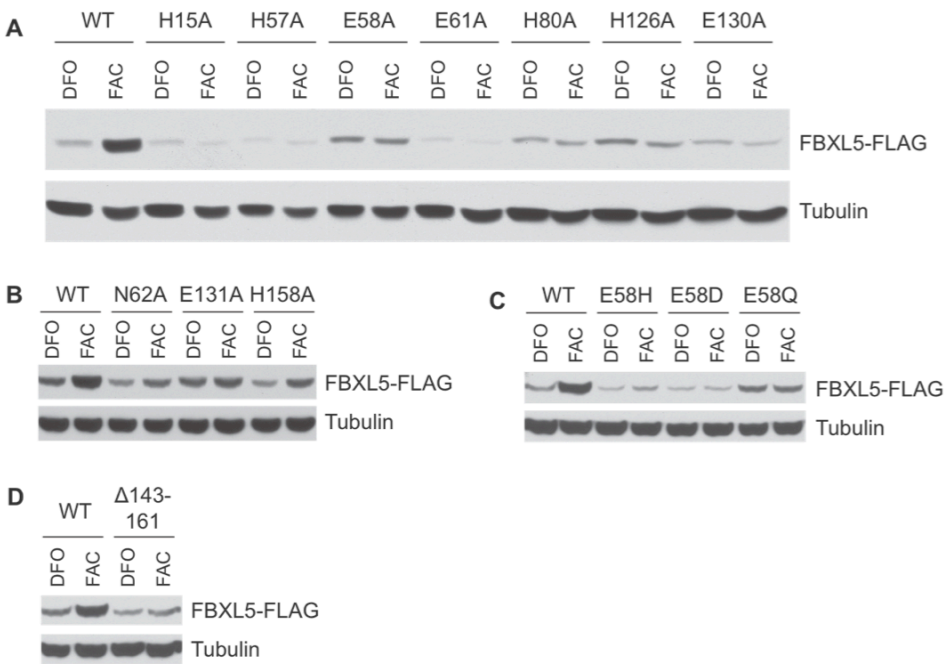

Figure 3-11. Features of the FBXL5 Hemerythrin Domain Required for Iron Dependent Regulation of FBXL5.

(**A-D**) Eight hours post-transfection, HEK 293T cells were treated with either DFO or FAC. FBXL5 accumulation was assessed by immunoblot analysis. (**A**) Analysis of mutations to residues comprising the primary iron coordination shell. (**B**) Analysis of mutations to residues comprising the second iron coordination shell. (**C**) Analysis of FBXL5 E58 mutations. (**D**) Analysis of a FBXL5 construct lacking helix α5 (Δ143-161).

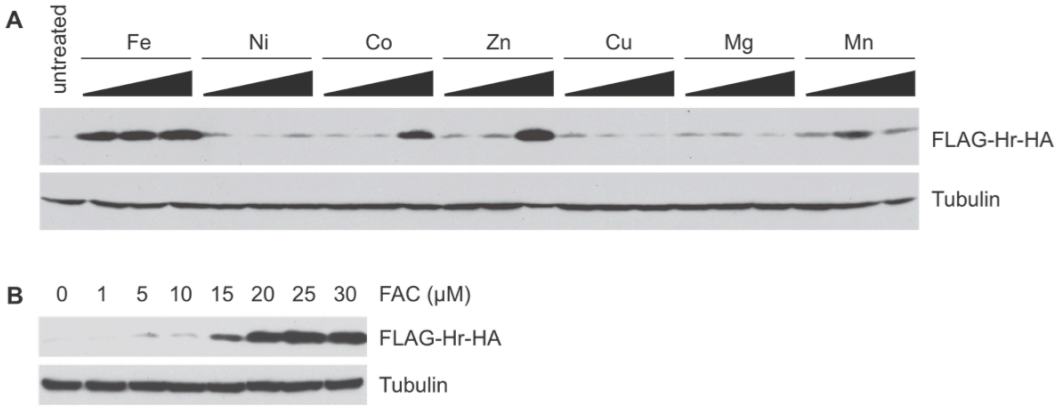

Figure 3-12. The FBXL5 Hemerythrin Domain Preferentially Responds to Iron Treatment. (**A**) Assessment of FBXL5 Hr accumulation in DFO treated HEK 293 cells by immunoblot analysis following addition of 30 μM, 100 μM, or 300 μM FAC, nickel chloride, cobalt chloride, zinc chloride, cupric sulfate, magnesium chloride, or manganese chloride. (**B**) Immunoblot analysis of FBXL5 Hr accumulation in DFO treated HEK 293 cells following addition of FAC at low concentrations.

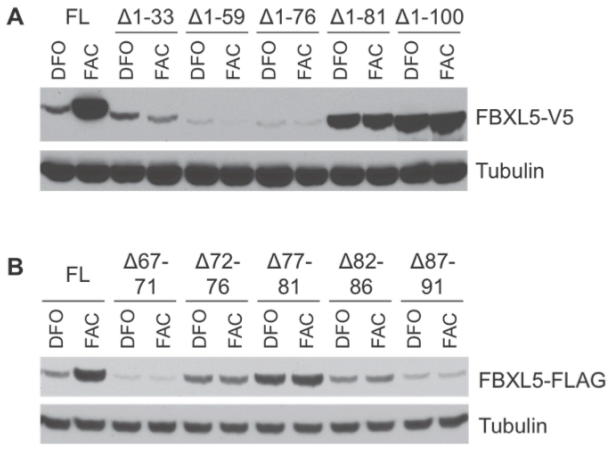

Figure 3-13. Mapping of a Degron in the FBXL5 Hemerythrin Domain

(**A**) FBXL5 protein accumulation was measured via immunoblot analysis in HEK 293T cells transfected with increasingly longer N-terminal de3letion constructs and treated with DFO or FAC. (**B**) Various FBXL5 constructs containing five amino acid deletions as indicated were transfected into HEK 293T cells and incubated with DFO or FAC. Protein accumulation was measured by immunoblot analysis.

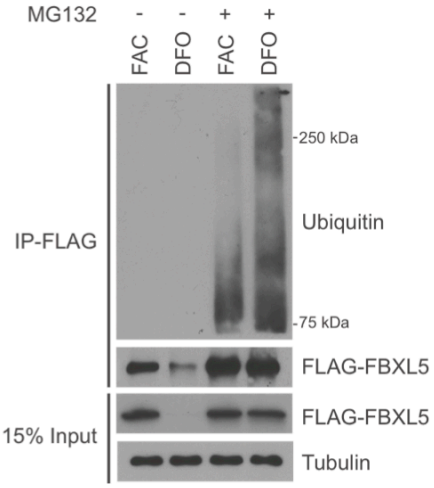

Figure 3-14. FBXL5 Displays Increased Polyubiquitination When Iron is Limiting
HEK 293 cells stably expressing FBXL5 were treated with FAC or DFO in the absence or presence of MG132. Immunoprecipitation of FBXL5 followed by immunoblot analysis demonstrated that FBXL5 displays increased polyubiquitination when iron is scarce compared to when it is abundant. (Figure courtesy of Julio Ruiz)

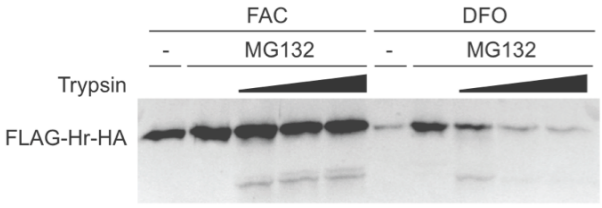

Figure 3-15. The FBXL5 Hemerythrin Domain Undergoes a Conformational Change as a Function of Iron Availability
HEK 293 cells stably expressing the FBXL5 Hr domain were treated with FAC or DFO in the absence or presence of MG132. Lysates from cells treated with MG132 were incubated for one hour with increasing concentrations of trypsin. Subsequently, Hr protein degradation was measured in the various lysates by immunoblot analysis. (Figure courtesy of Srinivas Chollangi)

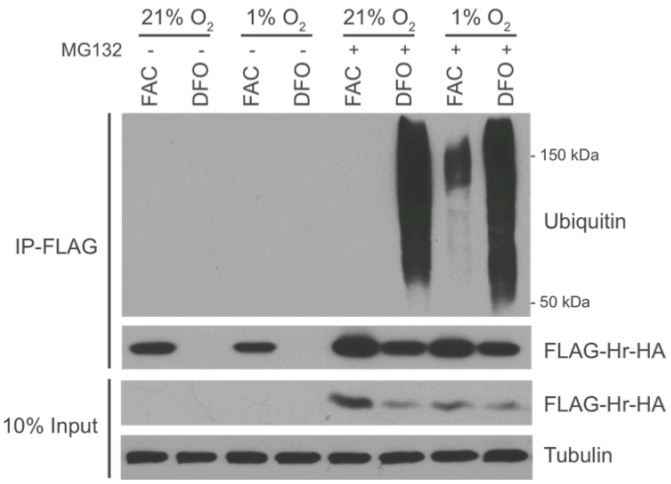

Figure 3-16. O_2 Dependent Regulation of the FBXL5 Hr Domain

HEK 293 cells stably expressing the FBXL5 Hr domain were treated with or without MG132 followed by addition of FAC or DFO. Cells were then incubated for 16 hours under high (~21%) or low (1%) O_2 conditions. The Hr domain was subsequently immunoprecipitated and subjected to immunoblot analysis to determine its polyubiquitination status. (Figure courtesy of Julio Ruiz)

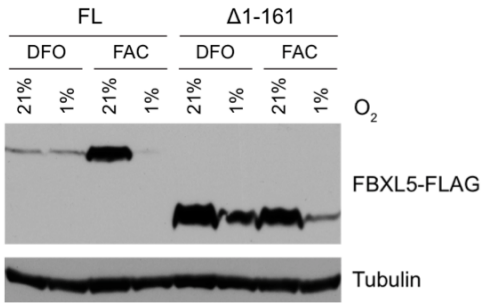

Figure 3-17. The Hemerythrin Domain is not Required for O_2 Dependent Regulation of FBXL5
Full-length (FL) and Δ1-161 FBXL5 constructs were transiently transfected into HEK 293T cells. Cells were treated with DFO or FAC and under high or low O_2 conditions. Protein accumulation was assessed via immunoblot analysis.

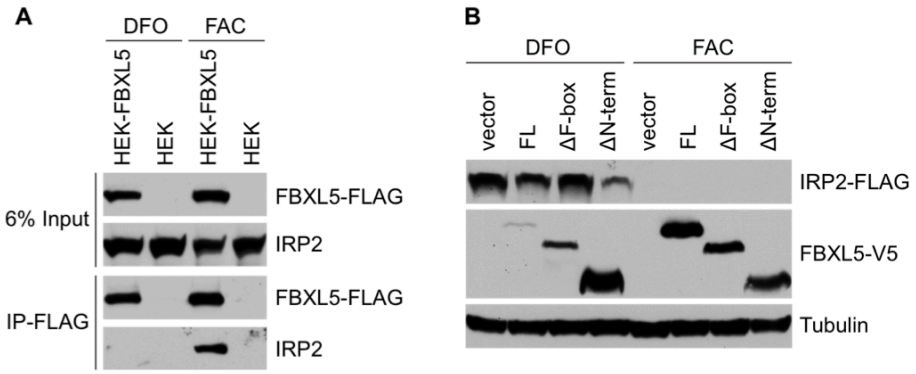

Figure 3-18. Iron Regulates FBXL5's Ability to Interact with IRP2
(**A**) IRP2 co-immunoprecipitates with FBXL5-FLAG in lysates from cells treated with FAC but not from cells treated with DFO. (**B**) HEK 293T cells were co-transfected with plasmids expressing IRP2-FLAG and FBXL5-V5 variants as indicated. Cells were treated with DFO or FAC and lysates were analyzed by immunoblotting. In DFO treated cells, overexpression of FBXL5 ΔN-term fails to degrade IRP2 to levels observed in FAC treated cells. (Salahudeen et al., 2009)

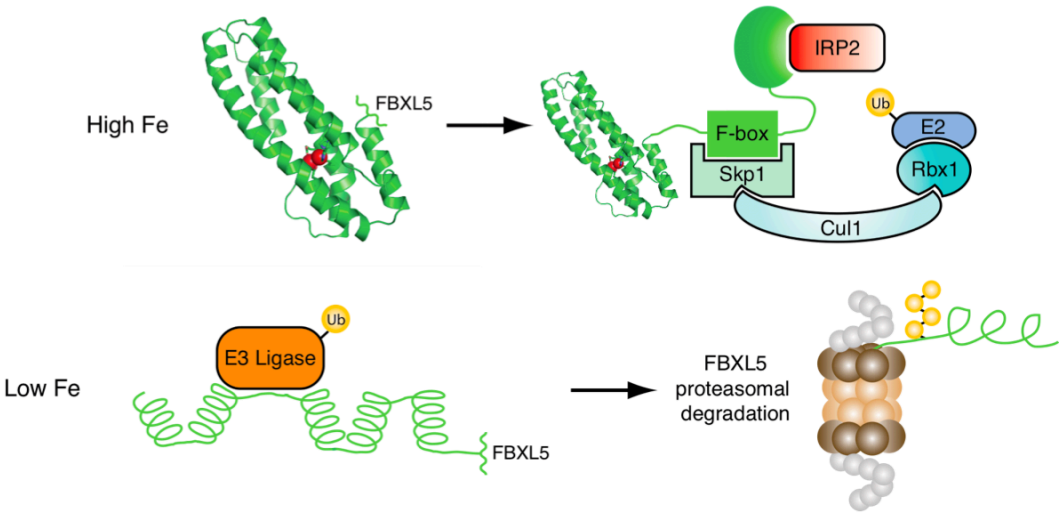

Figure 3-19. Model of How the N-terminal Hemerythrin Domain Controls Iron Dependent Stability of FBXL5

Under iron replete conditions the N terminus of FBXL5 adopts a hemerythrin fold, the protein is stabilized, and the SCF^{FBXL5} complex assembles. In contrast, under iron deficient conditions the Hr domain fails to bind iron resulting in a conformational change exposing a degron. Consequently, FBXL5 is polyubiquitinated by an unidentified E3 ligase and degraded in the proteasome.

CHAPTER FOUR

DISCUSSION AND FUTURE DIRECTIONS

Humans require adequate amounts of iron to sustain life. Failure to maintain sufficient amounts of iron impairs the function of many iron binding proteins and can lead to cell death. Conversely, excessive accumulation of free iron generates hydroxyl radicals that damage cellular components such as lipids, proteins, and nucleic acids. Since both iron deficiency and iron overload are deleterious to cells, it is no surprise that aberrant iron metabolism causes a number of human diseases. For example, inadequate levels of iron can lead to anemia and excess iron causes hemochromatosis. Thus, humans regulate iron homeostasis at the systemic and cellular levels to provide adequate concentrations of bioavailable iron while avoiding the detrimental affects of excess iron (Andrews and Schmidt, 2007; Muckenthaler et al., 2008).

Cellular iron homeostasis is regulated in part via the actions of Iron Regulatory Proteins. IRPs bind to cis-acting regulatory elements (IREs) in the 5' and 3' UTRs of a variety of genes involved in iron metabolism. Under iron depleted conditions, IRP binding to a single IRE in the 5' UTR of ferritin represses translation, whereas IRP binding to multiple IREs in the 3'UTR of TfR1 prevents endonucleolytic degradation of the mRNA. By virtue of their ability to regulate the expression of genes involved in iron import, utilization, and storage, IRPs coordinate the maintenance of cellular iron homeostasis (Hentze et al., 2004).

IRPs themselves are regulated as a function of iron availability. IRP1 alternates between two forms, an aconitase enzyme and an IRE binding protein. When iron is

plentiful, IRP1 ligates a Fe-S cluster and functions as a cytosolic aconitase. Under iron deficient conditions, IRP1 no longer binds a Fe-S cluster but instead recognizes IREs. Contrastingly, IRP2 is regulated through the UPS. Under iron replete conditions IRP2 is polyubiquitinated and degraded but when iron is scarce the protein is spared form this regulation, allowing it to accumulate to adequate levels to efficiently regulate IRE containing genes (Rouault, 2006).

From the 1990's through the 2000's a variety of groups attempted to delineate the mechanisms governing the iron dependent regulation of IRP2. Initially, many of these studies focused on the IDD region of IRP2 (Ishikawa et al., 2005; Iwai et al., 1998; Iwai et al., 1995; Kang et al., 2003; Yamanaka et al., 2003). Subsequently, several labs published data challenging the IDD dependent model and it was generally accepted that the IDD was not required for IRP2's regulation (Bourdon et al., 2003; Hanson et al., 2003; Wallander et al., 2006; Wang et al., 2004).

Taking the aforementioned reports into consideration it appeared that two fundamental question in the cellular iron homeostasis field remained unanswered. First, what is the E3 ligase that targets IRP2 for proteasomal degradation? Second, what are the mechanisms cells use to sense iron levels with concomitant regulation of IRP2 stability? With these outstanding questions as specific aims I began my dissertation research.

Iron Dependent Regulation of FBXL5 Stability

To identify the E3 ligase regulating IRP2 stability, an unbiased high throughput siRNA screen was performed. Based on the results of the screen, the SCF^{FBXL5} complex appeared to be the most promising candidate for an IRP2 E3 ligase. Knockdown of FBXL5 led to inappropriate accumulation of IRP2 in human cells. Moreover, loss of

FBXL5 expression causes increased IRP2 IRE binding activity with aberrant regulation of TfR1. Co-immunoprecipitation experiments showed an interaction between FBXL5 and IRP2. To determine whether FBXL5 could directly regulate IRP2 expression, the SCF^{FBXL5} complex was reconstituted in vitro and found to polyubiquitinate IRP2. In all, these results suggest that degradation of IRP2 requires the E3 ligase FBXL5.

With the identification of FBXL5, it appeared the first specific aim of my research had been answered. To address the second specific aim I focused my attention on further characterizing FBXL5. Interestingly, FBXL5 is regulated in a reciprocal fashion to IRP2. FBXL5 accumulates under conditions of excess iron, while its expression is downregulated when iron or O_2 is limiting. This led us to propose that the iron and O_2 dependent regulation of FBXL5 may have inverse affects on IRP2 stability.

However, at this point a mechanistic understanding of FBXL5's iron dependent regulation was lacking. Using a series of FBXL5 deletion constructs it was determined that iron dependent control of FBXL5 stability was mediated through its N terminus (residues 1-161). Bioinformatics predicted this region of FBXL5 encoded an iron binding hemerythrin (Hr) domain. Consistent with this prediction, X-ray crystallography revealed that the N-terminal portion of FBXL5 adopts a Hr fold with a diiron center. FBXL5 constructs in which the Hr domain's iron ligating residues have been individually mutated to alanine, fail to accumulate under iron replete conditions. Moreover, the Hr domain's expression is preferentially induced with iron treatment compared to six other metals tested. Together these data suggest that the Hr domain functions as an iron sensory module to regulate FBXL5 stability.

FBXL5's polyubiquitination status correlates with the protein's expression profile as a function of iron availability. Under iron replete conditions when the protein is expressed at high levels, FBXL5 exhibits low levels of polyubiquitination. Conversely, when cells are treated with the iron chelator DFO and FBXL5 accumulation is attenuated, the protein displays a more pronounced level of polyubiquitination. Additionally, treatment of cells with the proteasome inhibitor MG132 substantially increases FBXL5 expression, suggesting FBXL5 is regulated in a proteasome dependent manner. Consistent with these data, deletion experiments indicate that residues 77-81 of FBXL5 may be part of a degron. A limited proteolysis assay was performed to assess whether the FBXL5 Hr domain undergoes a conformation change as a function of iron availability. The Hr domain from cells treated with iron prior to lysis was insensitive to proteolysis. In contrast, Hr protein from DFO treated cells was efficiently degraded when incubated with protease following lysis.

The finding that an iron binding Hr domain regulates FBXL5 stability was particularly significant. This data suggested that iron functions as a ligand to regulate a molecular switch in the Hr domain to control FBXL5 stability. This type of ligand dependent regulation has been observed with multiple F-box proteins in plants and algae that bind small molecules such as Auxin and Jasmonate. For example, the association of the plant F-box TIR1 and its substrate Aux/IAA is positively regulated by Auxin binding to T1R1 (Tan et al., 2007). In a similar manner, binding of Jasmonate to the F-box protein COIl, enhances the interaction between COI1 and JAZ proteins (Chini et al., 2007; Thines et al., 2007). In red algae, Fbx3 binds Mg-protoporphyrin IX which negatively regulates binding to its substrate cyclin 1 (Kobayashi et al., 2011). While

multiple F-box proteins in plants and algae are known to sense metabolites in order to regulate downstream pathways, FBXL5 is the first example of a metazoan F-box protein to function in an analogous manner. However, in contrast to plant and algae F-box proteins, FBXL5 does not bind a small molecule but instead a metal. In addition, binding of iron via the Hr domain is not predicted to control an interaction with its substrate but instead regulate FBXL5 stability.

Iron binding to the FBXL5 Hr domain is predicted to regulate a molecular switch controlling the accessibility of a degron. This type of regulation is reminiscent of the yeast ER protein Pca1, which functions as an ATPase and exporter of the toxic metal cadmium. In the absence of cadmium, a degron is exposed and Pca1 is targeted for proteasomal degradation. However when cadmium levels are high, Pca1 binds cadmium eliciting a structural change that is purported to mask a degron and spare the protein from degradation. Upon binding cadmium and being stabilized, Pca1 may be excreted from the cell in order to control cadmium levels (Adle et al., 2009). Thus, both FBXL5 and Pca1 stabilities are dependent on binding of their cognate metals to cause a conformational change. Moreover, both proteins functions as sensors to maintain homeostasis of their respective metals.

Misfolded or damaged proteins are also regulated by conformational changes that bring normally buried degrons to the surface of the proteins. In some cases these degrons are assumed to be hydrophobic in nature promoting their interaction with chaperones, which eventually leads to protein degradation in the proteasome. In other cases, exposed hydrophobic patches promote formation of protein aggregates that are targeted for degradation via the UPS. These regulatory mechanisms are collectively known as the

quality control pathway (Kubota, 2009; Schrader et al., 2009; Sorokin et al., 2009). Our studies on FBXL5 suggest that residues 77-81 of the Hr domain may be part of a degron controlling the protein's stability. However, in contrast to the quality control degradation pathway, which as mentioned above recognizes proteins via their exposed hydrophobic residues or aggregation, FBXL5 does not appear to be regulated in this fashion. With the exception of V89, residues 77-81 of FBXL5's putative degron are not hydrophobic. However, additional studies will need to be performed in order to better define the degron sequence in the FBXL5 Hr domain. An X-ray crystal structure of the FBXL5 Hr domain in its apo form may be able to capture a conformational change and more clearly define potential regulatory sequences. In addition, bioinformatics could help determine whether the Hr domain contains any consensus sequences from degrons in the quality control pathway or in known E3 ligase substrates. Most importantly, identification of the E3 ligase regulating FBXL5 stability is needed for validating the importance of the residues currently proposed to form a degron. With an identified E3, the required elements for mediating an interaction with FBXL5 could be delineated.

Another mechanism that is known to be involved in F-box protein regulation is auto-ubiquitination (Cardozo and Pagano, 2004). This mode of regulation can occur in two forms, cis or trans. Auto-ubiquitination of F-box proteins in is believed to occur as a function of substrate availability. Under the auto-ubiquitination model, substrates shield their cognate F-box protein from ubiquitination. When substrates are abundant, the SCF complex catalyzes polyubiquitination of F-box protein substrates. However, when substrates have been depleted via proteasomal degradation, the SCF complex polyubiquitinates the F-box protein. Auto-ubiquitination in cis has been shown to

regulate the protein HOS. Deletion of the F-box domain from HOS greatly increases the protein's half-life and decreases its polyubiquitination status (Li et al., 2004) Alternatively, auto-ubiquitination can occur in trans when a specific F-box protein can interact with itself, and target its own SCF dependent degradation. One example of auto-ubiquitination of an F-box protein in trans may be Skp2. Skp2 is efficiently degraded in quiescent cells in an F-box independent but CUL1 dependent manner (Wirbelauer et al., 2000). Our data suggest that FBXL5 is not regulated through an autocatalytic mechanism. Deletion of the FBXL5 F-box domain still results in preferential protein accumulation under iron replete versus iron deplete conditions demonstrating that FBXL5 is not regulated by auto-ubiquitination in cis. Moreover, knockdown of FBXL5 has no affect on expression of the Hr domain alone, as the protein displays enhanced expression under high iron treatment, suggesting that FBXL5 is not regulated by auto-ubiquitination in trans (data not shown). However, work done by the Elledge lab demonstrated that FBXL5 accumulation increases with overexpression of a dominant-negative CUL1 construct (Yen and Elledge, 2008). These data suggest at least two possibilities regarding FBXL5's mechanism of regulation. First, an unknown SCF complex that does not contain FBXL5 may regulate FBXL5 expression levels. Second, because there are multiple SCF complexes with many substrates, inactivation of CUL1 may have pleiotropic effects on cells and cause non-specific stabilization of FBXL5.

Oxygen Dependent Regulation of FBXL5 Stability

In addition to iron availability, it was also discovered that FBXL5 stability is regulated as a function of oxygen. FBXL5 expression is downregulated when cells are deprived of O_2. Interestingly, analogous to its iron dependent regulation, O_2 dependent

regulation of FBXL5 occurs in a manner that is inverse to IRP2. This led us to propose that changes in O_2 availability leading to stabilization of IRP2 may be mediated through decreased FBXL5 stability.

The mechanisms controlling O_2 dependent regulation of FBXL5 have proven difficult to delineate. While the Hr domain of FBXL5 is both necessary and sufficient to confer iron regulation, this domain is not required to confer O_2 dependent regulation. An FBXL5 construct lacking the Hr domain is still destabilized under hypoxic conditions. Thus, it appears that O_2 regulates FBXL5 through multiple inputs. This may be necessary in order to fine-tune the expression of FBXL5 under different physiological conditions.

One of the methods we have utilized to delineate the mechanisms controlling oxygen dependent regulation of FBXL5 via its Hr domain is X-ray crystallography. Among the Hr domain structures solved to date, the FBXL5 Hr is most structurally homologous to the bacterial DcrH Hr. However, while the two Hrs share a similar protein fold, the manner in which these domains are regulated by O_2 appears to be distinct. The DcrH Hr contains a putative substrate channel purported to facilitate diffusion of O_2 to the diiron center and cause rapid autoxidation (Isaza et al., 2006), whereas such a pronounced channel does not exist in the FBXL5 Hr. Moreover, O_2 binding to the DcrH Hr causes a conformational change in which the N terminal loop becomes tightly packed to the helical bundle and is predicted to regulate the aerotactic signaling function of DcrH (Isaza et al., 2006). Conversely, in the FBXL5 Hr, no homologous N terminal loop exists. Instead, O_2 appears to regulate the stability of the FBXL5 Hr via the UPS.

In this study we have demonstrated that the FBXL5 Hr domain shows increased polyubiquitination and decreased protein accumulation under O_2 deficient conditions.

Nevertheless, despite our efforts to crystallize the FBXL5 Hr in different forms including oxy, we were only able to obtain structures in which O_2 was absent from the binding pocket. One possible explanation for lack of O_2 binding is that under the conditions used to purify and crystallize the domain it is not possible to capture the O_2 bound form. Another explanation is that the domain does not bind O_2. Alternatively, it may be that the binding of O_2 is too transient to capture an oxy form of the domain. Such is the case for the bacterial Hr domain from DcrH. The DcrH protein binds O_2 with a $t_{1/2}$ of less than a minute (Xiong et al., 2000). This is in stark contrast to the Hr domains from marine invertebrates which have O_2 binding $t_{1/2}$ of ~20 hours (Farmer et al., 2000). Nevertheless, if the FBXL5 Hr does bind O_2 it is reasonable to predict that in its oxy form the domain adopts an alternative conformation to the one presented here. In this confirmation residues F123 and M127 would have to be displaced from the binding pocket and E58 would have to rotate away from the μ-hydroxyl allowing O_2 to interact with Fe2 and the μ-hydroxyl. Thus, the structure reported here may represent a moderately destabilized state where a degron is partially exposed. Consistent with this hypothesis are the disordered residues S81 and D82, and the primary iron coordination shell residue H80, which is in an unstructured region of the domain. In all Hr structures solved to date the primary coordination shell ligands are found within alpha helices (French et al., 2008). Interestingly, residues 80-81 may correspond to part of a degron as demonstrated by our molecular experiments. Future work will need to focus on using biophysical approaches such as electron paramagnetic resonance spectroscopy to determine whether the FBXL5 Hr domain binds O_2.

Many cellular processes such as oxidative phosphorylation and chromatin remodeling are dependent on both iron and O_2 (Ozer and Bruick, 2007). Therefore, it is not surprising that cells have evolved to coordinate the regulation of iron and oxygen metabolism. Similar to iron, O_2 levels must be maintained in an optimal range in order to provide sufficient amounts for critical cellular processes, while avoiding oxidative damage caused by excess levels (Peyssonnaux et al., 2008). In mammalian cells, oxygen homeostasis is maintained by the dimeric transcription factor hypoxia inducible factor (HIF). HIF contains a constitutively expressed β subunit and a differentially expressed α subunit. HIF-α is preferentially degraded under normoxic conditions precluding formation of an active HIF heterodimer. Conversely, under hypoxic conditions, the α subunit is stabilized promoting its interaction with the β subunit. The transcription factor is subsequently translocated to the nucleus where it regulates a cohort of genes to elicit and adaptive response to low O_2 availability (Huang et al., 1998; Salceda and Caro, 1997). HIF target genes are involved in various cellular processes such as growth, survival, proliferation, angiogenesis, glucose metabolism, and erythropoiesis (Semenza, 2003).

HIF-α is preferentially degraded when O_2 is plentiful via the UPS. An E3 ligase complex containing the substrate recognition motif VHL regulates HIF-α polyubiquitination. Under normoxic conditions, a series of enzymes called HIF prolyl hydroxylases (HPH) posttranslationally regulate HIF-α. As their name suggests, HPHs hydroxylate two proline residues on the HIF-α degron (Bruick and McKnight, 2001; Epstein et al., 2001; Ivan et al., 2002; Masson et al., 2001). Prolyl hydroxylation is a key

step in the regulation of HIF-α expression. Hydroxylation of proline residues on the HIF-α degron promotes an interaction with VHL, leading to ubiquitination and proteasomal degradation of HIF-α (Hon et al., 2002; Min et al., 2002). HPHs are thought of as oxygen sensors due to their requirement of O_2 binding for substrate hydroxylation. Consistent with this hypothesis, HPH's O_2 binding affinities correlate with their in vivo activities (Ozer and Bruick, 2007).

In addition to oxygen, HPH activity is dependent on intracellular iron availability. The O_2 in the active site of HPHs is ligated in part by iron. As a result, treating cells with the iron chelator DFO abolishes HPH activity and stabilizes HIF under normoxic conditions (Peyssonnaux et al., 2008). Due to HPH's dependence on iron for activity it has been hypothesized that it may function as an iron sensor in addition to sensing O_2 availability (Ozer and Bruick, 2007; Peyssonnaux et al., 2008).

Whether or not HPH function as an iron sensor under physiological conditions remains poorly understood. However, it is becoming increasingly evident that HIF plays an important role in iron homeostasis. Underscoring this notion is the number of HIF target genes involved in iron metabolism including, ceruloplasmin, transferrin, TfR1, DMT1, and hepcidin. (Salahudeen and Bruick, 2009). Moreover, intestine specific knockout of HIF-2α in mice inhibits enterocyte iron uptake resulting in reduced serum and liver iron levels with concomitant downregulation of hepcidin expression (Mastrogiannaki et al., 2009; Shah et al., 2009).

Another connection between iron an oxygen homeostasis is found in the IRP/IRE regulatory pathway. As discussed in Chapter One, HIF-2α contains an IRE in its 5'UTR (Sanchez et al., 2007). Similar to the regulation of ferritin, IRP binding to its IRE under

conditions of iron deficiency inhibits HIF-2α translation, while under iron replete conditions its expression is derepressed. Interestingly, IRP1 but not IRP2, appears to predominantly regulate HIF-2α expression via its IRE (Zimmer et al., 2008). HIF-2α displays high expression levels in the kidney where it functions to upregulate erythropoietin, a hormone that stimulates the production of erythrocytes. Thus, the IRP/IRE regulatory system may negatively regulate red blood cell production under conditions where iron is limiting. This would be advantageous to the organism by preventing the production of heme and/or hemoglobin deficient erythrocytes (Sanchez et al., 2007).

Whether the FBXL5 Hr directly binds O_2 or not, it is evident that FBXL5 is regulated by oxygen. Similar to the HPH family of enzymes that responds to changes in iron and oxygen availability to regulate HIF, FBXL5 responds to the same metabolites and controls IRP2 expression. Future work to characterize the mechanisms controlling O_2 dependent regulation of FBXL5 may uncover novel insights into the crosstalk between oxygen and iron homeostasis.

Iron Dependent Regulation of the IRP2-FBXL5 Interaction

Intracellular iron levels control FBXL5 stability. Moreover, the physical interaction between FBXL5 and IRP2 may also be regulated as a function of iron availability. IRP2's interaction with FBXL5 is suppressed under iron deficient conditions. Consistent with an iron dependent interaction, overexpression of a Hr deficient FBXL5 construct that accumulates under iron deplete conditions, fails to degrade IRP2 to levels observed under iron replete conditions. Thus, in addition to the Hr domain that function

as an iron sensor to control FBXL5 stability, there may be other mechanisms by which iron regulates this E3 ligase subunit.

It is not surprising that FBXL5 is regulated at multiple levels, as this is a common phenomenon in biology. Many genes are regulated at the transcriptional, posttranscriptional, and posttranslational levels. Moreover, many biological pathways have multiple regulatory steps in order to assure tight regulation. With FBXL5 it appears that the protein is regulated by multiple posttranslational mechanisms. However, theses results raise new questions. How is the interaction between FBXL5 and IRP2 being regulated? Is FBXL5 or IRP2 being posttranslationally modified as a function of iron availability to enhance their interaction? Similar to iron dependent regulation of FBXL5 stability via its Hr domain, is FBXL5 binding a metal or other small molecule to facilitate its binding to IRP2? Alternatively, is an ancillary protein that is regulated by intracellular iron levels necessary for the interaction between FBXL5 and IRP2?

To identify interaction partners of FBXL5 that may mediate this iron dependent phenomenon one could use a proteomics approach. Proteomics can also be employed to identify posttranslational modifications on FBXL5. Work done by the Leibold lab using 2-D gel electrophoresis and mass spectrometry to characterize IRP2 modifications revealed that IRP2 is phosphorylated in an iron independent manner (Wallander et al., 2008). To date, no other posttranslational modifications of IRP2 have been identified. Therefore, it is tempting to speculate that FBXL5 is modified as a function of iron availability and not its substrate. If this conjecture were true, then this would be unique for the F-box family of proteins. Many F-box substrates are posttranslationally modified to enhance the interaction with their cognate F-box proteins (Cardozo and Pagano, 2004;

Ravid and Hochstrasser, 2008; Schrader et al., 2009). However, an F-box protein being posttranslationally modified to control binding to its target proteins has not been described.

The region of FBXL5 that is required for its interaction with IRP2 is also unknown. FBXL5 contains six predicted leucine rich repeats, which are known to function as substrate recognition motifs in other F-box proteins (Kobe and Kajava, 2001). However, which, if any of these repeats are required for FBXL5 substrate binding remains an open question. Using truncation constructs lacking the different domains found in FBXL5 one could identify the required regions for substrate interaction. Once the region of FBXL5 responsible for mediating its interaction with IRP2 has been identified it will be easier to determine whether that region is modified in response to fluctuations in iron availability.

Obtaining a crystal structure of full-length FBXL5 may also help address how its interaction with substrates such as IRP2 is regulated as a function of cellular iron levels. For these experiments it would be ideal to express recombinant FBXL5 in human cells to ensure that a soluble protein is produced in a system that ostensibly contains the regulatory mechanisms controlling FBXL5. HEK 293 F cells is one example of a cell line that is amenable to suspension culture and expresses relatively high levels of recombinant protein compared to other mammalian cells. Thus, FBXL5 could be expressed in 293 F cells under iron replete and iron deplete conditions, followed by purification. If crystals of the protein were obtained and their respective structures solved, a conformational change to the protein or binding of a ligand to a domain other then the Hr may be observed. Moreover, co-crystallizing FBXL5 and IRP2 would also be important for

demonstrating how the two proteins interact. Delineating the mechanisms that regulate the interaction between FBXL5 and IRP2 may reveal additional iron sensing factors and/or mechanisms that control iron homeostasis via FBXL5 and the IRP/IRE regulatory system.

Our data indicates that IRP2 and apo-IRP1 are SCF^{FBXL5} substrates. A previous report suggests that $p150^{Glued}$, a protein involved in vesicular transport, is also a FBXL5 substrate (Zhang et al., 2007). One could imagine that besides these three substrates there are additional FBXL5 targets. To address this question, a proteomics approach could be used. Using either affinity purification of a substrate trapping FBXL5 mutant, or stable isotope labeling with amino acids in cell culture (SILAC) using FBXL5 knockdown cell lines, other putative substrates can be identified. Future studies identifying additional FBXL5 targets could reveal that FBXL5 plays a role in regulating iron and oxygen homeostasis independent of the IRP/IRE regulatory system.

Another intriguing question is whether or not FBXL5 uses the same protein domains to recognize all of its substrates or if unique domains or conformations can regulate substrate recognition. Moreover, are all FBXL5-substate interactions regulated by iron availability, or are there regulatory mechanisms that confer selectivity? It is reasonable to propose that based on FBXL5's stability, it would be unable to regulate its target genes under low iron or low oxygen availability. However, substrate recognition does not necessarily have to be regulated as a function of iron availability.

FBXL5's Physiological Role in Iron Homeostasis

Abrogation of FBXL5 expression via RNAi leads to inappropriate accumulation of IRP2 under iron replete conditions in a variety of human cell lines. The IRP2 that

aberrantly accumulates following decreased FBXL5 expression is functionally active and binds IREs. Moreover, under these conditions IRP2 misregulates the IRE containing genes. Together these data suggest that FBXL5 is necessary for maintaining iron homeostasis.

While the aforementioned data demonstrate that FBXL5 is necessary for maintaining proper iron homeostasis in mammalian cell culture models, they do not address its relevance for iron homeostasis in a physiological setting. It could be speculated that deletion of FBXL5 in an animal model would lead to constitutive IRP2 stabilization with aberrant IRE gene expression similar to cell culture studies. Consistent with this postulate is the zebrafish mutant *shiraz*. The *shiraz* fish contains a mutation to grx5, a gene involved in the synthesis of Fe-S clusters. Loss of grx5 functions inhibits Fe-S biogenesis and causes IRP1 to assume a constitutive apo form. Apo-IRP1 IRE binding activity is refractory to changes in iron availability and as such constitutively binds IRE containing genes. Due to apo-IRP1 inhibiting translation of eALAS, the rate-limiting step in heme biosynthesis, the *shiraz* fish have an embryonic lethal phenotype caused by hypochromic anemia (Wingert et al., 2005). Similar to zebrafish with loss of grx5 expression, humans with grx5 mutations develop anemia in addition to some iron overload (Camaschella et al., 2007). Thus, FBXL5$^{-/-}$ mice might be expected to develop similar phenotypes due to constitutive stabilization of IRP2 and apo-IRP1.

Recently a study was published where several groups conducted a forward genetics screen in mice. One of the mice strains obtained from this screen contained a FBXL5 mutant where methionine 127 has been changed to lysine. Mice homozygous for this mutation display embryonic lethality, demonstrating that FBXL5 is required for

murine development (Ching et al., 2010). However, this group did not characterize the cause of the embryonic lethality and therefore it is unknown whether or not the phenotype is caused by defects in iron homeostasis. To address this question inducible and tissue specific FBXL5 knockout mice may need to be generated. Of particular interest will be mice lacking FBXL5 in the intestine, liver, and brain, to determine whether FBXL5 plays a role in iron absorption, hepcidin expression, and neurodegeneration, respectively. However, due to the possibility that FBXL5 has multiple substrates outside the IRE/IRP regulatory system, it may be that loss of FBXL5 expression in mice causes pleiotropic affects that mask FBXL5's function in iron homeostasis.

In addition to mouse models to determine FBXL5's physiological role in regulating iron homeostasis, of great interest will be clinical studies to determine if patients with iron related diseases have mutations in FBXL5. Similar to zebrafish with constitutively active IRP1, humans with diminished FBXL5 function may have aberrantly elevated levels of IRP2 and apo-IRP1. Under this scenario one could predict that genes such as ferritin and eALAS that contain IREs in their 5'UTRs would be downregulated. Consequently, iron storage and heme synthesis would be inhibited. For genes such as DMT1 and TfR1 that contain IREs in their 3'UTR, inappropriately activated IRPs may cause a decrease in their expression leading to decreased iron export and import. Together, these globally misregulated IRE containing genes may cause anemia, iron overload, or contribute to the pathogenesis of neurodegenerative diseases. Future work genotyping patients with iron related disorders where no known mutation can be found may lead to the identification of disease causing FBXL5 mutations.

Summary

Collectively, using functional genomics, biochemistry, molecular biology, and structural biology, the data presented in this dissertation suggest a model in which its N-terminal Hr domain regulates iron dependent stability of FBXL5. Under this model, when intracellular iron levels are abundant, the Hr domain binds iron and adopts a conformation where its degron is less accessible. This results in stabilization of FBXL5, formation of the SCF^{FBXL5} complex, and degradation of IRP2. Conversely, when bioavailable iron levels are low, the FBXL5 Hr domain is unable to form a diiron center resulting in a structural change exposing a degron. In this more accessible state the degron is recognized by an unknown E3 ligase and FBXL5 is polyubiquitinated and degraded in the proteasome. Central to this model is the ability of the Hr domain to function as an iron sensing module to control FBXL5 stability. Iron dependent regulation of FBXL5 is predicted to be critical as it controls IRP2 expression levels, which in turn regulates key iron homeostasis genes. Thus, FBXL5 via its Hr domain enables cells to gauge bioavailable iron levels and control IRP2 expression accordingly, resulting in a tightly regulated circuit in the maintenance of iron homeostasis (Fig 4-1).

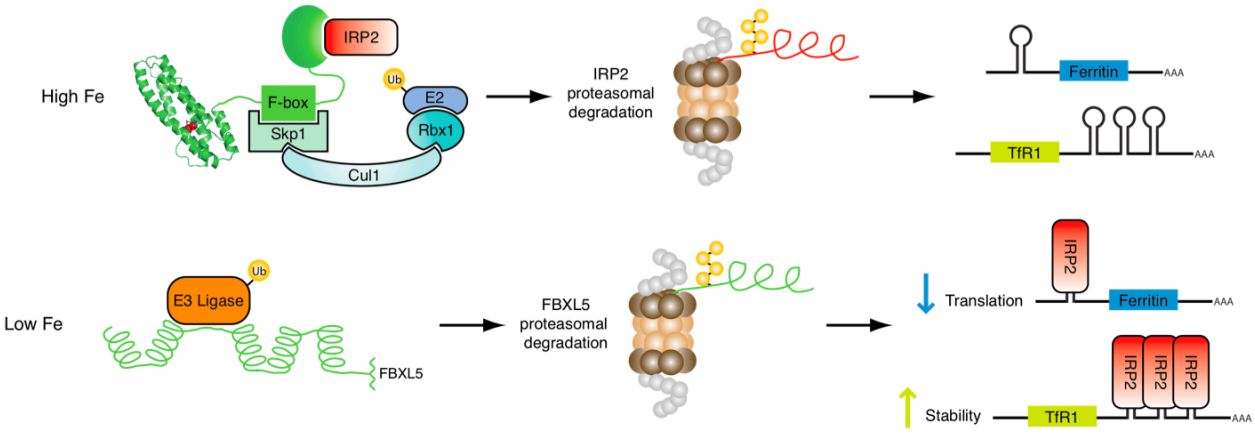

Figure 4-1. Model of How FBXL5's Iron Dependent Regulation Contributes to the Maintenance of Cellular Iron Homeostasis.

CHAPTER FIVE

METHODS

Cell Culture and Reagents

Non-tumorigenic immortalized human bronchial epithelial HBEC-30 cells (Ramirez et al., 2004; kindly provided by M. White), were grown in keratinocyte serum free medium supplemented with recombinant epidermal growth factor and bovine pituitary extract (Gibco). All other cell lines were grown in Dulbecco's Modified High Glucose Eagle Medium (HyClone). Tetracycline inducible cells were supplemented with 10% tetracycline-free fetal bovine serum (Clontech) while all other cells were supplemented with 10% fetal bovine serum (Atlanta Biologicals). All experiments carried out at 1% O_2 concentrations were performed in a hypoxic glove box (Coy Laboratory Products Inc). Transient transfections of plasmid DNA were carried out using Lipofectamine 2000 (Invitrogen) according to the manufacturer's instructions. Typically, $5x10^4$ cells were plated per well of a 24-well plate and incubated for 16 hr followed by transfection with 500 ng of DNA. Neomycin-resistant cells stably expressing epitope-tagged IRP2 or FBXL5 proteins were isolated over two rounds of clonal selection in the presence of 400 μg/mL G418 (Research Products Inc). HEK 293 cells stably expressing an N-terminal 3X FLAG and a C-terminal HA tagged FBXL5 hemerythrin construct and HEK 293 cells stably expressing 3X FLAG-FBXL5-HA were also generated over two rounds of clonal selection in the presence of 400 μg/mL G418. IRP1 and IRP1$^{3C>3S}$ Flp-In T-Rex HEK 293 cells were kindly provided by R. Eisenstein. FBXL5 shRNA knockdown cells were generated by stable transfection of HEK 293 TRex cells (Invitrogen) with

pSuperior vector (Oligoengine) encoding the FBXL5 shRNA: 5′- gaccccGCACAACA CUGCUCUCAGAuucaagagaUCUGAGAGCAGUGUUGUGCuuuuua-3′. Individual cell lines were isolated over two rounds of clonal selection in the presence of 1 μg/mL puromycin (Sigma). FBXL5 shRNA expression was induced upon addition of 1 μg/mL tetracycline hydrochloride (Sigma) to the culture medium for 72 hr.

RNAi

Transient transfections of siRNAs (Table 5, Appendix; Dharmacon) were carried out using Lipofectamine 2000 (Invitrogen) according to the manufacturer's instructions. Typically, $2x10^4$ cells were reverse transfected in 24-well plates with 20 pmoles siRNA duplex/well. Following 48 hr incubation, cells were treated with either 100 μM ferric ammonium citrate (FAC) or 100 μM deferoxamine mesylate (DFO) and incubated an additional 16 hr.

Plasmids

Human FBXL5 cDNA (NM_012161) was amplified from a human placenta cDNA library (kindly provided by C. Mendelson) using the oligonucleotides 5′-GGAGTCTAGAACCTTCGCCAGAGCGGCAGCAGG and 5′-GGAGGGATCCACCA TGGCGCCCTTTCCTGAAGAAGTGGAC and cloned into the pcDNA3.1/V5 vector (Invitrogen). FBXL5 cDNA was subcloned into the pCI-FLAG vector (kindly provided by X. Wang) using the 5′- GGAGGTCGACTCATTCGCCAGAGCGGCAGC and 5′- G GAGGGATCCACCATGGCGCCCTTTCCTGAAGAAGTGGAC oligonucleotides. Human IRP2 was amplified from a human cDNA library using the oligonucleotides 5′-AATTGGATCCACCATGGACGCCCCAAAAGCAGGATAC and 5′- CCTCCTCTAG ATGAGAATTTTCGTGCCACAAAG and cloned in frame with a C-terminal 3xFLAG

epitope tag into the pcDNA3.1 vector. The oligonucleotide 5′- TCGGATCCATGGCCG CCTACCCCTACGACGTGCCCGACTACGCCGGTGACGCCCCAAAAGCAGG was used to incorporate an N-terminal HA tag. Where appropriate, the overlap extension PCR method was utilized to construct deletion and point mutants using oligonucleotides listed in Table 6 (Appendix). For constructs containing a V5 epitope tag the pcDNA 3.1 vector was used while constructs containing a FLAG epitope were generated in the pCI vector. Full length human IRP2 was cloned into the pPICZb vector 3 (Invitrogen) in frame with C-terminal 1xMyc and 6xHIS epitope tags, and then cloned into the yeast centromeric shuttle vector pRS316 (kindly provided by B. Tu) downstream of the S. Cerevisiae GAL1 promoter. The vector was transformed into a protease deficient *S. cerevisiae* W303 strain using a standard Lithium Acetate protocol (Gietz and Woods, 2002). Transformants were isolated and maintained on SD-URA medium. All constructs were confirmed by sequencing.

Immunoblot Analysis

Samples were resuspended in SDS sample buffer and proteins were resolved by SDS-PAGE prior to immunoblot analysis. Rabbit anti-IRP1 antibody was kindly provided by R. Eisenstein. The Myc 9E10 antibody was purified (Harlow and Lane, 1988) on protein G agarose (Roche) from 9E10 hybridoma (ATCC) grown in Hybridoma SFM media (Gibco). α-FBXL5 antibody was generated from rabbits immunized with 6xHis-tagged FBXL5 (1-691) expressed in *E. coli* and further affinity purified from serum. Mouse monoclonal antibodies were obtained as follows: FLAG (Sigma, cat# F3165), V5 (Invitrogen, cat# R960-25), Tubulin (Sigma, cat# T6199), and Ubiquitin (Santa Cruz, cat# sc-8017). Immune complexes were detected by enhanced

chemiluminescence using peroxidase-conjugated secondary antibodies. Immunoblots using antibodies specific for tubulin were used as loading controls.

AlphaScreen Assay

To identify candidate E3 ubiquitin ligase(s) responsible for iron-dependent IRP2 ubiquitination, a library of 800 siRNA pools (Qiagen; 4 siRNA sequences/ pool/ gene), each designed to suppress expression of an individual human gene, was assembled. Included in the library were siRNAs targeting genes encoding proteins known to play a role in ubiquitination as well as proteins containing domains found within previously identified E3 ligase complexes (Ardley and Robinson, 2005; Hershko and Ciechanover, 1998; Li et al., 2008; Willems et al., 2004). HEK 293 cells stably transfected with the HA-IRP2-FLAG expression construct were reverse-transfected with siRNA using Lipofectamine 2000 (Invitrogen) in 96-well plates. Following 48 hr incubation, cells were treated with either 25 μM FAC or 100 μM DFO and incubated for 16 hr. Media was removed and 50 μL assay mixture/well (1X PBS, 0.5% TritonX-100, 5 ng/μL streptavidin donor beads (PerkinElmer), 5 ng/μL M2 FLAG acceptor beads (PerkinElmer), 2 pg/μL biotinylated α-HA antibody (Genscript), 250 μM phenylmethylsulfonyl fluoride (PMSF; Sigma), and 1X protease inhibitor cocktail (Sigma)) was added. Plates were incubated in the dark with gentle rocking for 4 hr and data collected with an EnVision microplate reader (PerkinElmer). Assays were performed in triplicate with bars indicating standard error. Validation of the top ~70 hits was performed using individual siRNAs (Dharmacon).

Electrophoretic Mobility Shift Assay

HA-IRP2-FLAG HEK 293 cells were transfected with siRNAs and treated with

either 100 μM FAC or 100 μM DFO for 16 hr. Cells were washed with 1X PBS, incubated in lysis buffer (20 mM HEPES (pH 7.4), 3 mM MgCl2, 40 mM KCl, 5% glycerol, 0.2% Nonidet P-40, 1 mM DTT, 250 μM PMSF, 1X protease inhibitor cocktail (Sigma)), and centrifuged at 17,000g for 15 min. Lysate containing 10 μg total protein was incubated in the presence of 100 kcpm ^{32}P-labeled in vitro transcribed RNA encompassing the rat L-ferritin IRE in a reaction mixture containing 1 mM DTT, 0.06 U/μL RNase inhibitor (New England Biolabs), 5% glycerol, 20 mM HEPES (pH 7.4), 40 mM KCl, and 3 mM MgCl2 for 1.5 hr at 4°C. For supershift reactions, 1 μL of α-IRP1 antibody or α-FLAG antibody was added to the mixture. Heparin was added to 2 mg/mL and the samples incubated another 10 min at 4°C. Protein-bound DNA complexes were resolved by electrophoresis in a 5% nondenaturing polyacrylamide gel at 4° C and visualized by phosphorimager analysis.

Quantitative Real Time PCR

Total RNAs were prepared using the Rneasy Mini Kit (Qiagen), treated with DNAse I (Roche) and converted to cDNA using Superscript II Reverse Transcriptase (Invitrogen) and random primers p(dN)6 (Roche). qRT-PCR was performed using the Power SYBR Green PCR Master Mix (ABI) on the 7900HT Fast Real-Time PCR System (ABI) using primer sets for human TfR1 (5′- GGTGACCCTTACACACCTGGATT and 5′-TGATGACCGAGATGGTGGAA), FBXL5 (5′- CTTACCCAGACTGACATTTCAG ATTC and 5′- GAAGACTCTGGCAGCAACCAA), and the 18S rRNA (5′- GATATGC TCATGTGGTGTTG and 5′- AATCTTCTTCAGTCGCTCCA) control. The thermal cycle conditions were as follows: 2 min at 50°C and 10 min at 95°C followed by 40 cycles of 95°C for 15 sec and 60°C for 1 min. Melting curves were performed at 95°C for

15 sec, 60°C for 15 sec and 95°C for 15 sec. All tests were performed in triplicate and all experiments were repeated three times. The mathematical transformations for primary data analysis were done by SDS2.0 (ABI). The amplification data were analyzed based on the equation: R (ratio) = $2^{-(\Delta Ct \text{ sample} - \Delta Ct \text{ control})}$. The results were expressed as fold changes of the treatment groups compared to the controls. p-values were determined by using Student's unpaired t-test.

Co-Immunoprecipitations

HA-IRP2-FLAG HEK 293 cells were transiently transfected using Lipofectamine 2000 (Invitrogen). Twenty-four hours after transfection, cells were treated with 10 μM MG132 (Boston Biochem) to block IRP2 and FBXL5 degradation for 1 hr followed by incubation with 100 μM FAC for an additional 6 hr. Cells were then washed with PBS, and incubated in lysis buffer containing 50 mM Tris/Cl (pH 8.0), 150 mM NaCl, 1.0% NP40, 250 μM PMSF, and 1X protease inhibitor cocktail (Sigma), and centrifuged at 17,000g for 15 min. Lysate (~500 μg) was incubated with 5 μL α-FLAG M2 affinity resin (Sigma) overnight, washed three times with lysis buffer, and the precipitates were subjected to immunoblot analysis. For co-immunoprecipitation of endogenous IRP2, reactions were carried out as described with two exceptions. Following incubation with MG132, FBXL5-FLAG expressing HEK 293T cells were treated with either 100 μM FAC or 100 μM DFO for 6 hrs and immunoprecipitates were eluted from the α-FLAG M2 affinity resin using a competitor FLAG-peptide prior to immunoblotting.

Recombinant Protein Expression and Purification

Bacteria, yeast, and insect cells were cultured under standard conditions unless otherwise specified. Recombinant E1 enzyme and ubiquitin were purchased from Boston

Biochem. K_0-GST-Ubiquitin was expressed in *E. coli* and purified by glutathione agarose (GE Healthcare). UbcH5a E2 was expressed and purified under similar conditions, except the GST tag was released by Thrombin protease (GE Healthcare) and removed using glutathione agarose. For recombinant IRP2 expression, yeast were grown to mid-log phase in YPGL medium and induced with galactose (2% w/v) for 16 hours (Caron et al., 1994). IRP2 was purified in anaerobic conditions (<1ppm O_2) in a Coy glovebox by Ni-NTA chromatography and gel filtration on a Superdex 200 column equilibrated in deoxygenated buffer. SCF^{FBXL5} was expressed in Sf9 cells grown in Sf900IIM media using the Bac to Bac system (Invitrogen). Briefly, SKP1, CUL1, and RBX1 were cloned into pFastBac HT vectors and FBXL5 was fused to a C-terminal 3xFLAG epitope tag in the pFastBac 1 vector. Recombinant baculovirus was generated according to the manufacturer's protocol, and SCF^{FBXL5} was expressed by infecting Sf9 cells in log phase growth. Optimal expression was observed at 55-60 hr with a ratio of 4:1:6:6 of FBXL5:SKP1:CUL1:RBX1 viruses. Soluble SCF^{FBXL5} was purified by binding to FLAG M2 Resin and eluted with FLAG peptide. Eluted fractions were dialyzed in a Slide-A-Lyzer (MWCO 10kDa; Pierce) or subjected to size exclusion chromatography in a Superdex 200 column in buffer containing 10 mM HEPES (pH 7.5), 1.5 mM MgCl2, 10 mM KCl, and 100 mM NaCl. The FBXL5 Hr domains was amplified by PCR using the oligonucleotides 5′-GGAGGGATCCGATGGCGCCCTTTCCTGAAGAAGTG and cloned into the pGST-parallel vector (Caron et al., 1994). Soluble GST-fusion protein was expressed in *E. coli* grown in media supplemented with 100 μM FAC and purified using glutathione agarose. The GST fusion tag was cleaved upon incubation with TEV protease for 6 hr at 24°C and the liberated Hr domain was purified by anion exchange

chromatography (HiTrap Q, GE Healthcare). Lastly, the protein was ran over a MonoQ anion exchange column. A centricon (VivaSpin MWCO 5kDa) was then employed to exchange the FBXL5-Hr domain into a buffer composed of 24mM Tris pH 8.0 and 50 mM NaCl, 4-5 mM BME and 0.5 mM TCEP. The resultant protein solution was then passed through a 0.22 μm filter.

In Vitro Ubiquitination Assay

Typical reactions are composed of 10 μg ubiquitin, 1 μg IRP2, 40 ng E1, 200 ng UbCH5a, and 1-3 μg of SCF^{FBXL5} in 50 μL reaction buffer containing 10 mM HEPES (pH 7.5), 10 mM KCl, 100 mM NaCl, 1.5 mM MgCl2, 1 mM DTT, 2 mM ATP, and 50 μM ferrous sulfate. Reactions were incubated at room temperature for 2 hr and resolved by electrophoresis in a 6% SDS polyacrylamide gel.

Crystallization and X-ray Diffraction Data Collection

Crystals of FBXL5-Hr (Native 1) were grown using the hanging-drop vapor diffusion method from drops containing 1 μL protein (5 mg/ml) and 1 μL of reservoir solution (10% PEG 6000, 0.1M HEPES pH 6.5) and equilibrated over 200 μL of reservoir solution. Plate-like crystals appeared after 1 day at 20°C and grew to their maximal extent by 2-3 days. Crystals were large in two dimensions (0.2 x 0.5 mm) and relatively thin (0.1 mm thickness). Cryoprotection was performed by transferring the crystals to a final solution of 25% ethylene glycol, 10% PEG6000, 0.1 M HEPES pH 6.5, increasing in 5% steps of ethylene glycol over the course of 10 minutes at 20°C. Crystals were flash frozen using liquid nitrogen. Native 1 crystals exhibited the symmetry of space group C2 with unit cell parameters of a=60.1 Å, b=75.8 Å, c=78.7 Å and b=111.8° and

contained two molecules of FBXL5-Hr per asymmetric unit. Native 1 crystals diffracted isotropically to a d_{min} of 1.85 Å when exposed to synchrotron radiation.

Crystals of the second form of FBXL5-Hr (Native 2) were obtained using an identical purification scheme as above, but protein was exchanged into buffer lacking reducing agent and allowed to incubate at 4°C for 24 hours. Native 2 crystals were grown using the hanging-drop vapor diffusion method from drops containing 1 μL protein (5 mg/ml) and 1 μL of reservoir solution (0.1 M Hepes pH 7.4, 25% PEG 3,350) and equilibrated over 50 μL of reservoir solution. Plate-like crystals appeared after 1 day at 20°C and grew to their maximal extent by 2-3 days. Crystals were similar in morphology to Native 1 crystals, i.e. large in two dimensions (0.2 x 0.5 mm) and relatively thin (0.1 mm thickness). Cryoprotection was performed by transferring the crystals to a final solution of (0.1 M Hepes pH 7.4, 25% PEG 3,350, 20% ethylene glycol) increasing in 5% steps of ethylene glycol over the course of 10 minutes at 20°C. Crystals were flash frozen using liquid nitrogen. Native 2 crystals exhibited the symmetry of space group $P2_1$ with unit cell parameters of a=76.3 Å, b=54.4 Å, c=78.2 Å and d=90.02° and contained four molecules of FBXL5-Hr per asymmetric unit. Native 2 crystals diffracted isotropically to a d_{min} of 2.10 Å when exposed to synchrotron radiation. Data were indexed, integrated and scaled using the HKL-3000 program package (Minor et al., 2006). Data collection statistics are provided in Table 3 (Appendix).

Phase Determination and Structure Refinement

Phases for Native 1 crystals of FBXL5-Hr were obtained from a two-wavelength anomalous dispersion experiment using the native iron atoms with data to a resolution of 2.5 Å. Four iron and two sulfur sites were located using the program SHELXD

(Schneider and Sheldrick, 2002); this represented two single-occupancy iron sites and one methionine sulfur site per FBXL5-Hr monomer. Phases were refined with the program MLPHARE (Otwinowski, 1991), resulting in an overall figure-of-merit of 0.59 for data between 44.7 and 2.5 Å. Phases were further improved by density modification and two-fold non-crystallographic averaging with the program DM (Cowtan and Main, 1998) resulting in a figure-of-merit of 0.85. An initial model containing about 86% of all residues was automatically generated by alternating cycles of the programs ARP/wARP (Morris et al., 2004). Additional residues were manually modeled in the programs O (Jones et al., 1991). Refinement was performed with native data to a resolution of 1.85 Å using the program PHENIX (Adams et al., 2002) with a random 5.1% of all data set aside for an R_{free} calculation. The current model contains two FBXL5-Hr monomers; included are residues 4-74, 77-80, 84-159 in molecule A and residues 4-74, 77-80, 84-160 in molecule B and 168 waters. The R_{work} is 0.170, and the R_{free} is 0.211. A Ramachandran plot generated with Molprobity (Davis et al., 2007) that 98.3% of all protein residues are in the most favored regions with the remaining 1.7% in additionally allowed regions.

Phases for the Native 2 crystals of FBXL5-Hr were obtained via molecular replacement in the program PHASER (McCoy et al., 2007) using the coordinates of FBXL5-Hr as a search model. Model building and refinement was performed as described above. The current model contains four FBXL5-Hr monomers; included are residues 5-80 and 83-159 in molecule A, residues 5-73, 77-80 and 83-159 in molecules B and C, residues 5-73, 77-80 and 84-160 in molecule D and 257 waters. The R_{work} is 0.200, and the R_{free} is 0.277. A Ramachandran plot generated with Molprobity indicated that 98.5% of all protein residues are in the most favored regions with the remaining 1.5% in

additionally allowed regions. Phasing and model refinement statistics are provided in Table 3 (Appendix).

Cell Culture Based Ubiquitination Assay

HEK 293 cells stably expressing an N-terminal 3X FLAG and C-terminal HA tagged FBXL5 Hemerythrin domain (HEK-Hr) were treated with or without 30 μM MG132 (Boston Biochem) for 1 hour followed by addition of 50 μM FAC or 50 μM DFO. Cells were then incubated for 16 hours under high (~21%) or low (1%) oxygen conditions. Cell extracts were prepared by adding lysis buffer containing 50 mM Tris-HCl (pH 8), 150 mM NaCl, 1% triton X-100, 250 μM PMSF (Sigma), 1X protease inhibitor cocktail (Sigma) and 10 mM N-ethylmaleimide. Lysates were incubated 20 minutes at 4°C, and cysteine (0.1% final concentration) was added to neutralize the N-ethylmaleimide. Lysates were clarified by centrifugation at 17,000 x g for 20 minutes and protein concentration was determined by the Bradford assay. Lysates (~1 mg) were incubated with 12 μL of FLAG M2 resin (Sigma) overnight to immunoprecipitate the Hr domain. Resin was washed three times with lysis buffer, and immunoprecipitated Hr was eluted using FLAG peptide. Proteins were resolved by SDS-PAGE and analyzed by immunoblotting. Hr protein levels were assessed using a FLAG antibody whereas an ubiquitin antibody was used to determine the polyubiquitination status of the immunoprecipitated Hr domain. The ubiquitination assay of full length FBXL5 was carried out using HEK 293T cells stably expressing a N-terminal 3X FLAG tagged FBXL5 construct. Cells were treated with or without 30 μM MG132 for 1 hour followed by incubation with 50 μM FAC or 50 μM DFO for 6 hours. The remainder of the assay was carried out as described for the aforementioned protocol of the Hr domain.

Limited Trypsin Proteolysis

HEK-Hr cells were treated in the presence or absence of 30 μM MG132 for 1 hour followed by treatment with either 50 μM FAC or 50 μM DFO for 6 hours. Cells were washed with ice cold PBS and lysed in 37 mM Tris-HCl (pH 8.0) containing 150 mM NaCl, 1% TritonX-100 and protease inhibitor cocktail (Sigma) at 4^{o}C for 10 minutes. Lysed cells were then centrifuged at 16,000g for 20 minutes and the supernatant was assessed for protein concentration using the Bradford assay (Biorad). Desired amount of trypsin (1 μg, 2 μg, or 3 μg; Promega) was then added to lysates containing 100 mg of total protein. Proteolysis was carried out at 37^{o}C for 1 hour after which the reaction was quenched by adding phenylmethylsulfonyl fluoride to a final concentration of 0.2 mM. The amount of undigested Hr in each sample was assessed by immunoblot analysis using a FLAG antibody.

FBXL5 Hemerythrin Metal Responsiveness Assay

HEK-Hr cells were treated 16 hours with 15 μM DFO to induce basal levels of Hr protein expression. Cells were subsequently left untreated or treated for six hours with 30 μM, 100 μM, or 300 μM, of either FAC, nickel chloride (Sigma), cobalt chloride (Sigma), zinc chloride (Sigma), cupric sulfate (Sigma), magnesium chloride (Fisher), or manganese chloride (Sigma). Hr protein accumulation was determined by immunoblot analysis using a FLAG antibody.

Luciferase Gene Reporter Assay

Following 24 hr of transfection, HEK 293T cells were treated with either100 μM FAC or 100 μM DFO and incubated an additional 24 hr under atmospheric (~21% O_2) or low (1%) O_2 conditions. Cells were lysed in buffer (30 mM Tricine (pH 7.8), 8 mM

MgAc, 0.2 mM EDTA, 1% Triton) on ice, transferred to a 96-well plate, and ATP, CoA, β-mercaptoethanol, and Dluciferin (Molecular Probes) added to final concentrations of 375 μM, 375 μM, 50 mM, and 125 μM respectively. Luminescence was measured in a plate reader (Bio-Tek, Synergy HT). Assays were performed in triplicate with bars indicating standard error.

Appendix

Table 1. Data Set Primary RNAI screen

Rank	Gene	Score	Rank	Gene	Score
1	ANUBL1	177.20	41	ZNF295	90.25
2	VHLL	174.31	42	ZBTB8	89.91
3	FBXL5	158.37	43	CRBN	89.67
4	KIAA0182	153.63	44	KCTD16	88.86
5	RHOBTB2	148.63	45	MARCH5	88.47
6	TRIM32	148.01	46	TRIM63	87.84
7	BIRC8	142.00	47	KLHL11	87.69
8	ZBTB5	132.49	48	KCNA6	87.65
9	SF3B3	124.88	49	ZBTB10	86.52
10	KCTD17	119.64	50	ZBTB6	86.20
11	WDR76	119.20	51	TRIM45	86.06
12	KLHL14	118.41	52	CPSF1	85.52
13	KCTD15	116.55	53	RNF113B	83.80
14	RNF11	114.54	54	UBE2J1	83.36
15	CUL1	108.62	55	WDR5B	82.49
16	KLHL22	108.38	56	FBXL21	82.34
17	HIC2	107.77	57	UBE3B	81.91
18	ZBTB7A	106.66	58	ZBTB2	80.99
19	ZBTB43	106.46	59	UBE2Q1	80.99
20	FBXL15	106.11	60	C2orf37	80.43
21	WWP1	105.76	61	SMU1	80.09
22	LONRF2	105.27	62	LINCR	80.04
23	KBTBD2	103.96	63	UBE2L3	79.81
24	KLHL20	103.73	64	MARCH3	79.20
25	MICAL1	103.23	65	MYCBP2	78.73
26	VHL	103.00	66	TRAIP	78.54
27	ZBTB16	102.87	67	RSPRY1	78.53
28	TRIM9	99.88	68	TRIM11	78.36
29	MGRN1	99.09	69	MARCH2	77.23
30	CUL7	97.80	70	FBXO21	76.47
31	FBXO5	97.11	71	NFX1	76.05
32	GZF1	96.55	72	PJA1	75.33
33	NEURL	94.35	73	RNF207	75.09
34	UBE2O	94.27	74	OTUD7A	75.07
35	FBLIM1	93.94	75	ZMYND11	74.80
36	MARCH10	93.62	76	KCTD12	74.70
37	BTBD8	91.88	77	BTBD10	72.61
38	ZFAND3	91.39	78	BTBD11	72.02
39	TRIM8	90.89	79	SKP2	71.84
40	PIAS4	90.52	80	KCTD18	71.25

Rank	Gene	Score
81	TNFAIP1	71.14
82	COMMD4	70.96
83	DTL	70.69
84	KLHL26	70.42
85	ZBTB45	70.04
86	WDR26	69.73
87	FBXW10	69.33
88	C16orf44	69.25
89	COMMD8	68.93
90	ZBTB47	68.69
91	FBXO10	68.41
92	PCGF3	68.07
93	KBTBD8	67.26
94	NOSIP	66.61
95	AMBRA1	66.33
96	ZBTB37	64.54
97	WDR12	63.68
98	KLHL13	63.60
99	ZNF423	63.56
100	RUFY1	63.46
101	ARIH1	63.29
102	KLHL18	63.25
103	FBXL10	62.70
104	ZBTB3	62.15
105	RNF20	62.01
106	RC3H1	61.84
107	PRPF19	61.62
108	ZBTB48	61.61
109	RNF208	61.47
110	KCTD9	60.60
111	RNF40	60.47
112	WDSOF1	59.79
113	LRRC41	59.59
114	TRAF3	59.25
115	WDR32	59.11
116	ZFAND6	58.93
117	RING1	58.48
118	KCTD2	58.19
119	KLHL30	57.88
120	BTBD5	57.76
121	NEURL2	57.65
122	FBXO17	57.48
123	BTBD2	57.06

Rank	Gene	Score
124	VPS41	56.87
125	RNF122	56.87
126	RNF157	56.84
127	RNF12	56.65
128	PCGF5	56.63
129	RNF183	56.44
130	BTBD6	56.43
131	BTBD9	56.37
132	PCGF6	55.95
133	WDR40A	55.77
134	BTBD14B	55.43
135	ZBTB11	55.06
136	ZBTB1	54.96
137	MLL3	54.53
138	SHKBP1	54.46
139	KLHL3	54.43
140	UBE2D2	54.41
141	GNB2	54.13
142	TRIM2	54.09
143	ZBTB32	53.93
144	ZBTB20	52.68
145	FBXO45	51.65
146	RNF34	51.38
147	GRWD1	50.79
148	UBE2M	50.59
149	UBE2S	50.46
150	DET1	50.40
151	HECW1	49.77
152	VPS18	49.35
153	WDTC1	49.14
154	ZBTB7B	48.68
155	NSMCE1	47.99
156	MKRN2	47.55
157	ZFYVE19	46.59
158	WDR61	46.30
159	FHL1	46.22
160	SUGT1	46.08
161	KLHL32	45.82
162	PXMP3	45.71
163	MARCH6	45.70
164	DZIP3	45.64
165	KBTBD10	45.46
166	TRIM58	45.39

Rank	Gene	Score
167	FANCL	45.23
168	DTX3L	45.20
169	MSL2L1	45.16
170	TRIM60	45.04
171	RNF103	45.04
172	CBLC	44.74
173	FBXO9	44.61
174	UBE3C	44.49
175	TRIM25	44.43
176	WHSC1L1	44.42
177	UBE2Z	44.14
178	KBTBD6	44.13
179	KLHL9	44.10
180	DDA1	43.53
181	ASB4	43.49
182	LNX1	43.33
183	PCGF1	43.30
184	FBXO6	43.09
185	MARCH8	42.97
186	KBTBD7	42.95
187	RNF151	42.72
188	RHOBTB3	42.72
189	MIB2	42.37
190	TRAF6	42.35
191	KLHL7	42.21
192	ZNF650	42.15
193	WSB2	42.14
194	ZNFX1	41.31
195	STUB1	40.65
196	KLHL25	40.61
197	GMCL1L	40.47
198	TRPC4AP	40.35
199	KLHL6	40.10
200	KCTD4	40.03
201	ZBTB39	40.00
202	ZBTB38	39.95
203	COMMD2	39.87
204	SOCS1	39.85
205	KLHL2	39.69
206	PWP1	38.99
207	ZNRF3	38.91
208	TRIM37	38.71
209	UBE1C	38.63

Rank	Gene	Score
210	UBE2R2	38.49
211	UBE2E1	38.41
212	TRIM41	38.33
213	C4orf30	38.13
214	KCNV1	37.74
215	TRIM26	37.71
216	SH3RF1	37.60
217	TRIM69	37.43
218	RBX1	37.39
219	ZBTB4	36.31
220	SPSB2	36.18
221	RFPL4A	36.13
222	ZBTB41	36.06
223	ASB9	35.96
224	ASB16	35.93
225	CUL5	35.90
226	COMMD3	35.86
227	RCBTB1	35.75
228	C12orf51	35.70
229	ZNF645	35.49
230	ZBTB7C	35.42
231	FBXW7	35.41
232	RNF186	35.27
233	WDSUB1	35.25
234	SOCS3	35.06
235	SPRYD5	34.98
236	EDD1	34.94
237	ASB3	34.90
238	RBBP4	34.81
239	OSTM1	34.77
240	RNF180	34.39
241	MYNN	34.16
242	RNF175	34.11
243	IFRG15	33.93
244	PDZRN4	33.89
245	UBE2Q2	33.61
246	HACE1	33.60
247	RNF7	33.58
248	IRF2BP2	33.50
249	KCTD3	33.46
250	LIMK2	33.42
251	RNF185	33.38
252	ZBTB9	33.36

Rank	Gene	Score
253	TCEB2	33.36
254	RFPL2	33.22
255	KLHDC5	33.05
256	MID1	33.01
257	SKP1A	32.98
258	UBE2D4	32.81
259	SPSB1	32.80
260	ABTB2	32.72
261	CSRP1	32.71
262	BRWD1	32.70
263	ZNRF4	32.44
264	ARIH2	32.22
265	ASB11	32.14
266	TRIM52	32.14
267	CIAO1	31.91
268	FBXO38	31.87
269	HECTD2	31.81
270	BTBD1	31.75
271	ASB2	31.67
272	RNF4	31.41
273	KCTD14	31.36
274	MID2	31.35
275	ANKIB1	31.16
276	RNF44	31.14
277	OTUD7B	30.89
278	KCNC1	30.81
279	CUL3	30.75
280	FBXO46	30.74
281	RNF190	30.72
282	ARMC5	30.61
283	COMMD10	30.59
284	COMMD5	30.42
285	FBXO16	30.42
286	NFXL1	30.42
287	RNF167	30.41
288	RNF113A	30.27
289	WDR51B	30.02
290	ZNF313	29.96
291	INTS12	29.89
292	SOCS6	29.77
293	RAI1	29.62
294	HERC3	29.27
295	TRIM47	29.23

Rank	Gene	Score
296	UBOX5	29.06
297	FBXO39	29.06
298	EED	28.98
299	DPF1	28.93
300	KLHL1	28.92
301	RKHD3	28.89
302	TRIM17	28.86
303	UBE2B	28.68
304	VPRBP	28.54
305	TRIM7	28.52
306	UBE2L6	28.42
307	RNF141	28.29
308	ZNF294	28.28
309	UBE1L2	27.97
310	PIAS1	27.93
311	COPS5	27.91
312	KCNA7	27.83
313	GMCL1	27.74
314	RAB40A	27.70
315	C1orf164	27.65
316	KIAA0614	27.65
317	ASB10	27.63
318	UBE2E2	27.61
319	RNF145	27.53
320	CUL2	27.51
321	TRIM16L	27.46
322	TRIM65	27.43
323	RNF126	27.41
324	ASB8	27.40
325	TRIML1	27.38
326	RKHD1	27.28
327	LONRF1	27.27
328	KCTD8	27.22
329	ZBTB33	27.19
330	CBLL1	27.17
331	KLHL12	27.16
332	KCND2	27.16
333	KLHL34	27.11
334	SPOP	27.07
335	KLHL24	26.94
336	COMMD7	26.80
337	UBE2G1	26.66
338	SYVN1	26.62

Rank	Gene	Score
339	TRIM43	26.60
340	WDR5	26.52
341	BMI1	26.52
342	FBXO27	26.38
343	PARK2	26.30
344	TRIM72	26.21
345	RNF38	26.15
346	TRIM39	26.12
347	RNF148	26.04
348	FBXO36	26.01
349	BTBD14A	25.99
350	UBE2V2	25.79
351	RNF214	25.73
352	MKRN4	25.63
353	FBXO33	25.62
354	ZNRF1	25.60
355	SOCS5	25.59
356	ZBTB46	25.58
357	TNFAIP3	25.57
358	ZSWIM2	25.54
359	KCNS2	25.54
360	CISH	25.53
361	CUL4A	25.47
362	SOCS4	25.36
363	ASB7	25.28
364	BTBD16	25.25
365	TLE1	25.18
366	NSMCE2	25.15
367	TRIM59	25.12
368	TULP4	25.07
369	KCTD6	25.04
370	WHSC1	24.90
371	KBTBD1	24.90
372	SPSB4	24.79
373	C10orf46	24.76
374	BAZ1B	24.70
375	TRAF5	24.68
376	KCTD7	24.68
377	RNF165	24.58
378	UBE2A	24.55
379	LONRF3	24.50
380	UBE2G2	24.48
381	SHPRH	24.47

Rank	Gene	Score
382	KCNA5	24.46
383	RAD18	24.40
384	PPIL5	24.36
385	NHLRC1	24.27
386	ASB18	24.26
387	ASB12	24.22
388	TRIM50	24.19
389	RNF5	24.07
390	ZNF179	24.05
391	TRIM36	23.99
392	PIAS2	23.96
393	COMMD1	23.83
394	UBE2D3	23.81
395	TLE2	23.80
396	BIRC6	23.80
397	PJA2	23.72
398	ZBTB17	23.71
399	RNF168	23.70
400	CCNF	23.68
401	ZBTB44	23.68
402	KCNS1	23.65
403	TRIM21	23.57
404	RKHD4	23.54
405	FBXO31	23.52
406	IBRDC1	23.51
407	DTX1	23.38
408	RNF121	23.37
409	DTX2	23.28
410	BCL6B	23.18
411	ZNF449	23.00
412	RNF8	22.85
413	UBE2U	22.84
414	TRIM4	22.83
415	KBTBD5	22.76
416	UBE2F	22.65
417	IBRDC2	22.65
418	KCTD10	22.64
419	RNF212	22.60
420	WDR42A	22.60
421	TRIM54	22.59
422	TRIM5	22.55
423	TRIM56	22.46
424	C14orf4	22.40

Rank	Gene	Score
425	LRSAM1	22.31
426	ITCH	22.23
427	TRIM23	22.23
428	UBE1L	22.23
429	RNF13	22.19
430	ASB17	22.12
431	KLHL5	22.10
432	PCGF2	22.08
433	NEDD8	22.06
434	UBE2N	22.05
435	FBXW9	22.03
436	KCND3	21.99
437	TRIM24	21.96
438	RFFL	21.94
439	RNF144	21.94
440	FBXO30	21.89
441	ZBTB25	21.82
442	BACH2	21.65
443	KLHDC6	21.63
444	WDR22	21.62
445	FASTKD5	21.62
446	LGALS3BP	21.61
447	BCL6	21.60
448	RNF146	21.57
449	UHRF2	21.53
450	FBXL14	21.53
451	RNF123	21.46
452	LOC123103	21.42
453	UBR4	21.42
454	FBXO15	21.39
455	RAG1	21.37
456	BIRC2	21.30
457	39515	21.28
458	PEX10	21.28
459	ZNRF2	21.16
460	HERC2	21.13
461	TRIM64	21.12
462	PRDM16	21.09
463	TRIM68	21.09
464	EGFL9	20.94
465	BSN	20.92
466	LOC399940	20.92
467	SMURF2	20.83

Rank	Gene	Score
468	FBXW2	20.71
469	FBXW11	20.63
470	TRIM35	20.62
471	RNF150	20.61
472	BIRC7	20.53
473	PAFAH1B1	20.49
474	UBE4B	20.45
475	UBR2	20.45
476	ZBTB26	20.43
477	FBXL20	20.40
478	MIB1	20.38
479	FBXO7	20.29
480	LOC399937	20.28
481	ZMIZ1	20.27
482	KLHL10	20.25
483	GAN	20.19
484	FBXL16	20.17
485	TRIM15	20.16
486	KCTD13	20.16
487	RNF182	20.13
488	ZBTB24	20.08
489	IBRDC3	20.02
490	KCNA10	19.96
491	ANAPC2	19.94
492	ENC1	19.89
493	DDB1	19.88
494	TRIM42	19.85
495	TRIM48	19.84
496	TRAF7	19.81
497	KCTD20	19.81
498	WBP7	19.80
499	LOC339745	19.67
500	RAPSN	19.66
501	IPP	19.50
502	KIAA1542	19.48
503	UHRF1	19.47
504	ASB14	19.44
505	RNF25	19.40
506	BIRC3	19.40
507	TRIM10	19.37
508	MNAB	19.29
509	RNF32	19.28
510	KLHL21	19.27

Rank	Gene	Score
511	C16orf28	19.16
512	RNF133	19.14
513	DTX4	19.13
514	BIRC4	19.10
515	MICAL2	19.06
516	HERC6	19.02
517	FBXL4	19.02
518	LNX2	19.00
519	UBE1	18.98
520	ASB5	18.93
521	PHF17	18.93
522	UBE2V1	18.92
523	RAB40C	18.91
524	BACH1	18.77
525	ZNF509	18.75
526	RBCK1	18.74
527	RNF166	18.71
528	RNF14	18.69
529	KCTD1	18.69
530	ZNF364	18.68
531	RKHD2	18.67
532	KCNA1	18.66
533	KLHL8	18.66
534	COMMD9	18.60
535	TRIM40	18.59
536	SIAH1	18.57
537	RFPL1	18.54
538	RNF149	18.52
539	KIAA0317	18.51
540	FBXL13	18.51
541	FBXL3	18.50
542	TRIM6	18.50
543	PHF1	18.49
544	KCNS3	18.45
545	RNF135	18.39
546	SH3RF2	18.37
547	ERCC8	18.33
548	LZTR1	18.31
549	IBTK	18.29
550	FLJ20186	18.28
551	RCBTB2	18.27
552	CUL4B	18.23
553	FBXL18	18.17

Rank	Gene	Score
554	FBXL22	18.12
555	BARD1	18.09
556	UBE2H	18.08
557	TRIM61	18.06
558	FBXO18	18.02
559	KLHL17	18.01
560	FBXO40	18.00
561	ZBTB12	17.98
562	RFWD3	17.94
563	MDM2	17.93
564	GTF2H2	17.92
565	HUWE1	17.88
566	LOC283116	17.87
567	TRIM22	17.87
568	CGRRF1	17.84
569	TRIM62	17.77
570	FBXO25	17.74
571	FBXO34	17.73
572	PEX12	17.73
573	WDR68	17.72
574	HECTD3	17.72
575	EVI1	17.71
576	FBXO11	17.69
577	BRCA1	17.69
578	CHFR	17.68
579	CBLB	17.66
580	HECW2	17.63
581	FBXO44	17.61
582	LOC51136	17.61
583	SIAH2	17.58
584	ZNF598	17.54
585	CCIN	17.52
586	UBE2I	17.46
587	FEM1B	17.42
588	KCNC3	17.35
589	FBXW8	17.35
590	RNF39	17.26
591	RNF139	17.15
592	TOPORS	17.14
593	RNF181	17.14
594	RNF31	17.13
595	FBXL11	17.12
596	LOC389768	17.11

Rank	Gene	Score
597	FBXO3	17.09
598	HERC4	16.96
599	PHF7	16.96
600	RBBP6	16.89
601	C8ORFK36	16.87
602	UBE2NL	16.87
603	RFPL3	16.86
604	PLEKHM1	16.85
605	RNF2	16.83
606	ASB6	16.82
607	RNF10	16.82
608	WDR21A	16.82
609	DCST1	16.80
610	BRAP	16.72
611	TCEB3	16.70
612	UBE3A	16.65
613	WWP2	16.56
614	RNF169	16.51
615	HIC1	16.45
616	RNF24	16.37
617	TRIM46	16.37
618	DTX3	16.26
619	FBXW12	16.25
620	RNF26	16.23
621	39508	16.21
622	FBXO42	16.18
623	SPSB3	16.15
624	TRIM16	16.12
625	CBL	16.12
626	C1orf166	16.08
627	KCND1	16.07
628	TRIM67	16.03
629	BFAR	16.02
630	FBXW5	16.01
631	IVNS1ABP	15.93
632	SOCS2	15.89
633	TRAF4	15.88
634	TRIM49	15.88
635	FBXL8	15.82
636	PHF21A	15.81
637	BTBD3	15.80
638	RNF19	15.73
639	ZFP161	15.69

Rank	Gene	Score
640	HERC1	15.67
641	LOC150739	15.67
642	FBXO43	15.62
643	PHF10	15.61
644	ZNF238	15.57
645	TRIM31	15.57
646	KCNC4	15.47
647	ASB13	15.46
648	TRIM38	15.35
649	CDC34	15.32
650	TRIM71	15.32
651	HLTF	15.29
652	KCNG1	15.27
653	LOC388419	15.16
654	ZC3H5	15.11
655	KCNB1	15.09
656	TRIM27	15.08
657	RABGEF1	15.08
658	PARC	14.99
659	MARCH7	14.97
660	ASB15	14.97
661	KCNA4	14.96
662	PHOSPHO2	14.91
663	DDB2	14.91
664	ABTB1	14.88
665	RBBP5	14.88
666	WDR53	14.80
667	ZMIZ2	14.80
668	KCNA3	14.76
669	KCTD5	14.75
670	TRIM34	14.68
671	MAP3K1	14.63
672	RNF170	14.60
673	KLHL23	14.54
674	MDM4	14.50
675	TRAF2	14.50
676	RNF152	14.47
677	RNF130	14.46
678	FBXL6	14.36
679	PHIP	14.28
680	AIRE	14.26
681	TRIM55	14.17
682	NUP43	14.11

Rank	Gene	Score
683	MKRN1	14.10
684	FBXO28	14.07
685	VPS11	14.05
686	NLE1	13.98
687	RNF43	13.88
688	FBXL12	13.88
689	KCNRG	13.83
690	HIP2	13.83
691	RNF17	13.82
692	PHF14	13.81
693	FBXL17	13.81
694	UBE4A	13.77
695	RNF111	13.70
696	ZBTB40	13.69
697	RNF41	13.67
698	TRIM75	13.66
699	FBXO22	13.64
700	UBE2J2	13.58
701	BTRC	13.56
702	TRIM13	13.52
703	BTBD7	13.52
704	KCNG3	13.48
705	KCNB2	13.46
706	ZFAND5	13.44
707	TTC3	13.43
708	RNF187	13.42
709	RHOBTB1	13.37
710	CNOT4	13.36
711	PIAS3	13.36
712	ANKFY1	13.34
713	TRIM74	13.30
714	IQWD1	13.27
715	ZFYVE27	13.21
716	DPF2	13.21
717	ATRX	13.18
718	KCNC2	13.18
719	ZFPL1	13.13
720	LOC441061	13.11
721	RBBP7	13.04
722	RNF128	12.95
723	WSB1	12.93
724	MLL2	12.92
725	TRIP12	12.83

Rank	Gene	Score
726	WDR57	12.70
727	PDZRN3	12.64
728	FBXO32	12.64
729	UBE2D1	12.60
730	TCEB1	12.58
731	KBTBD3	12.58
732	KATNB1	12.52
733	C17orf27	12.45
734	RNF125	12.40
735	LRRC29	12.36
736	NEDD4	12.30
737	KLHL15	12.25
738	RNF138	12.24
739	KBTBD11	12.19
740	KCNA2	12.12
741	ASB1	12.03
742	TLE3	12.01
743	UBE2T	11.99
744	KCTD21	11.99
745	VPS8	11.96
746	FBXO24	11.95
747	FBXL19	11.90
748	TRIM29	11.90
749	RAB40B	11.89
750	UBE1DC1	11.85
751	MNAT1	11.82
752	LOC390231	11.80
753	RCHY1	11.57
754	RFWD2	11.57
755	UBR1	11.43
756	COMMD6	11.41
757	AMFR	11.41
758	ZBTB22	11.39
759	LOC389072	11.32
760	FBXO8	11.31
761	FBXL7	11.31
762	KEAP1	11.24
763	UBE2E3	11.14
764	RP3-509I19.5	11.14
765	C13orf7	11.14
766	FBXW4	11.10
767	PPIL2	11.10
768	PATZ1	11.08

Rank	Gene	Score
769	LOC399939	11.08
770	MKRN3	11.04
771	SOCS7	10.98
772	FBXO41	10.92
773	FBXL2	10.89
774	UBE2C	10.88
775	HERC5	10.78
776	TRIM28	10.73
777	KBTBD4	10.68
778	IRF2BP1	10.61
779	ANAPC11	10.48
780	NEDD4L	10.47
781	TRIM33	10.21
782	TRIAD3	10.18
783	KBTBD9	10.17
784	RNF215	10.11
785	WDR59	10.09
786	KLHL4	10.05
787	SMURF1	9.91
788	WDR23	9.91
789	PML	9.84
790	CCNB1IP1	9.81
791	LOC120824	9.61
792	FBXO2	9.44
793	RNF6	9.32
794	TRIM3	8.89
795	UBE2W	8.66
796	DCAF15	8.61
797	MYLIP	7.64
798	FBXO4	7.62
799	BAZ1A	7.53
800	HECTD1	6.70

Table 2. Data Set Secondary RNAi Screen under 25 μM FAC

Rank	Oligo	Score	Rank	Oligo	Score
1	FBXL5-4	132.58	45	RBX1-3	31.94
2	TRIM8-3	117.82	46	KCNA6-2	31.80
3	FBXL5-1	113.01	47	TRAF3-3	31.63
4	FBXL5-3	110.23	48	CRBN-3	31.05
5	KCTD17-4	107.09	49	RING1-4	30.00
6	SKP1-4	106.63	50	RING1-2	29.40
7	CUL1-2	99.77	51	ZBTB5-4	29.01
8	WSB2-2	94.33	52	VHL-2	28.92
9	KCTD17-3	92.05	53	FBXO5-1	28.57
10	OTUD7-2	89.14	54	VHLL-3	28.29
11	SKP1-3	82.48	55	CRBN-1	27.44
12	CUL1-4	74.81	56	TRAF3-1	27.40
13	FBXO17-4	70.34	57	CUL1-3	27.30
14	SKP1-2	65.99	58	NEURL-4	27.21
15	FBXL5-2	64.59	59	TRIM9-4	27.17
16	FBXO6-3	60.57	60	LINCR-3	26.98
17	BTBD8-4	53.62	61	KLHL22-1	26.96
18	RBX1-1	52.75	62	OTUD7-3	26.93
19	CUL7-3	50.16	63	KLHL14-2	26.92
20	MARCH9-4	48.96	64	MGRN1-2	26.80
21	MARCH3-4	48.35	65	FBXO9-2	26.62
22	KLHL22-3	46.61	66	PJA1-3	26.37
23	RBX1-4	45.44	67	KLHL11-2	26.34
24	ZBTB7-2	43.52	68	RNF11-3	26.14
25	FBXL15-1	41.38	69	KCNA6-1	25.99
26	RC3H1-4	39.31	70	CRBN-4	25.98
27	RC3H1-2	38.33	71	BIRC8-4	25.96
28	FBXL10-4	37.61	72	NICAL-2	25.26
29	IVNS1ABP-1	36.72	73	WSB2-1	24.95
30	TNFAIPI-4	36.36	74	NEURL-1	24.95
31	KCTD15-1	36.36	75	FBXO6-4	24.80
32	TRIM8-4	35.69	76	VHL-3	24.43
33	CUL1-1	35.64	77	MARCH2-2	24.35
34	KCTD15-3	34.44	78	NEURL-3	23.95
35	RHOBTB2-4	34.05	79	RNF207-4	23.82
36	TRIM8-2	33.91	80	TRAF3-4	23.79
37	KLHL14-2	33.58	81	PXMP3-2	23.78
38	BTBD8-3	33.53	82	SMU1-1	23.77
39	WSB2-3	33.50	83	KCTD17-1	23.65
40	LINCR-1	33.48	84	TRIM9-3	23.63
41	DTX3L-4	33.00	85	PJA1-4	23.60
42	VPS41-3	32.90	86	TNFAIPI-3	23.60
43	FBX045-4	32.59	87	KLHL14-1	23.51
44	VHL-4	32.56	88	ASB4-4	23.21

Rank	Oligo	Score
89	DTX3L-1	22.88
90	FBXO17-1	22.82
91	VHLL-4	22.50
92	CUL7-4	22.38
93	RNF183-4	22.30
94	NICAL-3	22.28
95	BIRC8-2	22.28
96	BTBD8-1	22.28
97	CRBN-2	22.24
98	SMU1-2	22.16
99	MARCH2-1	22.15
100	WHSC1L1-4	22.13
101	LONRF2-4	22.08
102	VHLL-1	22.03
103	RSPRY1-2	22.03
104	ASB4-2	22.01
105	FBXL3P-4	21.92
106	RNF113B-2	21.83
107	RSPRY1-4	21.80
108	RNF11-4	21.77
109	DTX3L-3	21.70
110	VHL-1	21.49
111	FBX045-2	21.40
112	TRIP-4	21.34
113	CUL7-1	21.30
114	MARCH3-2	21.15
115	RAMP-3	21.13
116	RNF111-1	21.02
117	LINCR-4	20.99
118	FBLP-1-2	20.84
119	KLHL14-1	20.57
120	FBXL10-2	20.53
121	TRIM32-4	20.53
122	WDR5B-4	20.29
123	PXMP3-4	20.14
124	TRIP-3	20.13
125	FBXL15-4	20.01
126	ANUBL1-3	19.99
127	MARCH3-1	19.81
128	BTBD8-2	19.77
129	MARCH2-4	19.75
130	FBXL15-3	19.64
131	MARCH4-1	19.62
132	WHSC1L1-2	19.49
133	TNFAIPI-1	19.43

Rank	Oligo	Score
134	RNF207-1	19.43
135	NFX-4	19.36
136	KCNA6-4	19.22
137	WSB2-4	19.20
138	RING1-3	19.16
139	FBX021-3	18.99
140	RNF183-2	18.93
141	PJA1-1	18.89
142	KLHL14-3	18.87
143	MARCH3-3	18.84
144	PJA1-2	18.84
145	MARCH4-3	18.82
146	ZBTB5-1	18.73
147	FBX010-3	18.73
148	FLJ12973-4	18.67
149	IVNS1ABP-4	18.33
150	WDR5B-2	18.31
151	TNFAIPI-2	18.29
152	RNF113B-4	18.25
153	RNF111-2	18.24
154	NFX-1	18.19
155	FBXO17-3	18.19
156	TRIM9-2	18.14
157	FLJ12973-2	17.96
158	FLJ12973-1	17.92
159	ANUBL1-1	17.64
160	BIRC8-1	17.62
161	RHOBTB2-3	17.53
162	RC3H1-3	17.47
163	RNF11-2	17.44
164	ZBTB7-3	17.32
165	FBX010-1	17.30
166	KLHL14-3	17.24
167	VPS41-2	17.21
168	WHSC1L1-3	17.20
169	RING1-1	17.16
170	KLHL22-4	16.93
171	KLHL22-2	16.92
172	RNF113B-3	16.84
173	NICAL-4	16.65
174	FBXL3P-3	16.61
175	TRIM32-1	16.57
176	FBXO17-2	16.56
177	NFX-3	16.40
178	TRAF3-2	16.31

Rank	Oligo	Score
179	FBXL10-3	16.31
180	ASB4-1	16.30
181	LINCR-2	16.30
182	KIAA0182-2	16.21
183	ZBTB5-3	16.21
184	FBXL15-2	16.20
185	RAMP-4	16.07
186	SMU1-4	16.01
187	RNF207-3	15.80
188	TRIP-2	15.67
189	FBX045-1	15.58
190	ANUBL1-4	15.57
191	FBX010-4	15.51
192	ASB4-3	15.50
193	VPS41-4	15.44
194	NEURL2-3	15.42
195	KLHL14-4	15.41
196	WDR5B-3	15.35
197	MGRN1-3	15.29
198	NICAL-1	15.28
199	FBXO9-1	15.24
200	RNF183-1	15.23
201	KLHL14-4	15.16
202	MARCH9-2	14.99
203	KCTD17-2	14.93
204	MARCH9-3	14.89
205	KCNA6-3	14.79
206	TRIM32-3	14.74
207	NEURL-2	14.65
208	OTUD7-4	14.56
209	FBXL3P-1	14.55
210	FBXO9-3	14.37
211	IVNS1ABP-2	14.35
212	VPS41-1	14.31
213	MARCH2-3	14.29
214	RSPRY1-1	14.20
215	PXMP3-3	14.20
216	SKP2-3	14.12
217	WDR5B-1	14.04
218	RSPRY1-3	13.99
219	TRIM9-1	13.97
220	EDD1-1	13.91
221	NEURL2-1	13.77
222	SKP2-4	13.76

Rank	Oligo	Score
223	NFX-2	13.72
224	MGRN1-4	13.69
225	RNF11-1	13.67
226	TRIM32-2	13.67
227	FBLP-1-3	13.62
228	RNF113B-1	13.60
229	KIAA0182-3	13.55
230	RNF207-2	13.53
231	FBXO5-2	13.48
232	KLHL11-1	13.46
233	KCTD15-2	13.31
234	NEURL2-2	13.27
235	NEURL2-4	13.23
236	FBXO9-4	13.11
237	LONRF2-3	13.06
238	KIAA0182-4	12.88
239	FBX021-4	12.85
240	RAMP-2	12.51
241	RC3H1-1	12.31
242	EDD1-4	12.07
243	MARCH4-2	12.04
244	KCTD15-4	12.02
245	FBLP-1-4	11.90
246	ANUBL1-2	11.85
247	FBX045-3	11.73
248	BIRC8-3	11.71
249	ZBTB7-4	11.61
250	RAMP-1	11.53
251	OTUD7-1	11.51
252	PXMP3-1	11.51
253	FBX021-2	11.48
254	RHOBTB2-2	11.42
255	RNF111-4	11.35
256	LONRF2-2	11.31
257	FLJ12973-3	11.20
258	RNF111-3	11.16
259	FBLP-1-1	11.14
260	LONRF2-1	10.92
261	FBXO5-3	10.92
262	ZBTB5-2	10.83
263	MGRN1-1	10.82
264	EDD1-3	10.80
265	FBXO6-2	10.60
266	KLHL11-3	10.56

Rank	Oligo	Score
267	EDD1-2	10.52
268	IVNS1ABP-3	10.48
269	WHSC1L1-1	10.28
270	RBX1-2	10.26
271	VHLL-2	10.18
272	RHOBTB2-1	10.11
273	TRIP-1	9.84
274	TRIM8-1	9.83
275	SKP2-2	9.57
276	FBXO5-4	9.35
277	CUL7-2	9.35
278	ZBTB7-1	9.35
279	KLHL11-4	9.24
280	KIAA0182-1	9.20
281	SMU1-3	9.16
282	FBXL3P-2	9.05
283	FBX021-1	9.01
284	SKP1-1	8.93
285	DTX3L-2	8.83
286	SKP2-1	8.79
287	FBX010-2	8.42
288	RNF183-3	8.23
289	MARCH9-1	7.90
290	FBXL10-1	7.83
291	MARCH4-4	7.10
292	FBXO6-1	6.46

Table 3. Data collection, phasing and refinement statistics for FBXL5 Hr structure

Crystal	Native 1	Fe[a] *peak*	Fe[a] *inflection point*	Native 2
Space group	C2	C2	C2	$P2_1$
Energy (eV)	12,559.6	7,122.6	7,118.8	12,779.4
Resolution range (Å)	44.7 – 1.85 (1.88 – 1.85)	44.7 – 2.50 (2.54 – 2.50)	34.0 – 2.50 (2.54 – 2.50)	31.7 – 2.10 (2.14 – 2.10)
Unique reflections	28,254 (1,433)	11,365 (564)	11,319 (574)	37,291 (1,845)
Multiplicity	5.0 (5.0)	4.9 (4.0)	4.9 (3.9)	2.7 (2.5)
Data completeness (%)	99.8 (100.0)	99.6 (98.9)	99.5 (99.0)	97.5 (98.8)
R_{merge} (%)[b]	4.7 (69.0)	5.5 (11.2)	4.8 (9.8)	6.3 (59.7)
I/σ(I)	29.2 (2.0)	55.6 (19.2)	53.6 (19.2)	15.8 (1.8)
Wilson B-value ($Å^2$)	29.8	50.3	51.3	32.0
Phase determination				
Anomalous scatterers	iron, 4 out of 4 possible sites; sulfur, 2 sites[c]			
Figure of merit (44.7-2.50 Å)	0.59 (0.85 after density modification)			
Refinement statistics				
Crystal	Native 1		Native 2	
Resolution range (Å)	27.7 – 1.85 (1.92– 1.85)		29.3 – 2.10 (2.16 – 2.10)	
No. of reflections R_{work}/R_{free}	28,019/1,412 (2,677/134)		36,670/1,832 (2,690/118)	
Data completeness (%)	99.8 (100.0)		97.3 (98.0)	
Atoms (non-H protein/solvent/Fe)	2,612/168/4		5,127/257/8	
R_{work} (%)	17.0 (21.0)		20.0 (27.2)	
R_{free} (%)	21.1 (28.6)		27.7 (36.3)	
R.m.s.d. bond length (Å)	0.008		0.010	
R.m.s.d. bond angle (°)	0.872		1.01	
Mean B-value ($Å^2$) (protein/solvent/Fe)	48.0/47.9/26.6		51.9/48.3/33.2	
Ramachandran plot (%) (favored/additional/disallowed)[d]	98.3/1.7/0.0		98.5/1.5/0.0	
Maximum likelihood coordinate error	0.54		0.12	
Missing residues, by chain	A: 1-3, 75-76, 81-83, 160-161. B: 1-3, 75-76, 81-83, 161.		A: 1-4, 81-82, 160-161. B: 1-4, 74-76, 81-82, 160-161. C: 1-4, 74-76, 81-82, 160-161. D: 1-4, 74-76, 81-83, 161.	

Data for the outermost shell are given in parentheses

[a]Bijvoet-pairs were kept separate for data processing

[b]R_{merge} = 100 $\Sigma_h\Sigma_i|I_{h,\,i} - \langle I_h\rangle|/\Sigma_h\Sigma_i I_{h,\,i}$, where the outer sum (h) is over the unique reflections and the inner sum (i) is over the set of independent observations of each unique reflection

[c]Two well-ordered methionine sulfur atoms were located in *SHELXD* and refined in *MLPHARE*

[d]As defined by the validation suite MolProbity (Davis et al., 2007)

Table 4. Bond distances (Å) for FBXL5 diiron site

Structure	Fe1 – Fe2	Fe1 – O	Fe2 – O	E58 Oe2 – O
Native 1, chain A	3.16	2.01	1.99	2.75
Native 1, chain B	3.14	2.08	1.96	2.77
Native 2, chain A	3.13	2.03	2.11	2.95
Native 2, chain B	3.10	2.03	1.99	2.78
Native 2, chain C	3.13	1.86	2.11	2.87
Native 2, chain D	3.06	2.13	2.00	2.66
Mean	3.12	2.02	2.03	2.80

Table 5. siRNA sequences

siRNA	Catalog #	Targeting Sequence
FBXL5 #1	D-012424-04	CCUUAGAGGUCUUAGCCUA
FBXL5 #2	D-012424-17	CCUCAAGAGUUAUGUCGAU
FBXL5 #3	D-012424-01	GCACAACACUGCUCUCAGA
SKP1 #1	D-003323-09	CGCAAGACCUUCAAUAUCA
SKP1 #2	D-003323-10	CCAAUAUGAUCAAGGGGAA
CUL1 #1	D-004086-03	GGUUAUAUCAGUUGUCUAA
CUL1 #2	D-004086-05	CAACGAAGAGUUCAGGUUU
RBX1 #1	D-004087-01	GAAGCGCUUUGAAGUGAAA
RBX1 #2	D-004087-03	GCAUAGAAUGUCAAGCUAA
NT	D-001210-01	

Table 6. Primer sequences

Construct	FBXL5 Primers
Δ1-197	5'-GGAGGATCCACCATGGTGTCAGAACACTCCACAGG
Δ208-248	5'-GGTATAACCCATTACCCTGTTCATTGGGCCAGAG 5'-ATGAACAGGGTAATGGGTTATACCTGTGGAGTGTTCTGA
Δ252-350	5'-CTTTACCCTGTTATTTTAGAGCTTTGTCCTAACC 5'-GCTCTAAAATAACAGGGTAAAGATGTTTCC
Δ355-408	5'-ATTTTAGAGCTTGGAATTCTGACATCTCATC 5'-GTCAGAATTCCAAGCTCTAAAATCTGCCTAAC
Δ411-595	5'-GCTCTTGGAATTACTGGACGTGTACTTCTGTTTC 5'-CACGTCCAGTAATTCCAAGAGCTCTGGAAATC
Δ596-650	5'-CTGATCAAGAGTGTCCTTCTCTGAATGATG 5'-CAGAGAAGGACACTCTTGATCAGATTTTTCAC
Δ651-691	5'-GGTGTCTAGAACCTGCTGAAACCAAATCCTGCAGGCCTG
Δ1-161	5'-GGAGGATCCACCATGAAGGATACTGCAGAACTCCTTAGAGG
1-161	5'-GGATCTAGATCACTGAGAGCAGTGTTGTGCAATCAC
H57A	5'-GTTCAAAATGGCTGAGCAGATTGAAAATGAATAC 5'-CAATCTGCTCAGCCATTTTGAACTCCTTGAAAG
E61A	5'-GAGCAGATTGCAAATGAATACATTATTGGTTTG 5'-GTATTCATTTGCAATCTGCTCATGCATTTTG
N62A	5'-CAGATTGAAGCTGAATACATTATTGGTTTGCTTCAA 5'-GTATTCATTTGCAATCTGCTCATGCATTTTG
E131A	5'-GAAAGAGGAAGCAGAGGTTTTTCAGCCCATGTT 5'-GAAAAACCTCTGCTTCCTCTTTCATGTGAGGAA
H158A	5'-GCACAAGCCTGCTCTCAGAAGGATACTGCA 5'-CTGAGAGCAGGCTTGTGCAATCACTTTCTTTTT
E58H	5'-GTTCAAAATGCATCATCAGATTGAAAATGAATACATTATTGG 5'-CATTTTCAATCTGATGATGCATTTTGAACTCCTTGAA
E58D	5'-CAAAATGCATGATCAGATTGAAAATGAATACATT 5'-CATTTTCAATCTGATCATGCATTTTGAACTCCTTG
E58Q	5'-CAAAATGCATCAGCAGATTGAAAATGAATAC 5'-TTTCAATCTGCTGATGCATTTTGAACTCCTTGAAAG
E58A	5'-CAAAATGCATGCGCAGATTGAAAATGAATAC 5'-TTTCAATCTGCGCATGCATTTTGAACTCCTTG
H80A	5'-CATTTATAATGTAGCTTCTGACAATAAACTCTCCGAG 5'-TATTGTCAGAAGCTACATTATAAATGGTCTGGC
H126A	5'-GATTTTCTTCCTGCCATGAAAGAGGAAGAGGAGG 5'-CTCTTTCATGGCAGGAAGAAAATCTCTTGTAA
E130A	5'-CATGAAAGAGGCAGAGGAGGTTTTTCAGCCCA 5'-AAACCTCCTCTGCCTCTTTCATGTGAGGAAGA
Δ1-33	5'-GGAGGATCCACCATGGCGTTTTCCAACAACAACGATTTCCG
Δ1-59	5'-GGAGGATCCACCATGGCGATTGAAAATGAATACATTATTGGTTTG

Δ1-76	5’-GGAGGATCCACCATGTATAATGTACATTCTGACAATAAACTCTCC
Δ1-81	5’-GGAGGATCCACCATGGCGGACAATAAACTCTCCGAGATGCT
Δ1-100	5’-GGAGGATCCACCATGGCGAATGAATATGAACAGTTAAATTATGCAA
Δ67-71	5’-GAATACATTATTCGCAGCCAGACCATTTATAATGTACATTCTG 5’-GGTCTGGCTGCGAATAATGTATTCATTTTCAATCTG
Δ72-76	5’-TTGCTTCAACAATATAATGTACATTCTGACAATAAACTCTCCG 5’-ATGTACATTATATTGTTGAAGCAAACCAATAATGTATTC
Δ77-81	5’-AGCCAGACCATTGACAATAAACTCTCCGAGATG 5’-GAGTTTATTGTCAATGGTCTGGCTGCGTTGTTG
Δ82-86	5’-AATGTACATTCTGAGATGCTTAGCCTCTTTGAAAAGG 5’-GCTAAGCATCTCAGAATGTACATTATAAATGGTCTGGC
Δ87-91	5’-AATAAACTCTCCTTTGAAAAGGGACTGAAGAATGTTAAGAATG 5’-TCCCTTTTCAAAGGAGAGTTTATTGTCAGAATGTACATTATA
Δ143-161	5’-GAATATTTTACCAAGGATACTGCAGAACTCCTTAGA 5’-TGCAGTATCCTTAAAATATTCCATTAACATGGGCTG
Construct	**IRP2 Primers**
Δ73	5’- CTTCAGTAAAGAACCTGAAACAGTGTTAAA 5’-TTTCAGGTTCTTTACTGAAGTCAATTTGTA

BIBLIOGRAPHY

Adams, P.D., Grosse-Kunstleve, R.W., Hung, L.W., Ioerger, T.R., McCoy, A.J., Moriarty, N.W., Read, R.J., Sacchettini, J.C., Sauter, N.K., and Terwilliger, T.C. (2002). PHENIX: building new software for automated crystallographic structure determination. Acta Crystallogr D Biol Crystallogr *58*, 1948-1954.

Addess, K.J., Basilion, J.P., Klausner, R.D., Rouault, T.A., and Pardi, A. (1997). Structure and dynamics of the iron responsive element RNA: implications for binding of the RNA by iron regulatory binding proteins. J Mol Biol *274*, 72-83.

Adle, D.J., Wei, W., Smith, N., Bies, J.J., and Lee, J. (2009). Cadmium-mediated rescue from ER-associated degradation induces expression of its exporter. Proc Natl Acad Sci U S A *106*, 10189-10194.

Andrews, N.C. (2008). Forging a field: the golden age of iron biology. Blood *112*, 219-230.

Andrews, N.C., and Schmidt, P.J. (2007). Iron homeostasis. Annu Rev Physiol *69*, 69-85.

Ardley, H.C., and Robinson, P.A. (2005). E3 ubiquitin ligases. Essays Biochem *41*, 15-30.

Aziz, N., and Munro, H.N. (1987). Iron regulates ferritin mRNA translation through a segment of its 5' untranslated region. Proc Natl Acad Sci U S A *84*, 8478-8482.

Beaumont, C., Delaunay, J., Hetet, G., Grandchamp, B., de Montalembert, M., and Tchernia, G. (2006). Two new human DMT1 gene mutations in a patient with microcytic anemia, low ferritinemia, and liver iron overload. Blood *107*, 4168-4170.

Bourdon, E., Kang, D.K., Ghosh, M.C., Drake, S.K., Wey, J., Levine, R.L., and Rouault, T.A. (2003). The role of endogenous heme synthesis and degradation domain cysteines in cellular iron-dependent degradation of IRP2. Blood Cells Mol Dis *31*, 247-255.

Bruick, R.K., and McKnight, S.L. (2001). A conserved family of prolyl-4-hydroxylases that modify HIF. Science *294*, 1337-1340.

Bush, J.A., Jensen, W.N., Athens, J.W., Ashenbrucker, H., Cartwright, G.E., and Wintrobe, M.M. (1956). Studies on copper metabolism. XIX. The kinetics of iron metabolism and erythrocyte life-span in copper-deficient swine. J Exp Med *103*, 701-712.

Camaschella, C., Campanella, A., De Falco, L., Boschetto, L., Merlini, R., Silvestri, L., Levi, S., and Iolascon, A. (2007). The human counterpart of zebrafish shiraz shows sideroblastic-like microcytic anemia and iron overload. Blood *110*, 1353-1358.

Cardozo, T., and Pagano, M. (2004). The SCF ubiquitin ligase: insights into a molecular machine. Nat Rev Mol Cell Biol *5*, 739-751.

Caron, P.R., Watt, P., and Wang, J.C. (1994). The C-terminal domain of Saccharomyces cerevisiae DNA topoisomerase II. Mol Cell Biol *14*, 3197-3207.

Casey, J.L., Di Jeso, B., Rao, K., Klausner, R.D., and Harford, J.B. (1988a). Two genetic loci participate in the regulation by iron of the gene for the human transferrin receptor. Proc Natl Acad Sci U S A *85*, 1787-1791.

Casey, J.L., Hentze, M.W., Koeller, D.M., Caughman, S.W., Rouault, T.A., Klausner, R.D., and Harford, J.B. (1988b). Iron-responsive elements: regulatory RNA sequences that control mRNA levels and translation. Science *240*, 924-928.

Casey, J.L., Koeller, D.M., Ramin, V.C., Klausner, R.D., and Harford, J.B. (1989). Iron regulation of transferrin receptor mRNA levels requires iron-responsive elements and a rapid turnover determinant in the 3' untranslated region of the mRNA. EMBO J *8*, 3693-3699.

Ching, Y.H., Munroe, R.J., Moran, J.L., Barker, A.K., Mauceli, E., Fennell, T., Dipalma, F., Lindblad-Toh, K., Abcunas, L.M., Gilmour, J.F.*, et al.* (2010). High resolution mapping and positional cloning of ENU-induced mutations in the Rw region of mouse chromosome 5. BMC Genet *11*, 106.

Chini, A., Fonseca, S., Fernandez, G., Adie, B., Chico, J.M., Lorenzo, O., Garcia-Casado, G., Lopez-Vidriero, I., Lozano, F.M., Ponce, M.R.*, et al.* (2007). The JAZ family of repressors is the missing link in jasmonate signalling. Nature *448*, 666-671.

Clarke, S.L., Vasanthakumar, A., Anderson, S.A., Pondarre, C., Koh, C.M., Deck, K.M., Pitula, J.S., Epstein, C.J., Fleming, M.D., and Eisenstein, R.S. (2006). Iron-responsive degradation of iron-regulatory protein 1 does not require the Fe-S cluster. EMBO J *25*, 544-553.

Cowtan, K., and Main, P. (1998). Miscellaneous algorithms for density modification. Acta Crystallogr D Biol Crystallogr *54*, 487-493.

Crichton, R.R., and Pierre, J.L. (2001). Old iron, young copper: from Mars to Venus. Biometals *14*, 99-112.

Davis, I.W., Leaver-Fay, A., Chen, V.B., Block, J.N., Kapral, G.J., Wang, X., Murray, L.W., Arendall, W.B., 3rd, Snoeyink, J., Richardson, J.S., *et al.* (2007). MolProbity: all-atom contacts and structure validation for proteins and nucleic acids. Nucleic Acids Res *35*, W375-383.

De Domenico, I., Ward, D.M., Langelier, C., Vaughn, M.B., Nemeth, E., Sundquist, W.I., Ganz, T., Musci, G., and Kaplan, J. (2007). The molecular mechanism of hepcidin-mediated ferroportin down-regulation. Mol Biol Cell *18*, 2569-2578.

de Silva, D.M., Askwith, C.C., and Kaplan, J. (1996). Molecular mechanisms of iron uptake in eukaryotes. Physiol Rev *76*, 31-47.

Donovan, A., Lima, C.A., Pinkus, J.L., Pinkus, G.S., Zon, L.I., Robine, S., and Andrews, N.C. (2005). The iron exporter ferroportin/Slc40a1 is essential for iron homeostasis. Cell Metab *1*, 191-200.

Dycke, C., Bougault, C., Gaillard, J., Andrieu, J.P., Pantopoulos, K., and Moulis, J.M. (2007). Human iron regulatory protein 2 is easily cleaved in its specific domain: consequences for the haem binding properties of the protein. Biochem J *408*, 429-439.

Epstein, A.C., Gleadle, J.M., McNeill, L.A., Hewitson, K.S., O'Rourke, J., Mole, D.R., Mukherji, M., Metzen, E., Wilson, M.I., Dhanda, A., *et al.* (2001). C. elegans EGL-9 and mammalian homologs define a family of dioxygenases that regulate HIF by prolyl hydroxylation. Cell *107*, 43-54.

Farmer, C.S., Kurtz, D.M., Jr., Phillips, R.S., Ai, J., and Sanders-Loehr, J. (2000). A leucine residue "Gates" solvent but not O2 access to the binding pocket of phascolopsis gouldii hemerythrin. J Biol Chem *275*, 17043-17050.

French, C.E., Bell, J.M., and Ward, F.B. (2008). Diversity and distribution of hemerythrin-like proteins in prokaryotes. FEMS Microbiol Lett *279*, 131-145.

Galy, B., Ferring, D., Minana, B., Bell, O., Janser, H.G., Muckenthaler, M., Schumann, K., and Hentze, M.W. (2005). Altered body iron distribution and microcytosis in mice deficient in iron regulatory protein 2 (IRP2). Blood *106*, 2580-2589.

Galy, B., Ferring-Appel, D., Kaden, S., Grone, H.J., and Hentze, M.W. (2008). Iron regulatory proteins are essential for intestinal function and control key iron absorption molecules in the duodenum. Cell Metab *7*, 79-85.

Gietz, R.D., and Woods, R.A. (2002). Transformation of yeast by lithium acetate/single-stranded carrier DNA/polyethylene glycol method. Methods Enzymol *350*, 87-96.

Gouider-Khouja, N. (2009). Wilson's disease. Parkinsonism Relat Disord *15 Suppl 3*, S126-129.

Gunshin, H., Fujiwara, Y., Custodio, A.O., Direnzo, C., Robine, S., and Andrews, N.C. (2005a). Slc11a2 is required for intestinal iron absorption and erythropoiesis but dispensable in placenta and liver. J Clin Invest *115*, 1258-1266.

Gunshin, H., Starr, C.N., Direnzo, C., Fleming, M.D., Jin, J., Greer, E.L., Sellers, V.M., Galica, S.M., and Andrews, N.C. (2005b). Cybrd1 (duodenal cytochrome b) is not necessary for dietary iron absorption in mice. Blood *106*, 2879-2883.

Guo, B., Phillips, J.D., Yu, Y., and Leibold, E.A. (1995). Iron regulates the intracellular degradation of iron regulatory protein 2 by the proteasome. J Biol Chem *270*, 21645-21651.

Guo, B., Yu, Y., and Leibold, E.A. (1994). Iron regulates cytoplasmic levels of a novel iron-responsive element-binding protein without aconitase activity. J Biol Chem *269*, 24252-24260.

Hamill, R.L., Woods, J.C., and Cook, B.A. (1991). Congenital atransferrinemia. A case report and review of the literature. Am J Clin Pathol *96*, 215-218.

Hanson, E.S., Rawlins, M.L., and Leibold, E.A. (2003). Oxygen and iron regulation of iron regulatory protein 2. J Biol Chem *278*, 40337-40342.

Harlow, E., and Lane, D. (1988). Antibodies: A Laboratory Manual (Cold Spring Harbor Laboratory Press).

Hentze, M.W., Caughman, S.W., Rouault, T.A., Barriocanal, J.G., Dancis, A., Harford, J.B., and Klausner, R.D. (1987). Identification of the iron-responsive element for the translational regulation of human ferritin mRNA. Science *238*, 1570-1573.

Hentze, M.W., Muckenthaler, M.U., and Andrews, N.C. (2004). Balancing acts: molecular control of mammalian iron metabolism. Cell *117*, 285-297.

Hentze, M.W., Muckenthaler, M.U., Galy, B., and Camaschella, C. (2010). Two to tango: regulation of Mammalian iron metabolism. Cell *142*, 24-38.

Hershko, A., and Ciechanover, A. (1998). The ubiquitin system. Annu Rev Biochem *67*, 425-479.

Ho, M.S., Ou, C., Chan, Y.R., Chien, C.T., and Pi, H. (2008). The utility F-box for protein destruction. Cell Mol Life Sci *65*, 1977-2000.

Holm, L., and Park, J. (2000). DaliLite workbench for protein structure comparison. Bioinformatics *16*, 566-567.

Holmes, M.A., Le Trong, I., Turley, S., Sieker, L.C., and Stenkamp, R.E. (1991). Structures of deoxy and oxy hemerythrin at 2.0 A resolution. J Mol Biol *218*, 583-593.

Holmes, M.A., and Stenkamp, R.E. (1991). Structures of met and azidomet hemerythrin at 1.66 A resolution. J Mol Biol *220*, 723-737.

Hon, W.C., Wilson, M.I., Harlos, K., Claridge, T.D., Schofield, C.J., Pugh, C.W., Maxwell, P.H., Ratcliffe, P.J., Stuart, D.I., and Jones, E.Y. (2002). Structural basis for the recognition of hydroxyproline in HIF-1 alpha by pVHL. Nature *417*, 975-978.

Huang, L.E., Gu, J., Schau, M., and Bunn, H.F. (1998). Regulation of hypoxia-inducible factor 1alpha is mediated by an O2-dependent degradation domain via the ubiquitin-proteasome pathway. Proc Natl Acad Sci U S A *95*, 7987-7992.

Isaza, C.E., Silaghi-Dumitrescu, R., Iyer, R.B., Kurtz, D.M., Jr., and Chan, M.K. (2006). Structural basis for O2 sensing by the hemerythrin-like domain of a bacterial chemotaxis protein: substrate tunnel and fluxional N terminus. Biochemistry *45*, 9023-9031.

Ishikawa, H., Kato, M., Hori, H., Ishimori, K., Kirisako, T., Tokunaga, F., and Iwai, K. (2005). Involvement of heme regulatory motif in heme-mediated ubiquitination and degradation of IRP2. Mol Cell *19*, 171-181.

Ivan, M., Haberberger, T., Gervasi, D.C., Michelson, K.S., Gunzler, V., Kondo, K., Yang, H., Sorokina, I., Conaway, R.C., Conaway, J.W.*, et al.* (2002). Biochemical purification and pharmacological inhibition of a mammalian prolyl hydroxylase acting on hypoxia-inducible factor. Proc Natl Acad Sci U S A *99*, 13459-13464.

Iwai, K., Drake, S.K., Wehr, N.B., Weissman, A.M., LaVaute, T., Minato, N., Klausner, R.D., Levine, R.L., and Rouault, T.A. (1998). Iron-dependent oxidation, ubiquitination, and degradation of iron regulatory protein 2: implications for degradation of oxidized proteins. Proc Natl Acad Sci U S A *95*, 4924-4928.

Iwai, K., Klausner, R.D., and Rouault, T.A. (1995). Requirements for iron-regulated degradation of the RNA binding protein, iron regulatory protein 2. EMBO J *14*, 5350-5357.

Jackson, A.L., and Linsley, P.S. (2004). Noise amidst the silence: off-target effects of siRNAs? Trends Genet *20*, 521-524.

Jin, J., Cardozo, T., Lovering, R.C., Elledge, S.J., Pagano, M., and Harper, J.W. (2004). Systematic analysis and nomenclature of mammalian F-box proteins. Genes Dev *18*, 2573-2580.

Jones, T.A., Zou, J.Y., Cowan, S.W., and Kjeldgaard, M. (1991). Improved methods for building protein models in electron density maps and the location of errors in these models. Acta Crystallogr A *47 (Pt 2)*, 110-119.

Kang, D.K., Jeong, J., Drake, S.K., Wehr, N.B., Rouault, T.A., and Levine, R.L. (2003). Iron regulatory protein 2 as iron sensor. Iron-dependent oxidative modification of cysteine. J Biol Chem *278*, 14857-14864.

Kao, W.C., Wang, V.C., Huang, Y.C., Yu, S.S., Chang, T.C., and Chan, S.I. (2008). Isolation, purification and characterization of hemerythrin from Methylococcus capsulatus (Bath). J Inorg Biochem *102*, 1607-1614.

Kaptain, S., Downey, W.E., Tang, C., Philpott, C., Haile, D., Orloff, D.G., Harford, J.B., Rouault, T.A., and Klausner, R.D. (1991). A regulated RNA binding protein also possesses aconitase activity. Proc Natl Acad Sci U S A *88*, 10109-10113.

Klausner, R.D., Rouault, T.A., and Harford, J.B. (1993). Regulating the fate of mRNA: the control of cellular iron metabolism. Cell *72*, 19-28.

Kobayashi, Y., Imamura, S., Hanaoka, M., and Tanaka, K. (2011). A tetrapyrrole-regulated ubiquitin ligase controls algal nuclear DNA replication. Nat Cell Biol.

Kobe, B., and Kajava, A.V. (2001). The leucine-rich repeat as a protein recognition motif. Curr Opin Struct Biol *11*, 725-732.

Kubota, H. (2009). Quality control against misfolded proteins in the cytosol: a network for cell survival. J Biochem *146*, 609-616.

LaVaute, T., Smith, S., Cooperman, S., Iwai, K., Land, W., Meyron-Holtz, E., Drake, S.K., Miller, G., Abu-Asab, M., Tsokos, M.*, et al.* (2001). Targeted deletion of the gene encoding iron regulatory protein-2 causes misregulation of iron metabolism and neurodegenerative disease in mice. Nat Genet *27*, 209-214.

Leibold, E.A., and Munro, H.N. (1988). Cytoplasmic protein binds in vitro to a highly conserved sequence in the 5' untranslated region of ferritin heavy- and light-subunit mRNAs. Proc Natl Acad Sci U S A *85*, 2171-2175.

Levy, J.E., Jin, O., Fujiwara, Y., Kuo, F., and Andrews, N.C. (1999). Transferrin receptor is necessary for development of erythrocytes and the nervous system. Nat Genet *21*, 396-399.

Li, W., Bengtson, M.H., Ulbrich, A., Matsuda, A., Reddy, V.A., Orth, A., Chanda, S.K., Batalov, S., and Joazeiro, C.A. (2008). Genome-wide and functional annotation of human E3 ubiquitin ligases identifies MULAN, a mitochondrial E3 that regulates the organelle's dynamics and signaling. PLoS ONE *3*, e1487.

Masson, N., Willam, C., Maxwell, P.H., Pugh, C.W., and Ratcliffe, P.J. (2001). Independent function of two destruction domains in hypoxia-inducible factor-alpha chains activated by prolyl hydroxylation. EMBO J *20*, 5197-5206.

Mastrogiannaki, M., Matak, P., Keith, B., Simon, M.C., Vaulont, S., and Peyssonnaux, C. (2009). HIF-2alpha, but not HIF-1alpha, promotes iron absorption in mice. J Clin Invest.

McCoy, A.J., Grosse-Kunstleve, R.W., Adams, P.D., Winn, M.D., Storoni, L.C., and Read, R.J. (2007). Phaser crystallographic software. J Appl Crystallogr *40*, 658-674.

McKie, A.T., Barrow, D., Latunde-Dada, G.O., Rolfs, A., Sager, G., Mudaly, E., Mudaly, M., Richardson, C., Barlow, D., Bomford, A.*, et al.* (2001). An iron-regulated ferric reductase associated with the absorption of dietary iron. Science *291*, 1755-1759.

Meyron-Holtz, E.G., Ghosh, M.C., Iwai, K., LaVaute, T., Brazzolotto, X., Berger, U.V., Land, W., Ollivierre-Wilson, H., Grinberg, A., Love, P.*, et al.* (2004a). Genetic ablations of iron regulatory proteins 1 and 2 reveal why iron regulatory protein 2 dominates iron homeostasis. EMBO J *23*, 386-395.

Meyron-Holtz, E.G., Ghosh, M.C., and Rouault, T.A. (2004b). Mammalian tissue oxygen levels modulate iron-regulatory protein activities in vivo. Science *306*, 2087-2090.

Mims, M.P., Guan, Y., Pospisilova, D., Priwitzerova, M., Indrak, K., Ponka, P., Divoky, V., and Prchal, J.T. (2005). Identification of a human mutation of DMT1 in a patient with microcytic anemia and iron overload. Blood *105*, 1337-1342.

Min, J.H., Yang, H., Ivan, M., Gertler, F., Kaelin, W.G., Jr., and Pavletich, N.P. (2002). Structure of an HIF-1alpha -pVHL complex: hydroxyproline recognition in signaling. Science *296*, 1886-1889.

Minor, W., Cymborowski, M., Otwinowski, Z., and Chruszcz, M. (2006). HKL-3000: the integration of data reduction and structure solution--from diffraction images to an initial model in minutes. Acta Crystallogr D Biol Crystallogr *62*, 859-866.

Morris, R.J., Zwart, P.H., Cohen, S., Fernandez, F.J., Kakaris, M., Kirillova, O., Vonrhein, C., Perrakis, A., and Lamzin, V.S. (2004). Breaking good resolutions with ARP/wARP. J Synchrotron Radiat *11*, 56-59.

Muckenthaler, M.U., Galy, B., and Hentze, M.W. (2008). Systemic iron homeostasis and the iron-responsive element/iron-regulatory protein (IRE/IRP) regulatory network. Annu Rev Nutr *28*, 197-213.

Nakayama, K.I., and Nakayama, K. (2006). Ubiquitin ligases: cell-cycle control and cancer. Nat Rev Cancer *6*, 369-381.

Nalepa, G., Rolfe, M., and Harper, J.W. (2006). Drug discovery in the ubiquitin-proteasome system. Nat Rev Drug Discov *5*, 596-613.

Nemeth, E., Tuttle, M.S., Powelson, J., Vaughn, M.B., Donovan, A., Ward, D.M., Ganz, T., and Kaplan, J. (2004). Hepcidin regulates cellular iron efflux by binding to ferroportin and inducing its internalization. Science *306*, 2090-2093.

Nicolas, G., Bennoun, M., Devaux, I., Beaumont, C., Grandchamp, B., Kahn, A., and Vaulont, S. (2001). Lack of hepcidin gene expression and severe tissue iron overload in upstream stimulatory factor 2 (USF2) knockout mice. Proc Natl Acad Sci U S A *98*, 8780-8785.

Nicolas, G., Chauvet, C., Viatte, L., Danan, J.L., Bigard, X., Devaux, I., Beaumont, C., Kahn, A., and Vaulont, S. (2002). The gene encoding the iron regulatory peptide hepcidin is regulated by anemia, hypoxia, and inflammation. J Clin Invest *110*, 1037-1044.

Nordlund, P., and Eklund, H. (1995). Di-iron-carboxylate proteins. Curr Opin Struct Biol *5*, 758-766.

Osaki, S., and Johnson, D.A. (1969). Mobilization of liver iron by ferroxidase (ceruloplasmin). J Biol Chem *244*, 5757-5758.

Otwinowski, Z. (1991). Maximum likelihood refinement of heavy atom paramaters. Paper presented at: Proceedings of the CCP4 Study Weekend (Cambridge, U.K., Science & Engineering Research Council).

Owen, D., and Kuhn, L.C. (1987). Noncoding 3' sequences of the transferrin receptor gene are required for mRNA regulation by iron. EMBO J *6*, 1287-1293.

Ozer, A., and Bruick, R.K. (2007). Non-heme dioxygenases: cellular sensors and regulators jelly rolled into one? Nat Chem Biol *3*, 144-153.

Peyssonnaux, C., Nizet, V., and Johnson, R.S. (2008). Role of the hypoxia inducible factors HIF in iron metabolism. Cell Cycle *7*, 28-32.

Philpott, C.C., Klausner, R.D., and Rouault, T.A. (1994). The bifunctional iron-responsive element binding protein/cytosolic aconitase: the role of active-site residues in ligand binding and regulation. Proc Natl Acad Sci U S A *91*, 7321-7325.

Ragan, H.A., Nacht, S., Lee, G.R., Bishop, C.R., and Cartwright, G.E. (1969). Effect of ceruloplasmin on plasma iron in copper-deficient swine. Am J Physiol *217*, 1320-1323.

Ramirez, R.D., Sheridan, S., Girard, L., Sato, M., Kim, Y., Pollack, J., Peyton, M., Zou, Y., Kurie, J.M., Dimaio, J.M.*, et al.* (2004). Immortalization of human bronchial epithelial cells in the absence of viral oncoproteins. Cancer Res *64*, 9027-9034.

Rao, K., Harford, J.B., Rouault, T., McClelland, A., Ruddle, F.H., and Klausner, R.D. (1986). Transcriptional regulation by iron of the gene for the transferrin receptor. Mol Cell Biol *6*, 236-240.

Ravid, T., and Hochstrasser, M. (2008). Diversity of degradation signals in the ubiquitin-proteasome system. Nat Rev Mol Cell Biol *9*, 679-690.

Roetto, A., Papanikolaou, G., Politou, M., Alberti, F., Girelli, D., Christakis, J., Loukopoulos, D., and Camaschella, C. (2003). Mutant antimicrobial peptide hepcidin is associated with severe juvenile hemochromatosis. Nat Genet *33*, 21-22.

Rouault, T.A. (2006). The role of iron regulatory proteins in mammalian iron homeostasis and disease. Nat Chem Biol *2*, 406-414.

Rouault, T.A., Haile, D.J., Downey, W.E., Philpott, C.C., Tang, C., Samaniego, F., Chin, J., Paul, I., Orloff, D., Harford, J.B.*, et al.* (1992). An iron-sulfur cluster plays a novel regulatory role in the iron-responsive element binding protein. Biometals *5*, 131-140.

Rouault, T.A., Hentze, M.W., Caughman, S.W., Harford, J.B., and Klausner, R.D. (1988). Binding of a cytosolic protein to the iron-responsive element of human ferritin messenger RNA. Science *241*, 1207-1210.

Rouault, T.A., Tang, C.K., Kaptain, S., Burgess, W.H., Haile, D.J., Samaniego, F., McBride, O.W., Harford, J.B., and Klausner, R.D. (1990). Cloning of the cDNA encoding an RNA regulatory protein--the human iron-responsive element-binding protein. Proc Natl Acad Sci U S A *87*, 7958-7962.

Salahudeen, A.A., and Bruick, R.K. (2009). Maintaining Mammalian iron and oxygen homeostasis: sensors, regulation, and cross-talk. Ann N Y Acad Sci *1177*, 30-38.

Salahudeen, A.A., Thompson, J.W., Ruiz, J.C., Ma, H.W., Kinch, L.N., Li, Q., Grishin, N.V., and Bruick, R.K. (2009). An E3 ligase possessing an iron-responsive hemerythrin domain is a regulator of iron homeostasis. Science *326*, 722-726.

Salceda, S., and Caro, J. (1997). Hypoxia-inducible factor 1alpha (HIF-1alpha) protein is rapidly degraded by the ubiquitin-proteasome system under normoxic conditions. Its stabilization by hypoxia depends on redox-induced changes. J Biol Chem *272*, 22642-22647.

Samaniego, F., Chin, J., Iwai, K., Rouault, T.A., and Klausner, R.D. (1994). Molecular characterization of a second iron-responsive element binding protein, iron regulatory protein 2. Structure, function, and post-translational regulation. J Biol Chem *269*, 30904-30910.

Sanchez, M., Galy, B., Muckenthaler, M.U., and Hentze, M.W. (2007). Iron-regulatory proteins limit hypoxia-inducible factor-2alpha expression in iron deficiency. Nat Struct Mol Biol *14*, 420-426.

Schaible, U.E., and Kaufmann, S.H. (2004). Iron and microbial infection. Nat Rev Microbiol *2*, 946-953.

Schneider, T.R., and Sheldrick, G.M. (2002). Substructure solution with SHELXD. Acta Crystallogr D Biol Crystallogr *58*, 1772-1779.

Schrader, E.K., Harstad, K.G., and Matouschek, A. (2009). Targeting proteins for degradation. Nat Chem Biol *5*, 815-822.

Semenza, G.L. (2003). Targeting HIF-1 for cancer therapy. Nat Rev Cancer *3*, 721-732.

Shah, Y.M., Matsubara, T., Ito, S., Yim, S.H., and Gonzalez, F.J. (2009). Intestinal hypoxia-inducible transcription factors are essential for iron absorption following iron deficiency. Cell Metab *9*, 152-164.

Sheriff, S., Hendrickson, W.A., and Smith, J.L. (1987). Structure of myohemerythrin in the azidomet state at 1.7/1.3 A resolution. J Mol Biol *197*, 273-296.

Smith, S.R., Ghosh, M.C., Ollivierre-Wilson, H., Hang Tong, W., and Rouault, T.A. (2006). Complete loss of iron regulatory proteins 1 and 2 prevents viability of murine zygotes beyond the blastocyst stage of embryonic development. Blood Cells Mol Dis *36*, 283-287.

Sorokin, A.V., Kim, E.R., and Ovchinnikov, L.P. (2009). Proteasome system of protein degradation and processing. Biochemistry (Mosc) *74*, 1411-1442.

Stenkamp, R.E. (1994). Dioxygen and Hemerythrin. Chemical Reviews *94*, 715-726.

Stenkamp, R.E., Sieker, L.C., Jensen, L.H., McCallum, J.D., and Sanders-Loehr, J. (1985). Active site structures of deoxyhemerythrin and oxyhemerythrin. Proc Natl Acad Sci U S A *82*, 713-716.

Tan, X., Calderon-Villalobos, L.I., Sharon, M., Zheng, C., Robinson, C.V., Estelle, M., and Zheng, N. (2007). Mechanism of auxin perception by the TIR1 ubiquitin ligase. Nature *446*, 640-645.

Theil, E.C. (2003). Ferritin: at the crossroads of iron and oxygen metabolism. J Nutr *133*, 1549S-1553S.

Thines, B., Katsir, L., Melotto, M., Niu, Y., Mandaokar, A., Liu, G., Nomura, K., He, S.Y., Howe, G.A., and Browse, J. (2007). JAZ repressor proteins are targets of the SCF(COI1) complex during jasmonate signalling. Nature *448*, 661-665.

Tokunaga, F., Sakata, S., Saeki, Y., Satomi, Y., Kirisako, T., Kamei, K., Nakagawa, T., Kato, M., Murata, S., Yamaoka, S., *et al.* (2009). Involvement of linear polyubiquitylation of NEMO in NF-kappaB activation. Nat Cell Biol *11*, 123-132.

Tsushima, R.G., Wickenden, A.D., Bouchard, R.A., Oudit, G.Y., Liu, P.P., and Backx, P.H. (1999). Modulation of iron uptake in heart by L-type Ca2+ channel modifiers: possible implications in iron overload. Circ Res *84*, 1302-1309.

Ullman, E.F., Kirakossian, H., Singh, S., Wu, Z.P., Irvin, B.R., Pease, J.S., Switchenko, A.C., Irvine, J.D., Dafforn, A., Skold, C.N., *et al.* (1994). Luminescent oxygen channeling immunoassay: measurement of particle binding kinetics by chemiluminescence. Proc Natl Acad Sci U S A *91*, 5426-5430.

Varshavsky, A. (1991). Naming a targeting signal. Cell *64*, 13-15.

Vulpe, C.D., Kuo, Y.M., Murphy, T.L., Cowley, L., Askwith, C., Libina, N., Gitschier, J., and Anderson, G.J. (1999). Hephaestin, a ceruloplasmin homologue implicated in intestinal iron transport, is defective in the sla mouse. Nat Genet *21*, 195-199.

Walden, W.E., Selezneva, A.I., Dupuy, J., Volbeda, A., Fontecilla-Camps, J.C., Theil, E.C., and Volz, K. (2006). Structure of dual function iron regulatory protein 1 complexed with ferritin IRE-RNA. Science *314*, 1903-1908.

Wallander, M.L., Leibold, E.A., and Eisenstein, R.S. (2006). Molecular control of vertebrate iron homeostasis by iron regulatory proteins. Biochim Biophys Acta *1763*, 668-689.

Wallander, M.L., Zumbrennen, K.B., Rodansky, E.S., Romney, S.J., and Leibold, E.A. (2008). Iron-independent phosphorylation of iron regulatory protein 2 regulates ferritin during the cell cycle. J Biol Chem *283*, 23589-23598.

Wang, J., Chen, G., Muckenthaler, M., Galy, B., Hentze, M.W., and Pantopoulos, K. (2004). Iron-mediated degradation of IRP2, an unexpected pathway involving a 2-oxoglutarate-dependent oxygenase activity. Mol Cell Biol *24*, 954-965.

Wang, J., Fillebeen, C., Chen, G., Biederbick, A., Lill, R., and Pantopoulos, K. (2007). Iron-dependent degradation of apo-IRP1 by the ubiquitin-proteasome pathway. Mol Cell Biol *27*, 2423-2430.

Willems, A.R., Schwab, M., and Tyers, M. (2004). A hitchhiker's guide to the cullin ubiquitin ligases: SCF and its kin. Biochim Biophys Acta *1695*, 133-170.

Wingert, R.A., Galloway, J.L., Barut, B., Foott, H., Fraenkel, P., Axe, J.L., Weber, G.J., Dooley, K., Davidson, A.J., Schmid, B.*, et al.* (2005). Deficiency of glutaredoxin 5 reveals Fe-S clusters are required for vertebrate haem synthesis. Nature *436*, 1035-1039.

Wirbelauer, C., Sutterluty, H., Blondel, M., Gstaiger, M., Peter, M., Reymond, F., and Krek, W. (2000). The F-box protein Skp2 is a ubiquitylation target of a Cul1-based core ubiquitin ligase complex: evidence for a role of Cul1 in the suppression of Skp2 expression in quiescent fibroblasts. EMBO J *19*, 5362-5375.

Xiong, J., Kurtz, D.M., Jr., Ai, J., and Sanders-Loehr, J. (2000). A hemerythrin-like domain in a bacterial chemotaxis protein. Biochemistry *39*, 5117-5125.

Yamanaka, K., Ishikawa, H., Megumi, Y., Tokunaga, F., Kanie, M., Rouault, T.A., Morishima, I., Minato, N., Ishimori, K., and Iwai, K. (2003). Identification of the ubiquitin-protein ligase that recognizes oxidized IRP2. Nat Cell Biol *5*, 336-340.

Yen, H.C., and Elledge, S.J. (2008). Identification of SCF ubiquitin ligase substrates by global protein stability profiling. Science *322*, 923-929.

Yu, Y., Radisky, E., and Leibold, E.A. (1992). The iron-responsive element binding protein. Purification, cloning, and regulation in rat liver. J Biol Chem *267*, 19005-19010.

Zahringer, J., Baliga, B.S., and Munro, H.N. (1976). Novel mechanism for translational control in regulation of ferritin synthesis by iron. Proc Natl Acad Sci U S A *73*, 857-861.

Zhang, N., Liu, J., Ding, X., Aikhionbare, F., Jin, C., and Yao, X. (2007). FBXL5 interacts with p150Glued and regulates its ubiquitination. Biochem Biophys Res Commun *359*, 34-39.

Zimmer, M., Ebert, B.L., Neil, C., Brenner, K., Papaioannou, I., Melas, A., Tolliday, N., Lamb, J., Pantopoulos, K., Golub, T.*, et al.* (2008). Small-molecule inhibitors of HIF-2a translation link its 5'UTR iron-responsive element to oxygen sensing. Mol Cell *32*, 838-848.

Zumbrennen, K.B., Hanson, E.S., and Leibold, E.A. (2008). HOIL-1 is not required for iron-mediated IRP2 degradation in HEK293 cells. Biochim Biophys Acta *1783*, 246-252.